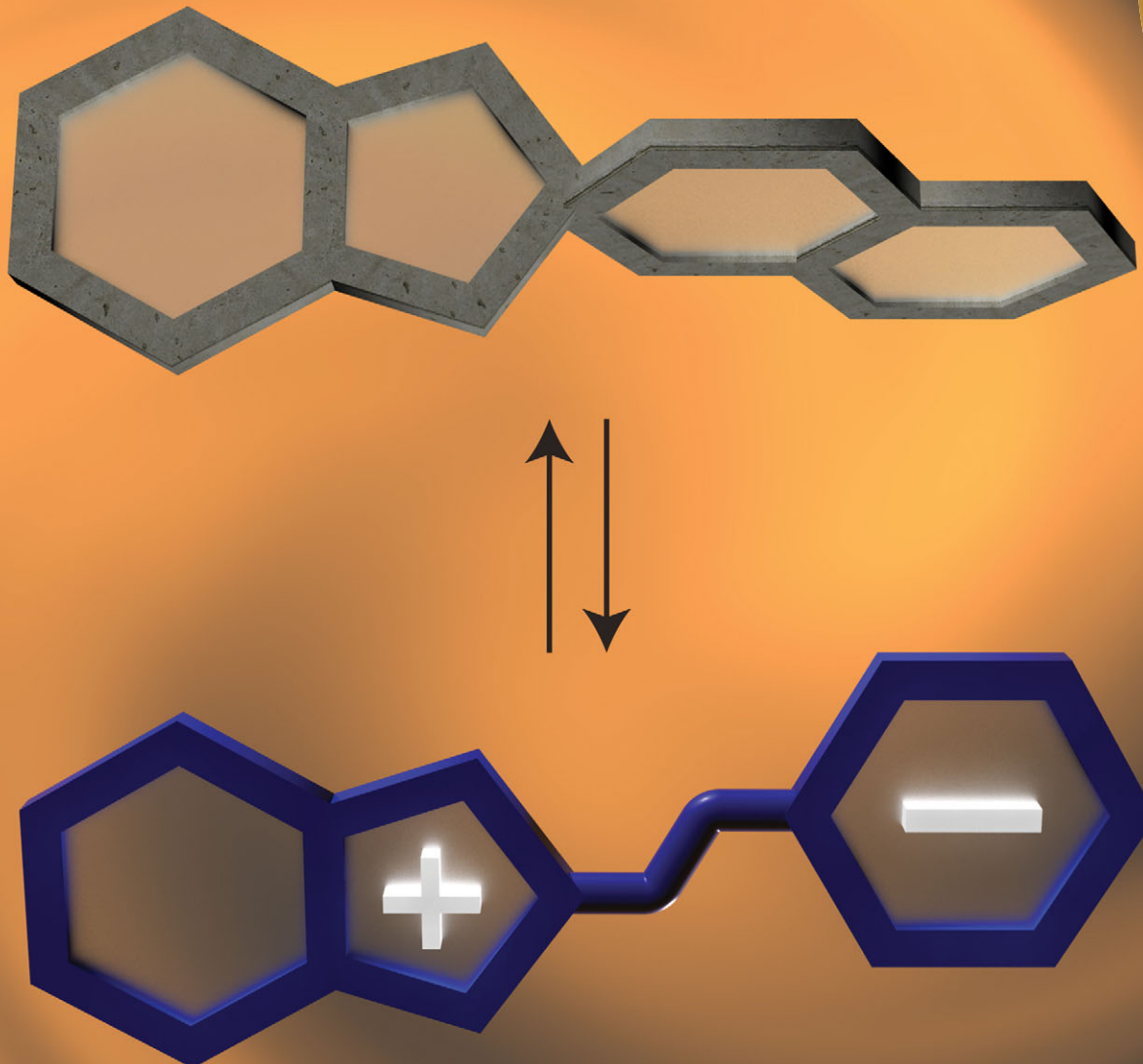


# Chem Soc Rev

Chemical Society Reviews

[www.rsc.org/chemscrev](http://www.rsc.org/chemscrev)



ISSN 0306-0012



ROYAL SOCIETY  
OF CHEMISTRY

REVIEW ARTICLE

Rafal Klajn

Spiropyran-based dynamic materials

## Spiropyran-based dynamic materials

Rafal Klajn

Cite this: *Chem. Soc. Rev.*, 2014, 43, 148

Received 3rd June 2013

DOI: 10.1039/c3cs60181a

[www.rsc.org/csr](http://www.rsc.org/csr)

In the past few years, spiropyran has emerged as the molecule-of-choice for the construction of novel dynamic materials. This unique molecular switch undergoes structural isomerisation in response to a variety of orthogonal stimuli, e.g. light, temperature, metal ions, redox potential, and mechanical stress. Incorporation of this switch onto macromolecular supports or inorganic scaffolds allows for the creation of robust dynamic materials. This review discusses the synthesis, switching conditions, and use of dynamic materials in which spiropyran has been attached to the surfaces of polymers, biomacromolecules, inorganic nanoparticles, as well as solid surfaces. The resulting materials show fascinating properties whereby the state of the switch intimately affects a multitude of useful properties of the support. The utility of the spiropyran switch will undoubtedly endow these materials with far-reaching applications in the near future.

### 1. Introduction

For centuries, nature has awed scientists with its rich repertoire of materials and systems that can reversibly adjust their structure and properties in response to environmental stimuli. Wide-ranging examples include heat-shock response in bacteria,<sup>1</sup> camouflage in cephalopods and chameleons,<sup>2</sup> colour changes in echinoderms in response to light,<sup>3</sup> and avian flocking in the presence of a predator.<sup>4</sup> In sharp contrast, nearly all traditional man-made materials are static in both form and function, and only quite recently are synthetic materials chemists gradually shifting their attention to dynamic materials.<sup>5–9</sup> Such dynamic materials have multiple advantages over their static counterparts: selected properties of interest can be reversibly “turned on” and “off” at will and the ability to reconfigure these materials imparts upon them many uses. Emerging applications include “smart” windows for the construction of energy-efficient buildings, self-erasing (reusable) paper or self-healing coatings, to name just a few.

Among the different forms of external inputs that can influence the state of a material, light has numerous advantages:<sup>10–16</sup> it can be delivered with high spatial and temporal precision, no chemical contaminants are introduced, closed systems can be actuated, and finally, light of specific wavelengths can be delivered. The last feature is of great value when photoswitchable molecules are used as light-harvesting elements; azobenzenes,<sup>17,18</sup> for example, isomerises between two forms when exposed to near-UV ( $\sim 350$  nm) and blue ( $\sim 420$  nm) light, respectively. Accordingly, various photoswitchable molecules – azobenzenes,<sup>17,18</sup> stilbenes,<sup>19,20</sup> spiropyrans,<sup>21–24</sup> diarylethenes,<sup>25,26</sup> fulgides,<sup>27,28</sup> and others<sup>29–31</sup> – have been widely investigated and employed for the

construction of light-responsive systems and materials. Each of these photoswitches has its advantages and disadvantages; azobenzenes, for example, are structurally simple and readily accessed synthetically; unfortunately the yield of the *trans*  $\rightarrow$  *cis* conversion is usually far from quantitative. Diarylethenes, on the other hand, are not ideal for the design of mechanically switchable architectures since their isomerisation is accompanied by a relatively small change in molecular conformation, but this class of molecules has shown superb resistance to photo-degradation<sup>11,32</sup> – a drawback which has traditionally been associated with spiropyrans (*cf.*, however, Section 1.3.6).

What makes spiropyrans unique among this broad spectrum of photoswitches, however, is that its two isomers (see Section 1.1) have vastly different properties. As a consequence, spiropyran is far more than just a simple photoswitch; the range of stimuli able to induce its reversible isomerisation is truly impressive and includes different solvents, metal ions, acids and bases, temperature, redox potential, and mechanical force. This versatility vis-à-vis input method highlights the far-reaching capabilities of new spiropyran-based dynamic materials. It is important to emphasise, however, that in order for the dynamic materials to be robust and ultimately meet the requirements of real-world applications, it is necessary for the active components – the spiropyran units – to be *covalently* attached to the support<sup>33</sup> (as elaborated in Section 1.3). For this reason, examples based on non-covalent association<sup>34–37</sup> of small-molecule spiropyrans with macromolecules or surfaces are not included in the current review.

Materials and systems covered in this review are divided according to the type of support spiropyrans are immobilised onto/within. These supports include polymer chains (Sections 2.1–2.7), biomacromolecules (Sections 3.1–3.8), inorganic nanoparticles (NPs) (Sections 4.1 and 4.2), and solid surfaces



(Sections 5.1–5.5). For consistency, the name “spiropyran” in this review applies to both the closed- and the open-ring isomers. The closed-ring isomer is abbreviated as “SP”; the open-ring isomer (or merocyanine) is abbreviated as “MC”.

### 1.1. Isomerisation of spiropyran

The structural formula of the parent closed-ring isomer of spiropyran is represented as **1** in Fig. 1A. The molecule comprises an indoline and a chromene moiety bound together *via* a spiro junction and oriented perpendicular with respect to one another. The optical spectrum of the closed-ring isomer shows two localised transitions (Fig. 1B, gray trace); the band located at  $\sim 272$ – $296$  nm is attributed to the  $\pi$ – $\pi^*$  electronic transition in the indoline part of the molecule, and the  $\sim 323$ – $351$  nm band corresponds to the chromene moiety.<sup>38,39</sup> UV ( $\lambda = 365$  nm) irradiation of SP gives rise to the open-ring isomer (MC; **2** in Fig. 1A) in a first-order process<sup>40</sup> whose mechanism has been

investigated extensively; the transformation begins with the cleavage of the C<sub>spiro</sub>–O bond, resulting in *cis*-MC<sup>41–43</sup> (see **5**, **6** Fig. 2) – an ephemeral species detectable by using transient absorption spectroscopy immediately after the UV pulse. The rotation about the central C–C bonds<sup>44,45</sup> in *cis*-MC ultimately yields *trans*-MC.<sup>18,19</sup> Interestingly, the SP  $\rightarrow$  MC isomerisation can also be accomplished using near-infrared (NIR) radiation (*via* two-photon excitation).<sup>46–50</sup> This property is important since (i) the use of an NIR laser significantly reduces photodegradation of the switch as compared to the wavelengths (UV) used for single-photon processes, and (ii) it opens the way to perform isomerisation in biological samples as discussed in Section 2.1. The MC  $\rightarrow$  SP reverse isomerisation usually occurs spontaneously, again following first-order kinetics,<sup>51</sup> and can be accelerated by visible light.

The ring-opening reaction can be represented either as a heterolytic C–O bond cleavage (Fig. 2, left) or as a  $6\pi$  electrocyclic ring opening (Fig. 2, right), leading to the zwitterionic (**7**) or the quinoidal (**8**) resonance forms, respectively.<sup>52</sup> The final MC product is a hybrid of these resonance forms (**9** in Fig. 2). Due to its planar structure and an extended  $\pi$ -conjugation between the indoline and the chromene moieties, MC shows a single delocalised transition shifted to the visible region, with  $\lambda_{\text{max}} = 550$ – $600$  nm in most non-polar solvents. The exact location of this band is dictated by the relative contributions of the two extreme resonance forms. Non-polar media, which preferentially stabilise the quinoidal form,<sup>53–55</sup> decrease the energy gap between the ground and excited states of MC, resulting in a bathochromic shift of the MC band<sup>43,56</sup> (“negative solvatochromism” of MC<sup>57,58</sup>). The strong dependence of MC absorption on the environment has been exploited for the construction of microcapillary-based systems capable of detecting specific solvents.<sup>59,60</sup>

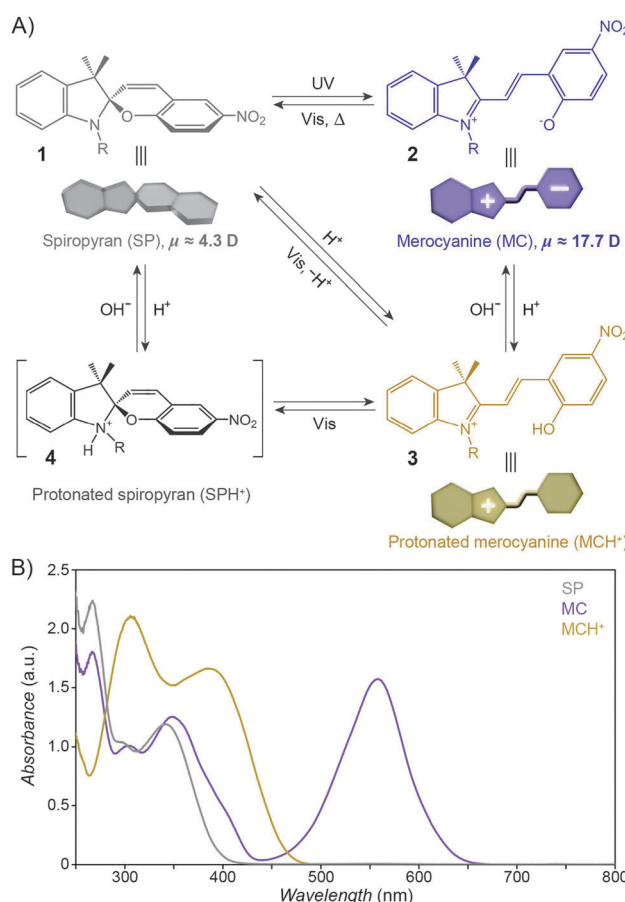


Fig. 1 Photochromism and acidochromism of spiropyran. (A) Reversible transformations between the four states: spiropyran (SP) **1**, merocyanine (MC) **2**, protonated merocyanine ( $\text{MCH}^+$ ) **3**, and protonated spiropyran ( $\text{SPH}^+$ ) **4** (note that although **4** is represented with the extra proton on the spiro N atom, it is also possible that the proton resides on the spiro O atom, or on the nitro group<sup>306</sup>). (B) UV-Vis spectra of the parent spiropyran ( $1',3',3'$ -trimethyl-6-nitrospiro[chromene-2,2'-indoline]) before (gray) and after (purple) UV irradiation (5 min;  $I = 0.7 \text{ mW cm}^{-2}$ ), and after the addition of 20 eq. of HCl (yellow). Spectra were recorded on a  $c = 0.231 \text{ mM}$  solution in acetonitrile; optical path length = 10 mm.

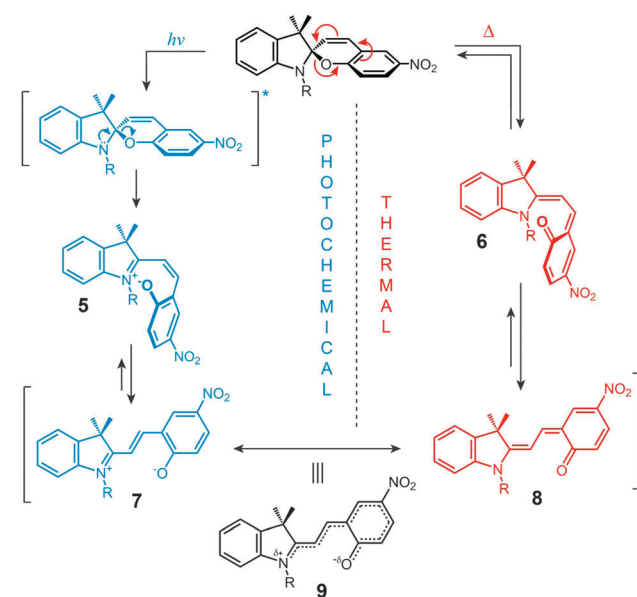


Fig. 2 Mechanism of photochemical and thermal isomerisation of spiropyran.



The widespread utility of the spiropyran switch lies in the fact that the SP and MC isomers have vastly different physicochemical properties. First and foremost, the charge separation in MC gives rise to a large electric dipole moment, particularly in comparison with the SP isomer. Density functional theory calculations<sup>61</sup> as well as electrical interferometry<sup>62</sup> and electro-optical absorption measurements<sup>63</sup> have shown that while the dipole moment of the parent (Fig. 1A) SP is in the range of  $\sim 4\text{--}6$  D, this changes drastically to  $\sim 14\text{--}18$  D for the MC form. Secondly, the SP and MC states show significant structural differences, whereby SP occupies less volume than MC. An elegant manifestation of these differences is the reversible increase, as a result of UV irradiation, in surface pressure within monolayers of a spiropyran-functionalised PMMA densely packed at the water-air interface.<sup>64\text{--}66</sup> Thirdly, the SP isomer is optically transparent in the visible region whereas MC absorbs strongly at  $\lambda_{\text{max}} = 550\text{--}600$  nm and appears deep blue. Fourthly, SP and MC differ markedly in their emission behaviour: while the SP isomer does not exhibit strong emission, ring-opening results in the appearance of an intense emission band centered at  $\lambda_{\text{max}} \approx 650$  nm (cf. Fig. 3A<sup>67</sup>). The resulting red emission can

subsequently be “turned off” as the pyran ring re-forms and the extended  $\pi$ -conjugation is broken. Fifthly, the MC isomer is significantly more basic than SP, and its protonation leads to  $\text{MCH}^+$  with a characteristic band at  $\sim 420$  nm (Fig. 1B). Still, while the acidic character of  $\text{MCH}^+$  originates from the 2-hydroxy-4-nitrophenyl moiety, the  $\text{p}K_{\text{a}}$  of  $\text{MCH}^{+70}$  ( $\sim 2.25$ ) is much lower than that of the parent 4-nitrophenol ( $\text{p}K_{\text{a}} = 7.15^{71}$ ). This dramatic stabilisation of the phenoxide anion (reduced basicity) can be attributed to the electronic conjugation within the molecule, with the quinoidal resonance form (8 in Fig. 2) favouring<sup>72</sup> the deprotonated MC. The low  $\text{p}K_{\text{a}}$  value is also due to the electron-withdrawing effect of the  $\text{NO}_2$  group located at the *para* position with respect to the phenolic OH – without it, the  $\text{p}K_{\text{a}}$  of  $\text{MCH}^+$  was estimated to be 6–7<sup>73</sup> (compare with  $\text{p}K_{\text{a}} = 10.0$  for phenol). It should be noted, however, that the solution value of  $\text{p}K_{\text{a}} = 2.25$  often is not accurate for the immobilised spiropyrans discussed in this review; the acidity of constrained species<sup>74</sup> is, in principle, system-dependent. Finally, the MC form has a higher affinity to different chemical species, in particular other zwitterions and metal ions.

The above differences in the characters of SP and MC are intimately linked to another unique feature of spiropyran: its responsiveness to multiple stimuli. In addition to being photochromic, its reversible isomerisation can be realised by several other independent stimuli, which include temperature<sup>21</sup> (thermochromism), pH<sup>75\text{--}77</sup> (acidochromism), solvent polarity<sup>78</sup> (solvatochromism), redox potential<sup>79</sup> (electrochromism), metal ions,<sup>45,46</sup> and even mechanical force<sup>80</sup> (mechanochromism). For example, treating SP with acids (Fig. 1A) or metal ions can induce ring opening even in the absence of any UV irradiation because of the high affinity of the open-ring form to  $\text{H}^+$  and metal ions (see Section 2.6). Likewise, polar environments – including solvents,<sup>81,82</sup> silica,<sup>83\text{--}86</sup> or reverse micelles<sup>87</sup> – can stabilise the zwitterionic MC to the extent that the  $\text{SP} \rightarrow \text{MC}$  transition occurs spontaneously in the dark. Under these conditions, SP represents the metastable state, which can exist only if the system is exposed to visible light. This property is referred to as *negative photochromism*<sup>58,88</sup> (sometimes also called inverse or reverse photochromism), and is of particular relevance in the context of water-based biological environments (see Sections 3.1–3.8).

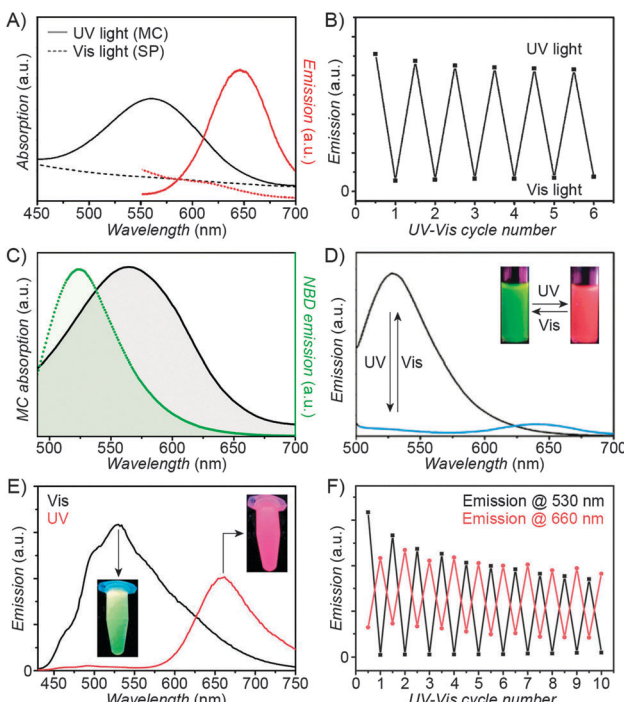


Fig. 3 Fluorescent properties of the SP–MC system. (A) Typical absorption (black) and emission (red) profiles of SP (dashed lines) and MC (solid lines). (B) Reversible fluorescence ( $\lambda_{\text{em}} = 645$  nm) switching in a spiropyran-decorated polymer upon exposure to UV and Vis light. (C) Overlap of the nitrobenzoxadiazolyl (NBD) fluorophore emission (green) and MC quencher absorption (gray) – a prerequisite for efficient FRET. (D) Photoswitchable FRET in dual-emissive polymer NPs based on spiropyran and NBD. (E) Photoswitchable FRET in dual-emissive polymer NPs based on spiro-pyran and a polythiophene derivative. (F) Green emission is quenched as red emission rises in dual-emissive polymer NPs shown in (E). [Adapted with permission from ref. 67 (Copyright 2010 Wiley-VCH) (A and B), ref. 159 (Copyright 2008 Royal Society of Chemistry) (C and D) and ref. 190 (Copyright 2003 Royal Society of Chemistry) (E and F).]

## 1.2. Aggregation of the open-ring isomer

An important consequence of the molecular structure of the MC isomer is its tendency to aggregate. Driven predominantly by the dipole–dipole interactions (along with the  $\pi$ – $\pi$  stacking), the aggregation occurs readily in hydrophobic solvents.<sup>89,90</sup> The MC units can stack in two different ways: “head-to-tail” (parallel) arrangement of the dipoles gives rise to so-called J-aggregates, whereas “side-by-side” (antiparallel; compare Fig. 7C) stacking yields H-aggregates. These two types of packing can easily be identified in the absorption spectra: while J-aggregation shifts the MC band to higher wavelengths (bathochromic/red shift), H-aggregation is manifested by the hypsochromic/blue shift (cf. Fig. 7A). Both J-aggregates<sup>91\text{--}96</sup> and



H-aggregates<sup>97–100</sup> of MC are well known, and occasionally are found to co-exist.<sup>101,102</sup>

In addition to its tendency to aggregate, MC can also form complexes with SP units.<sup>63,64</sup> Elegant experiments suggesting the existence of such heterocomplexes were performed with ~900 nm silica spheres and planar quartz surfaces – both functionalised with spiropyran. As expected, there were no attractive interactions between the spheres and the surfaces in the dark, but exposure of the system to UV induced adsorption of the silica onto quartz. Interestingly, such adsorption could also be induced when only *one* of the two components was UV-irradiated (and had its SP moieties converted to MC), therefore confirming that the SP–MC interactions were responsible for adsorption.<sup>103</sup>

MC aggregation stabilises the open-ring isomer and therefore it strongly retards<sup>101,104</sup> or even completely blocks<sup>105</sup> the ring-closing reaction. As such, the aggregation is counterproductive to the development of efficiently switching systems. Fortunately, immobilisation of the chromophore units can protect individual MC units from aggregation. Still, partial aggregation is often observed, with MC → SP decolouration kinetics that are best fitted by the superposition of two first-rate reactions.<sup>106,107</sup> For example, MC immobilised on the surface of silica spheres faded with  $k_1 = 4.2 \times 10^{-3} \text{ s}^{-1}$  and  $k_2 = 1.3 \times 10^{-3} \text{ s}^{-1}$ , which was attributed to the isomerisation of isolated and aggregated MC moieties, respectively.<sup>108</sup> Such biexponential decay of MC was also observed within monolayers on solid SiO<sub>2</sub>, wherein transient Brewster angle reflectometry showed that while the quantum efficiency of the ring opening occurred with a well-defined quantum efficiency of ~0.1, the MC signal decayed with quantum efficiencies of ~0.2 and ~0.03 assigned to isolated and stacked MC units, respectively.<sup>109</sup>

### 1.3. Benefits of immobilisation

Covalent attachment of spiropyran has numerous advantages over non-covalent association to the support:

**1.3.1. No leaching.** Spiropyran moieties remain permanently attached to the support and there is no risk of leaching. In photoresponsive systems based on non-covalent interactions, the issue of leaching is particularly acute due to distinctly different characters of the closed- and the open-ring isomers, which facilitates phase separation.<sup>110,111</sup>

**1.3.2. Improved processability.** Attachment of spiropyran to inorganic or macromolecular carriers allows one to take advantage of the desired mechanical properties, film formation capabilities, *etc.*, imparted by the carrier.

**1.3.3. Solvent compatibility.** The polymer backbone can have a much larger contribution to overall solubility than the pendant (SP/MC) groups. For example, the hydrophilic poly-(*N*-isopropylacrylamide) (PNIPAM) showed good solubility in water even when decorated with the hydrophobic SP (see Section 2.3) (it may be noted that for heavily substituted polymer chains, the opposite trend is observed and the solubility is determined by the side groups; *e.g.* polysaccharides modified with SP<sup>73,74</sup> could be dissolved in DMSO<sup>112,113</sup> and even in benzene<sup>114</sup>). Likewise, in the case of NPs functionalised with mixed monolayers

comprising SP/MC, solubility is determined by the majority component of the monolayer (“background ligand”).

**1.3.4. Enabling biocompatibility.** Attachment of spiropyran to biocompatible polymers was shown to give biocompatible photoresponsive materials,<sup>115,116</sup> therefore paving the way for photoswitching inside living organisms.

**1.3.5. Preventing MC aggregation.** Immobilisation of spiropyran moieties suppresses intermolecular interactions and therefore MC stack formation. Keeping MC units isolated from one another is important in the context of reversible isomerisation – under such conditions, fast and efficient switching is possible in both directions, even in non-polar solvents.<sup>117</sup>

**1.3.6. Reduced photodegradation.** Arguably the most important benefit of immobilising spiropyran is that it increases the resistance to “fatigue” (gradual degradation with increasing number of switching cycles). Although photoisomerisation of spiropyran is, in principle, a nondestructive process, side reactions can lead to by-products that lack the photoresponsive properties. Both mono- and bimolecular (with respect to spiropyran) pathways of photodegradation have been identified. The former mechanism is based on the interaction of the long-lived triplet excited state of spiropyran with triplet oxygen (<sup>3</sup>O<sub>2</sub>), which generates singlet oxygen (<sup>1</sup>O<sub>2</sub>) initiating irreversible oxidation of the photoswitch.<sup>118,119</sup> To tackle this issue, switching can be carried out in the presence of antioxidants<sup>120</sup> and/or in an airtight environment.<sup>121</sup> However, the dominant cause of fatigue is *via* the bimolecular (dependent on spiropyran concentration) pathway, again involving the triplet excited state of the photoswitch.<sup>122</sup> Consequently, isomerisation in non-polar solvents, which favour MC stacking, gives rise to pronounced photodegradation.<sup>114</sup>

Fortunately, bimolecular events become largely suppressed by placing the spiropyran units on supports.<sup>123</sup> In a study that compared photodegradation of spiropyran molecules moving around freely in solution with that of their immobilised counterparts, ten switching cycles induced degradation of ~55% of small molecules, but only ~21% of the immobilised version under the same irradiation conditions.<sup>124</sup> In another example, PMMA-based spiropyran homopolymers showed significant fatigue after only several isomerisation cycles whereas a copolymer containing 20 mol% of the chromophore units was significantly more stable.<sup>125</sup> Finally, 50 switching cycles induced degradation of ~40% of spiropyran immobilised on ~2 μm polystyrene beads<sup>126</sup> – compared with ~50% degradation of small molecules in solution after only 13 cycles.<sup>120</sup> The decay of the switch on the beads was likely due to bimolecular events caused by the beads coming into contact with one another. Yet when spiropyran was attached to a *planar* surface, an impressive 370 switching cycles were realised without significant fatigue!<sup>127</sup>

**1.3.7. Improved fluorescence.** Immobilisation of the MC moieties restricts their conformational flexibility and protects the fluorophores from quenching by nonradiative processes (*e.g.* *via* collisions with solution molecules). As a result, emission quantum yields are increased. Fluorescence of MC can further be enhanced by placing the fluorophores in the hydrophobic environment of vesicles<sup>128</sup> or polymeric NPs,<sup>116</sup> which



is particularly important in the development of switchable fluorescent probes for biological applications (see Section 2.1).

**1.3.8. Tailoring the behaviour of the switch.** The support (*e.g.* a polymer chain and a nanoparticle) to which spiropyran is bound often has a much larger effect on the behaviour of the switch than the solvent.<sup>129,130</sup> First, the support affects the optical properties of the chromophore. The absorption of small-molecule MC in benzene is centered at  $\sim 600$  nm, as compared to  $\sim 583$  nm for PMMA-immobilised MC in the same solvent.<sup>44</sup> This shift suggests that MC is preferentially stabilised by the polymer's ester groups rather than by benzene molecules. In other words, the support acts as a "buffer", stabilising the photoswitch against environmental (*e.g.* solvents) changes. Interestingly, this *intramolecular solvation* could be followed by transient absorption spectroscopy: MC generated immediately after the UV pulse appeared at  $\sim 592$  nm, and shifted to  $\sim 583$  nm within only 1  $\mu$ s.<sup>44</sup>

Second, the support can largely affect isomerisation kinetics: while a small-molecule MC dissolved in ether isomerised within a few minutes, the colour of the same dye residing on a chitosan chain, also dissolved in ether, persisted for 24 hours.<sup>131</sup> In another example demonstrating the buffering effect of the polymer "hosts", addition of hydrophilic mica particles to a toluene solution of a small-molecule MC stabilised the coloured form and greatly reduced the kinetics of decolouration, whereas it had virtually no effect on the fading of polymer-immobilised MC under otherwise identical conditions.<sup>130</sup> It is also worth noting that polymer-immobilised MC does not exhibit significant solvatochromism, in contrast to individual MC units (see Sections 1.2 and 1.3). The properties of the photoswitch can even be modulated solely by the length of the linker connecting it to the support: accordingly, ring-closing of MC attached to the surface of silica proceeded with  $k_{n=8} = 0.52 \times 10^{-3}$  s<sup>-1</sup> and  $k_{n=16} = 4.2 \times 10^{-3}$  s<sup>-1</sup> when the dye was connected through linkers comprising 8 and 16 atoms, respectively.<sup>108</sup> In principle, longer linkers allow for more conformational flexibility and encourage solvation by the solvent molecules – which consequently leads to faster decolouration.<sup>132–134</sup> It is important to emphasise here the need to decouple the photoswitch from the underlying surface (that is, a minimal linker length is necessary) to achieve efficient isomerisation.<sup>135</sup> While the direct attachment of spiropyran to polystyrene beads *via* physisorption was possible, the isomerisation yield was only  $\sim 20\%$  of that of the switch which had been chemisorbed through an eight-carbon chain linker.<sup>126</sup> Likewise, isomerisation of SP *physisorbed* on planar gold<sup>136</sup> proceeded with a quantum yield of only  $\sim 10^{-10}$ .

The effect of the support can in fact be strong enough in some cases to induce a transition between positive and negative photochromism.<sup>129</sup> For example, spiropyran on a poly(*N,N*-dimethylacrylamide) backbone displayed positive ("normal") photochromism despite the polymer being surrounded by a strongly hydrophilic silica gel matrix.<sup>137</sup> Interestingly, the SP  $\leftrightarrow$  MC equilibrium can also be affected by the surface of a nanoparticle: chromophores bound to CdSe NPs prepared with tri-*n*-octylphosphine as the capping agent showed positive photochromism, but in similar NPs prepared in the presence

of sodium dioctylsulfosuccinate, negative photochromism was observed.<sup>138</sup> The authors attributed the stabilisation of the MC isomer to the charged defects on the surface of NPs prepared by the latter approach.

**1.3.9. Stabilising ephemeral species.** Finally, polymers functionalised with spiropyrans have proven useful in studying the mechanism of switching; isomerisation of constrained spiropyrans within sterically hindered environments has enabled the stabilisation and characterisation of *cis*-MC<sup>139</sup> (see 5, 6 in Fig. 2) – an otherwise ephemeral intermediate during the SP  $\leftrightarrow$  *trans*-MC isomerisation.

## 2. Spiropyran-functionalised polymers

Various approaches to spiropyran-bound polymers have been developed. The spiropyran moiety is compatible with most polymerisation conditions; therefore routes based on both polymerisation of spiropyran-based monomers and grafting on pre-formed polymer chains have been employed. The grafting-on approach has been used to functionalise a variety of polymers, including polytetrafluoroethylene (PTFE),<sup>140</sup> polyaniline,<sup>141</sup> polyacrylates,<sup>39,142,143</sup> polysulfones,<sup>82,144</sup> polyphosphazenes,<sup>106</sup> and Pluronic.<sup>145</sup> Homopolymers are typically synthesised by means of ring-opening metathesis polymerisation (ROMP).<sup>146,147</sup>

Random copolymers are most commonly prepared *via* AIBN-initiated free radical polymerisation of terminal alkenes<sup>148–154</sup> (usually methacrylates) or by polycondensation reactions,<sup>155–158</sup> whereas for the synthesis of block copolymers, atom transfer radical polymerisation (ATRP)<sup>129,159,160</sup> and reversible addition-fragmentation transfer (RAFT) polymerisation<sup>128,161,162</sup> have proven successful. These controlled polymerisation methods have also been used to derivatise solid surfaces with spiropyran polymers – in such cases, the solids (*e.g.* glass,<sup>163</sup> silica colloids<sup>164</sup>) are pre-functionalised with polymerisation initiators and used as starting materials.

Examples of polymers incorporating disubstituted spiropyran units as a part of the polymer backbone are relatively rare; these polymers can be obtained by various polycondensation methods, including polyesterification,<sup>165,166</sup> diol-diisocyanide polycondensation,<sup>167</sup> and bis(indoline)-bis(salicylaldehyde) polycondensation.<sup>168</sup> Polymers having precisely one photoswitchable unit as a part of the polymer chain were synthesised by controlled polymerisation methods (single-electron transfer living radical polymerisation (SET-LRP)<sup>169</sup> and ATRP<sup>170</sup>) using disubstituted spiropyrans as initiators. Finally, end-labeled polymers were obtained by nucleophilic substitution reactions involving small-molecule spiropyrans and pre-formed polymer chains,<sup>171,172</sup> *via* ATRP using a spiropyran-based tertiary bromide initiator,<sup>173</sup> or by solid-phase synthesis.<sup>174</sup>

### 2.1. Photocontrol of polymer fluorescence

Over the past several years, fluorescent properties of spiropyran polymers have been studied extensively due to their potential applications in detection and imaging. Ideal for such applications are photoresponsive polymers in the form of spherical



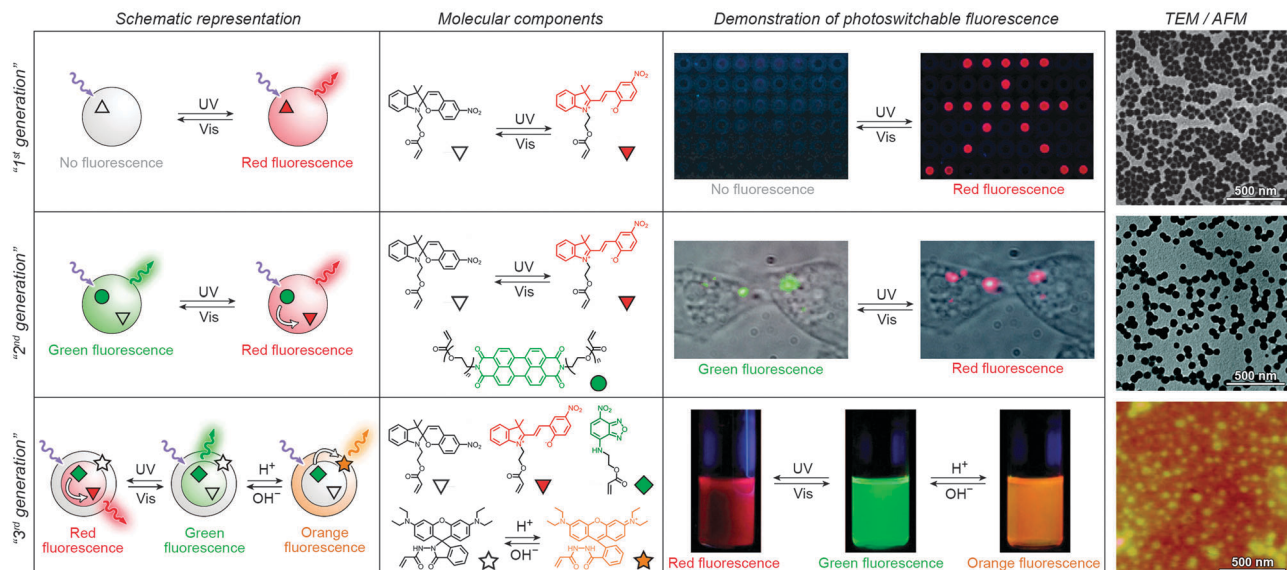


**Fig. 4** Polymer NPs exhibiting photoswitchable fluorescence. Top panel: In “1st generation” fluorescent NPs, MC fluorescence is reversibly “turned on” and “off”. Middle panel: “2nd generation” fluorescent NPs, whereby MC lights up at the expense of emission from a nearby fluorophore. Bottom panel: “3rd generation” fluorescent NPs capable of emitting light of three different wavelengths, depending on the environmental conditions. [Adapted with permission from ref. 68 (Copyright 2006 American Chemical Society) (top panel), ref. 186 (Copyright 2007 American Chemical Society) (middle panel) and ref. 161 (Copyright 2010 Wiley-VCH) (bottom panel).]

NPs, which have successfully been prepared using methods such as emulsion polymerisation<sup>68</sup> and ATRP followed by micellisation.<sup>159</sup> The resulting NPs are very bright (due to the compact packing of the fluorophores), often biocompatible, their surfaces can be functionalised with biomolecules,<sup>116</sup> and, most importantly, their fluorescence can be modulated remotely in a reversible fashion (Fig. 3 and 4).

In the simplest case, fluorescence of NPs is “turned on” and “off” upon exposure to UV and visible light, respectively. Such NPs, designated as “1st generation” in Fig. 4, were originally synthesised by Li and co-workers by means of emulsion polymerisation of a mixture containing *N*-isopropylacrylamide (NIPAM), styrene, divinylbenzene, and a spirobifluorene-methacrylate monomer.<sup>68</sup> Whereas the shells of the resulting NPs were hydrophilic (PNIPAM), thus providing them with good water solubility, the SP units resided in the hydrophobic cores. This gave rise to strong fluorescence of the MC form while significantly reducing photodegradation of the chromophore, as evidenced by only an ~5% decrease in MC fluorescence after five switching cycles.<sup>68</sup> This fatigue resistance, however, came at the expense of slow isomerisation kinetics of the photoswitch within the compact polymer matrix.<sup>68,69</sup> As a result, it took as long as ~5 min to reach the photostationary state under UV irradiation (compared with ~5 s for switching on semiconductor NPs under similar irradiation conditions<sup>175</sup>), and ~2 min (vs. ~90 s on the same semiconductor NPs) under visible light irradiation. The diameters of the NPs were readily controlled, in the 40–400 nm range, by varying the ratio of the monomers. This ability to control the particle size is important: ideally, NPs should be large enough to give an intense optical signal; however they should not be too large so as to minimise undesired light scattering.

Switchable fluorescence is the basis of *localisation microscopy*<sup>176</sup> – a recently developed<sup>177,178</sup> technique which enables imaging with nanometer-scale resolution – well below the diffraction limit – using standard fluorescence microscopy tools. Li *et al.* identified spirobifluorene as a switchable fluorophore which is well-suited for this application,<sup>179</sup> and developed a variant called photoactuated unimolecular logical switching-attained reconstruction (PULSAR) microscopy.<sup>180–182</sup> The principle of PULSAR is as follows: the sample is first irradiated with red light so as to set all the photoswitches to the dark state (closed-ring isomer), and to photobleach all adventitious (non-photoswitchable) fluorophores absorbing in that region. In each imaging cycle, a brief UV pulse ( $\lambda = 375$  nm) is used to “turn on” a small fraction of MC emitters, which are then imaged (with  $\lambda_{\text{excitation}} = 561$  nm<sup>182</sup>) until photobleaching/back-isomerisation takes place. Assuming that the distances between the active emitters are greater than the Abbe diffraction limit, each of them can be localised with nanometer precision by fitting the summed intensity data to a Gaussian mask. The process is then repeated over many cycles until the entire population of the fluorophores is photobleached. An overall image is reconstructed from the positions of individual MC molecules recorded during each cycle. The resolution of PULSAR is determined by the number of photons a single MC can emit before it photobleaches. This number is as large as  $1.8 \times 10^5$ , giving rise to imaging resolution down to 10 nm.<sup>180</sup>

Imaging capabilities of PULSAR microscopy are demonstrated in Fig. 5. Fig. 5B shows a single (left), two (center), and four (right) 70 nm spirobifluorene-polymer NPs arranged in a row. PULSAR clearly resolves individual 70 nm NPs<sup>180,181</sup> whereas conventional fluorescence microscopy (Fig. 5A) is unable to do so. Furthermore, the possibility to chemically functionalise the surfaces of these NPs<sup>115</sup> can turn them into



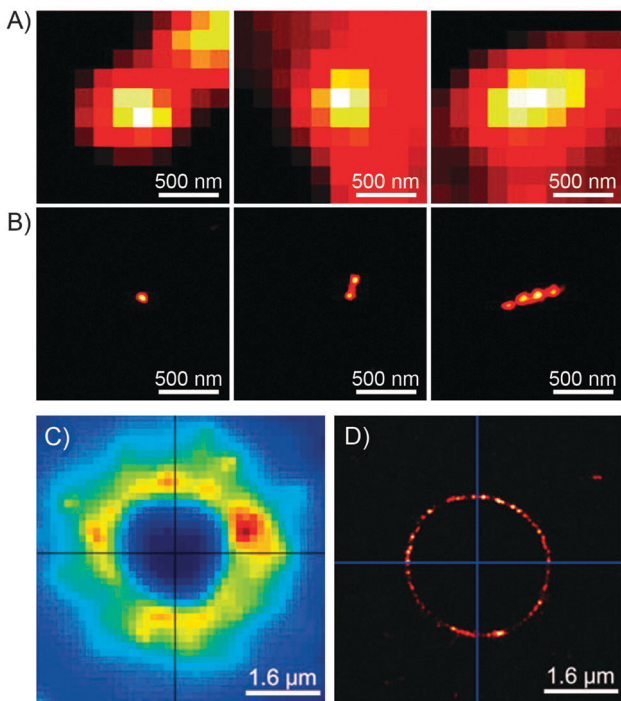


Fig. 5 Imaging power of the PULSAR microscopy. (A) Reversibly fluorescent NPs, 70 nm in diameter, imaged using conventional fluorescence microscopy. (B) Reconstructions of the same NPs obtained using PULSAR. Resolution improves by a factor of  $\sim 25$ . (C and D) Reversibly fluorescent NPs as markers for  $\text{CaCl}_2$  crystals – images obtained using conventional fluorescence microscopy (C) and PULSAR (D). [Adapted with permission from ref. 180 (Copyright 2008 American Chemical Society) (A and B) and ref. 182 (Copyright 2011 Royal Society of Chemistry) (C and D).]

valuable imaging markers. For example, NPs with polyacrylic acid-rich shells exhibited affinity to  $\text{CaCl}_2$  microcrystals and could be used to acquire high-resolution images thereof: the PULSAR image shown in Fig. 5D clearly shows a monolayer of NPs decorating a round crystal of  $\text{CaCl}_2$  (as compared to the diffraction-limited image of the same crystal in Fig. 5C).<sup>182</sup>

The combination of high resolution with the possibility to activate fluorescence “on demand” makes PULSAR microscopy of particular interest for imaging biological systems, where false positive signals due to cell autofluorescence are a ubiquitous problem. This background fluorescence, being non-photo-switchable, can easily be extracted from the signals due to the MC probe. Importantly, UV-induced cytotoxicity is not an inevitability since the SP–MC isomerisation can be induced not only by UV, but also by NIR light as discussed in Section 1.1. The excitation wavelength of  $\sim 780$  nm lies within the so-called NIR window, where both the absorption and scattering of biological tissues are minimal. Moreover, irradiation with an NIR laser enables not only the isomerisation, but also two-photon fluorescence of MC, thereby overcoming the problem of back-isomerisation of MC typically accompanying single-photon fluorescence.

A desirable feature of fluorescent probes – in the context of biological imaging – is the ability to reversibly switch between two different colours of emitted light (as opposed to a dark-bright

transition). Although the parent SP (**1** in Fig. 1A) is non-fluorescent, Li *et al.* have recently engineered dual-colour fluorescence in a series of spiroxans by functionalising the photoswitch with electron-donating or -withdrawing substituents.<sup>183,184</sup> For example, the MC form of a 5-cyano-substituted switch emitted red fluorescence, whereas the SP form was blue-fluorescent. The authors also prepared polymer NPs incorporating these novel spiroxans and demonstrated the ability to unambiguously stain intracellular objects by taking advantage of the reversible, two-colour fluorescence.<sup>183</sup>

Switching between two different wavelengths of emitted light can also be realised by using fluorescence resonance energy transfer (FRET). The advantage of this approach over dual-emitting dyes (previous paragraph) is that it offers more flexibility in terms of optical output. Recall that FRET efficiency is governed by the extent of overlap between the fluorophore emission band and the MC excitation band – *cf.* Fig. 3C<sup>159</sup> – as well as by the average distance between the two moieties;<sup>185</sup> both of these parameters are readily controllable within spiroxan-polymer NPs. One such example is shown in Fig. 4, middle panel (“2nd generation” switchable NPs), whereby spiroxan has been co-polymerised with a perylene diimide dye to form spherical,  $\sim 50$  nm polymer NPs.<sup>186</sup> In the closed form of the switch, these NPs emit green fluorescence due to the PDI units. An SP-to-MC photoisomerisation, however, activates a PDI-to-MC FRET, and the resulting NPs emit red light. A related example of emission control is shown in Fig. 3D,<sup>159</sup> whereby a fluorescent nitrobenzoxadiazole (NBD)-based dye within spiroxan-polymer NPs emitted green fluorescence while SP was in its closed form.<sup>67,187,188</sup> UV-triggered ring-opening induced FRET to the MC form resulting in red emission. Other fluorophores attached to/incorporated in spiroxan polymers include polythiophene<sup>189,190</sup> (Fig. 3E and F), poly(fluorenyl-*co*-benzothiadiazole) (PFBT),<sup>116</sup> boron-dipyrrromethene (BODIPY),<sup>191</sup> diphenylanthracene,<sup>192</sup> naphthalimide,<sup>193,194</sup> and even the green fluorescent protein (GFP).<sup>42,195</sup> In all of these examples, photo-switchable dual-colour emission was achieved.

More recently, approaches have emerged for the development of spiroxan-polymer NPs whose fluorescence can be controlled by *multiple* orthogonal stimuli (“3rd generation” NPs in Fig. 4). Thermoresponsive polymers, such as PNIPAM, can be used to introduce temperature responsiveness. PNIPAM is readily hydrated and highly water-soluble at room temperature. Upon warming of an aqueous solution, it undergoes volume phase transition and precipitates at the temperature ( $T = 32$  °C) which corresponds to its lower critical solution temperature (LCST) (“cloud point”),<sup>196,197</sup> as a result of entropically driven dehydration.<sup>198</sup> Liu and co-workers reported block copolymers comprising (i) PNIPAM copolymerised with an NBD acrylate-based fluorescence donor, and (ii) an MC methacrylate-based acceptor.<sup>164</sup> The block copolymers were supported on silica particles, resulting in overall core@shell@shell morphology. These particles could emit light of *three* different colours, depending on the external conditions: (1) under visible light irradiation, the spiroxan was in the SP (“off”) form and the colour of emitted light was green (and not affected by



temperature). (2) Under UV irradiation at  $T = 20$  °C (below the LCST), the solution appeared orange due to the large average distance between the FRET donors (NBD) and acceptors (MC), causing FRET to occur with moderate efficiency. (3) Under UV irradiation at  $T = 35$  °C, the solution appeared red as a result of PNIPAM collapsing, decreasing the average distance between the NBD and the MC groups, and enhancing FRET efficiency.<sup>164</sup> An even more sophisticated system is shown in Fig. 4, bottom panel. In addition to being photo- and thermoresponsive, this block copolymer (poly(St-*co*-NBD-*co*-SP)-*b*-poly(NIPAM-*co*-Rh), where St = styrene and Rh = rhodamine), incorporates rhodamine, whose fluorescence can be modulated by pH. The resulting NPs can exist in as many as eight different states, which can be toggled between each other by exposure to three orthogonal stimuli.<sup>161</sup>

## 2.2. Photocontrol of polymer solubility

The large difference in polarity between SP and MC can be exploited to construct systems in which aggregation is induced by light. Different studies demonstrating such photoinduced changes propose three alternative explanations for the behaviour. First, preferential *intramolecular* ‘‘solvation’’ of the MC isomer by the polymer backbone was suggested to play a role, as postulated by Irie *et al.*, who observed that UV irradiation of benzene solutions of a spirobifluorene-decorated PMMA resulted in decreased viscosities. This effect was attributed to intramolecular stabilisation of MC by the PMMA’s ester moieties.<sup>44,199</sup> The same rationale was used to explain the UV-induced decrease in the viscosity of SP-decorated poly(methacrylic acid) in methanol.<sup>200</sup> Evidence supporting this scenario was provided by studies of copolymers with different contents of spirobifluorene: in all cases, the photoinduced effect was most pronounced for copolymers containing relatively *low* (e.g., ~10%<sup>200</sup> or ~18%<sup>44</sup>) molar percentage of the switch.

In contrast, other experiments showed a linear dependence of the viscosity change on the spirobifluorene content, and suggested that direct interactions between the chromophore units are involved.<sup>201</sup> Depending on the solvent, these attractive interactions could take place between SP units, resulting in visible light-induced viscosity decrease (e.g. in DMSO)<sup>39</sup>/precipitation (in water; Fig. 6A<sup>202</sup>), or, more commonly, between the MC units,<sup>99,203–205</sup> giving rise to UV-induced aggregation (e.g. in dioxane; Fig. 6B<sup>206,207</sup>). The contribution of direct MC–MC interactions is also corroborated by MC fluorescence quenching which accompanies polymer aggregation.<sup>208</sup>

Finally, the third plausible explanation is based on the photo-induced loss of the solvation layer. Spirobifluorene-functionalised polystyrene precipitated from a cyclohexane solution when irradiated with UV light.<sup>117</sup> Comparison with a small-molecule analogue supported the negligible role of direct MC–MC interactions. This monomer, when exposed to UV, aggregated by means of MC–MC interactions, which stabilised the resulting aggregates and consequently inhibited redissolution by visible light. In contrast, the aggregated MC-polymer could be redissolved easily, thereby suggesting that direct MC–MC interactions play only a negligible role.<sup>117</sup> Overall, the light-induced aggregation

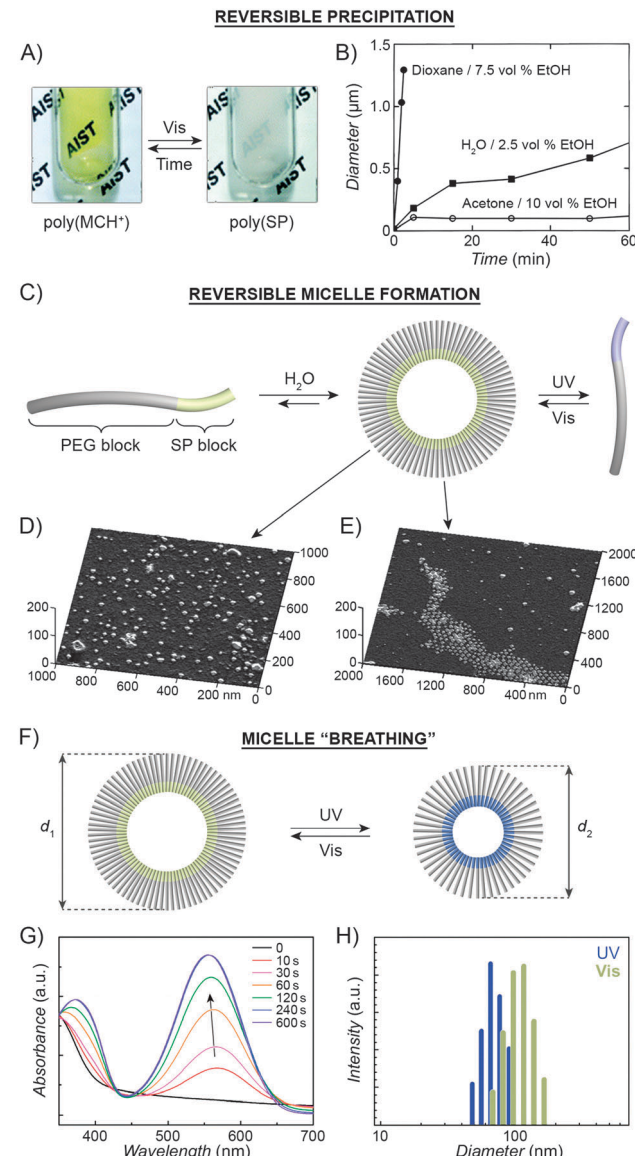


Fig. 6 Light-controlled aggregation of spirobifluorene-functionalised polymers. (A and B) Depending on the solvent, aggregation can be induced by either the SP (A) or the MC (B) state. (C) Schematic representation of light-induced micelle formation. (D) AFM image of micelles formed by self-assembly of a block copolymer containing a PEG block and an SP-functionalised block. (E) AFM image of micelles formed by exposure of the sample in (D) to UV light (disassembles the micelles) followed by Vis light (micelles re-form). (F) Schematic representation of reversible size change in micelles self-assembled from a block copolymer containing a PEG block and a (PMMA-*co*-SP) block. (G) Changes in the UV-Vis spectra of SP-rich micelles (left in (F)) exposed to UV. (H) Micelle size distribution as a function of light wavelength. [Adapted with permission from ref. 202 (Copyright 2006 Royal Society of Chemistry) (A), ref. 206 (Copyright 1997 American Chemical Society) (B), ref. 160 (Copyright 2007 Wiley-VCH) (D and E) and ref. 218 (Copyright 2010 Chemical Society of Japan) (G and H).]

behaviour is highly system-dependent and can likely be explained by a combination of the above mechanisms.

UV-Vis spectroscopy provides a convenient way to monitor interactions between the MC moieties as UV-irradiated polymers aggregate. Fig. 7A shows a series of absorption spectra of a



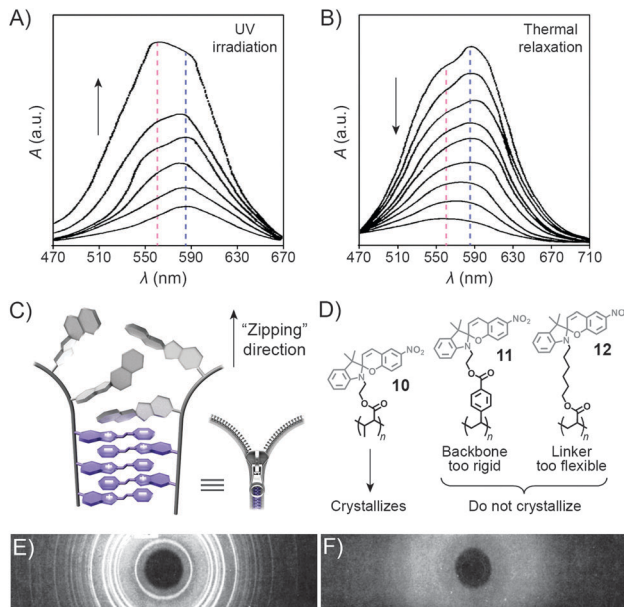


Fig. 7 Spectroscopic and structural evidence for MC stack formation. (A) SP  $\rightarrow$  MC isomerisation accompanied by MC aggregation during UV irradiation of a spirobifluorene-functionalised polymer **10**. (B) Thermal relaxation of the sample obtained in (A). (C) Schematic representation of “zipper crystallisation”. (D) Structural formulas of spirobifluorene-functionalised polymers **10–12** differing in their crystallisation behaviour. (E) X-ray powder diffraction pattern of **10**. (F) X-ray powder diffraction pattern of **11**. [Adapted with permission from ref. 100 (Copyright 1984 American Chemical Society) (A and B) and ref. 107 (Copyright 1984 American Chemical Society) (E and F).]

spiropyran-functionalised methacrylate in toluene upon increasing exposure to UV light. The initially observed band centered at  $\sim 585$  nm, attributed to individual MC units, develops a shoulder at  $\sim 560$  nm, which is attributed to MC stacks (H-aggregation).<sup>100</sup> Subsequent relaxation spectra clearly show that MC within these stacks re-isomerises considerably slower than the non-stacked MCs, such that after sufficiently long relaxation times, only the peak at  $\sim 560$  nm can be observed (Fig. 7B).

The controlled formation of such MC stacks governs a fascinating process first reported by Krongauz *et al.* which involves spontaneous ring-opening of SPs residing on polymer chains.<sup>209</sup> Slow solvent evaporation from 2-methyltetrahydrofuran (MTHF) solutions of poly(MMA-SP) (**10** in Fig. 7D) was found to result in red, *crystalline* (Fig. 7E) solids. In sharp contrast, *fast* evaporation of MTHF from the same solution yielded a white, amorphous precipitate. The red colour suggested that crystallisation entailed the SP  $\rightarrow$  MC isomerisation – indeed, UV-Vis spectra of the crystals showed only one band centered at  $\lambda \approx 560$  nm, attributed to stacked MCs. Equally impressive was the stability of MC within the resulting crystals: it did not back-isomerise even upon heating to  $150$  °C (at which point the polymer decomposes) – in contrast to MC within amorphous aggregates obtained from the same polymers, which faded within a few seconds at  $T \approx 50$  °C.<sup>107</sup> Surprisingly, such controlled crystallisation is *interrupted* by UV light – a stimulus usually used to induce SP  $\rightarrow$  MC isomerisation – in fact, crystalline solids could only be obtained in the dark. The

crystallisation process is thought to involve stepwise isomerisation along the polymer chain as the crystal forms – in other words, crystallisation and isomerisation mutually stimulate each other. The process can therefore be thought of as a molecular scale analog of closing a zipper and hence has aptly been called “zipper crystallisation”<sup>210</sup> (Fig. 7C). It is important that the polymer chain has certain degree of flexibility – when the SP units were located on a more rigid polystyrene chain, no crystalline order in the resulting material was observed (**11** in Fig. 7D and F).<sup>107</sup> On the other hand, the spirobifluorene groups cannot have *too* much conformational freedom: no crystals were observed in the case when spirobifluorene was attached to the polymer backbone through a long and flexible alkyl chain linker (**12** in Fig. 7D).

Advances in controlled polymerisation methods have enabled selective placement of the photoswitchable units at desired fragments of the polymer chains.<sup>211–214</sup> The resulting block copolymers can have a tendency to spontaneously assemble into micelles or vesicles, such as in the process called “polymerisation-induced self-assembly and reorganisation”.<sup>218</sup> Matyjaszewski and co-workers used ATRP to prepare block copolymers containing a long poly(ethylene glycol) (PEG) block appended with a short spirobifluorene-based block.<sup>160</sup> The hydrophobic nature of SP induced the formation of micelles in aqueous solutions (Fig. 6C and D). When UV-irradiated, the micelles disassembled. Subsequent exposure to visible light restored the SP isomer and regenerated the original micelles, as shown in Fig. 6E. The same concept was demonstrated using block copolymers comprising (i) a PEG block and a spirobifluorene-decorated poly-L-glutamic acid block,<sup>215</sup> as well as (ii) a spirobifluorene-appended PMMA block and a polysaccharide block.<sup>216</sup> Interestingly, however, opposite behaviour was observed in the case of block copolymers bearing precisely one spirobifluorene unit at the terminal position of the polymer chain<sup>173</sup> – in this case, UV-irradiation of well-solvated, PEG-rich polymers induced micellisation resulting from attractive MC–MC interactions.

*Dual-responsiveness* within spirobifluorene-incorporating block copolymers was encoded by substituting the PEG segment with a thermoresponsive block. Ji *et al.* reported a system based on a PDEGMMA-*b*-poly(SP) copolymer (where PDEGMMA = thermo-responsive poly(2-(2-methoxyethoxy)ethyl methacrylate)), which could exist in three different states – single molecules, micelles, and reverse micelles, depending on the environmental conditions.<sup>217</sup>

Finally, increasing the hydrophobic character of the spirobifluorene-incorporating block can stabilise the micellar structure such that no disassembly takes place even upon SP  $\rightarrow$  MC isomerisation. The resulting MC-rich blocks, instead of being solvated by water molecules, pack more compactly due to strong MC–MC interactions, and the average micelle size decreases. This process is reversible, giving rise to oscillations of the micelle diameters between  $\sim 110$  nm and  $\sim 90$  nm (“micelle breathing”; Fig. 6F and H).<sup>218</sup>

### 2.3. Photocontrol of volume phase transitions in thermoresponsive polymers

An interesting case of light-induced aggregation of polymers is the behaviour of thermoresponsive polymers incorporating spirobifluorene, and is best exemplified by PNIPAM-based copolymers.



In Section 2.1, we saw how thermally induced collapse of the PNIPAM chains decreased the distance between fluorescence acceptors (MC) and donors, thereby modulating FRET efficiency. The temperature at which this phase transition occurs – the LCST – can be increased or reduced by the incorporation of hydrophilic and hydrophobic groups, respectively, in the polymer backbone.<sup>219</sup> Being able to transform reversibly between a hydrophobic and a hydrophilic isomer, the spiropyran switch offers the possibility to prepare PNIPAM-based copolymers with solubilities controlled not only by temperature, but also by light. For a given poly(NIPAM-X) copolymer, a range of temperatures exist where the polymers are water-soluble when X = the hydrophilic MC, but readily precipitate when X = the hydrophobic SP.<sup>220</sup>

This behaviour is illustrated in Fig. 8 in an acidic (pH 4) solution of the copolymer. Under these conditions, the open form of the switch is protonated and the system exhibits negative photochromism, with the SP ring spontaneously opening in the dark. As shown in Fig. 8B, LCST of the thermally equilibrated,  $\text{MCH}^+$ -rich polymer is relatively high ( $T_{\text{MC}} \approx 35^\circ\text{C}$ ), whereas the closed-ring isomer reduces the LCST to  $T_{\text{SP}} \approx 30^\circ\text{C}$ .

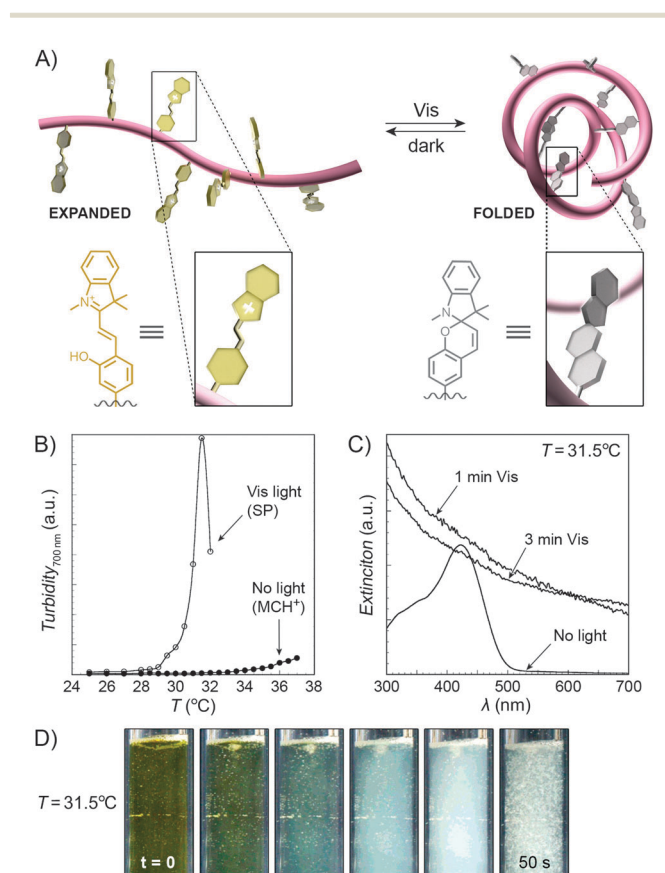


Fig. 8 Light-controlled aggregation of thermoresponsive polymers. (A) Schematic representation of the process. Conversion of the hydrophilic  $\text{MCH}^+$  to the hydrophobic SP induces dehydration of the polymer chain, which initiates the phase transition. (B) Thermally induced precipitation of SP- and MC-rich PNIPAM. (C) Photoinduced precipitation of spiropyran-functionalised PNIPAM taking place at a temperature  $T$  such that  $\text{LCST}_{\text{poly(NIPAM-MC)}} < T < \text{LCST}_{\text{poly(NIPAM-SP)}}$ . (D) Visible light-induced precipitation of poly(NIPAM-MC) from an aqueous solution. [Adapted with permission from ref. 73 (Copyright 2004 American Chemical Society) (B-D).]

As a consequence, the initially yellow (due to  $\text{MCH}^+$ ), transparent solution exposed to visible light in the temperature range  $T_{\text{MC}} < T < T_{\text{SP}}$  turns colourless and opaque in less than a minute (Fig. 8C and D). The fact that the effect can be observed with remarkably small amounts of the chromophore units – the copolymer in Fig. 8 had only 1 mol% of SP and the solution concentration was 0.1 wt% – led the authors to hypothesise<sup>73,221</sup> that the SP ring closing and the polymer dehydration could possibly accelerate each other. Another interesting aspect of the process is proton release accompanying the volume phase transition:  $(\text{MCH}^+)_n \xrightleftharpoons{\text{Vis}} (\text{SP})_n + n\text{H}^+$ . Indeed, a ten-fold increase in the  $\text{H}^+$  concentration was observed<sup>221</sup> upon visible light irradiation, suggesting that these polymers can be used for light-controlled proton delivery.

Despite the fact that the volume phase transition of the poly(NIPAM-SP) copolymers takes place abruptly at a well-defined temperature (LCST), continuous dehydration of the polymer<sup>222</sup> backbone can be observed well below the LCST

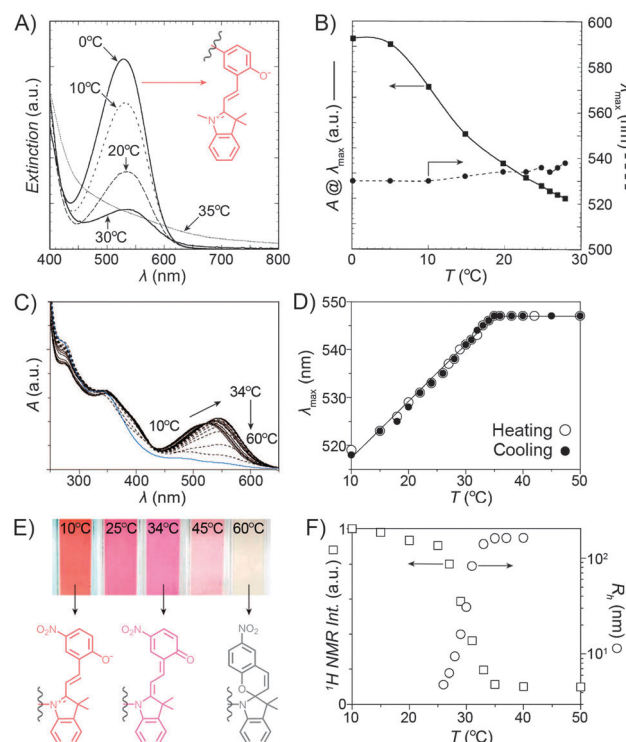


Fig. 9 Spiropyran as a probe for microenvironment polarity. (A) Thermally induced MC  $\rightarrow$  SP transition ( $0$ – $30^\circ\text{C}$ ) precedes precipitation of poly(NIPAM-SP) ( $35^\circ\text{C}$ ). (B) Changes in maximum absorbance values and wavelength absorption maxima at temperatures below the volume phase transition. (C) Optical response of a poly(NIPAM-SP) polymer pre-irradiated with UV as it is gradually heated from  $T = 10^\circ\text{C}$  to  $T = 60^\circ\text{C}$ . (D) Temperature-dependent changes in wavelength absorption maxima of the same copolymer. (E) Colour changes accompanying a gradual zwitterion  $\rightarrow$  quinoid conversion (observed spectrophotometrically in (C)). (F) Precipitous drop of the integrated intensity of the NIPAM's CH proton resonances (left) coincides with the rapid increase of the hydrodynamic radius (right). [Adapted with permission from ref. 223 (Copyright 2004 American Chemical Society) (A and B) and ref. 224 (Copyright 2009 American Chemical Society) (C–F).]

using the SP-MC pair as a probe.<sup>223,224</sup> Fig. 9A shows the dependence of MC absorbance on temperature: absorption decreases in a roughly linear fashion starting at  $T \approx 5$  °C, although precipitation does not take place until  $T \approx 35$  °C. It is important to note that this decrease in MC absorption accompanying a gradual MC  $\rightarrow$  SP ring closing is indeed due to an increasingly non-polar environment, and not a result of thermal isomerisation as evidenced by control experiments on monomeric spiropyran showing that temperature rise led to an *increase* in MC absorption (due to negative photochromism).<sup>223</sup> Additionally, a slight red-shift of the MC band can also be seen with increasing temperature. This can be attributed to an increasing contribution of the quinoidal resonance form of MC at the expense of its zwitterionic form (see Section 1.1) – yet another indication of dehydration. This latter effect is more pronounced in a related system based on PNIPAM incorporating a nitrospiropyran, as shown in Fig. 9C–F.<sup>224</sup> The dependence of  $\lambda_{\text{max}}$  on  $T$  is nearly linear over a broad range of temperatures (10–34 °C) and wavelengths (519–547 nm), indicating that this system can serve as a colorimetric thermometer within this temperature window. The large difference in  $\lambda_{\text{max}}$  values suggests significant contributions of the zwitterionic and quinoidal resonance forms at the low and high temperatures, respectively.

In order to develop robust PNIPAM-based photoresponsive materials and ultimately functional devices, use of crosslinked polymers, as opposed to linear polymer chains, becomes necessary. Crosslinking is typically achieved with *N,N'*-methylenebisacrylamide<sup>225–227</sup> and leads to hydrogels whose hydration (expansion) and dehydration (shrinkage) can be achieved upon exposure to UV and visible light, respectively. In an exemplary demonstration of the phenomenon, thin films of crosslinked gels exhibiting negative photochromism were exposed to blue light through a mask, causing volume phase transition and shrinkage in the irradiated regions. Irradiation times as short as 3 s were sufficient to decrease film thickness by  $\sim 30\%$ .<sup>227</sup> Moreover, multilevel patterns could be created by irradiating different areas of the same film for different amounts of time. MCH<sup>+</sup>-SP isomerisation in the irradiated areas was confirmed by preferential adsorption of negatively charged latex particles onto non-irradiated (carrying more positive charges) areas. Similar reversible shrinkage–swelling behaviour was reported for poly(NIPAM-SP) gels in the form of colloidal particles. Upon consecutive cycles of visible light irradiation and thermal equilibration in the dark, these particles performed “breathing” motion, with their hydrodynamic diameters oscillating between  $\sim 200$  nm and  $\sim 160$  nm.<sup>226</sup>

Optical control of the thermal threshold for volume changes has also been reported for thermoresponsive polymers other than PNIPAM – for example, the LCST of poly(2-(dimethylamino)ethyl methacrylate) (PDMAEMA) containing 1.3 mol% of spiropyran in the form of MC could be shifted from 44 °C to 34 °C upon exposure to visible light.<sup>129</sup> Block copolymers comprising thermoresponsive poly(*N,N*-dimethylacrylamide) (PDMA) and poly(2-(2-methoxyethoxy)ethyl methacrylate) (PDEGMMA) units were also investigated.<sup>228</sup> An intriguing aspect of the latter study is that *two* different photoswitchable

groups – spiropyran and azobenzene – were incorporated into the polymer backbones and their combined effect was studied.

As demonstrated in this section, spiropyran allows for the control of properties characteristic of thermoresponsive polymers (*i.e.* volume phase transition) by means of light, thereby effectively rendering them *photoresponsive*, and paving the way towards the development of a conceptually new family of photoswitchable materials. Structure and property changes which could previously be brought about thermally<sup>229</sup> can now be directed by light – using excellent spatial and temporal control – as well. The ability to shrink and expand crosslinked polymer gels in particular is interesting in the context of controlling transport phenomena (see Section 2.4).

## 2.4. Photocontrol of transport through polymeric systems

Sumaru and co-workers have pioneered the use of crosslinked poly(NIPAM-SP) hydrogels as the key components of light-actuated microvalves.<sup>230–233</sup> As described in the previous section, these gels contain spiropyran in the MCH<sup>+</sup> form, and can be dehydrated upon exposure to blue light, triggering ring closing and PNIPAM chain collapse. An example of the process is shown in Fig. 10A, where the surface area of a circular piece of gel irradiated with blue light decreases by a factor of two. The switchable

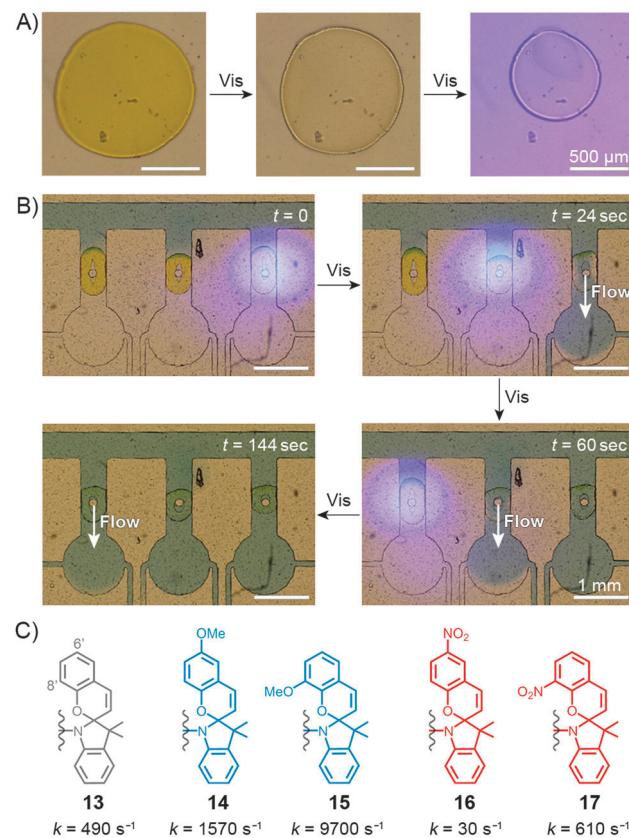


Fig. 10 Spiropyran-based microvalves. (A) Contraction of a poly(NIPAM-SP) gel induced by blue light. (B) Remote control of liquid flow by consecutive opening of poly(NIPAM-SP)-based microvalves using blue light. (C) Controlling the rate of SP ring closure by the substitution pattern on the chromene moiety. [Adapted with permission from ref. 231 (Copyright 2007 Elsevier) (A and B).]



polymers can conveniently be deposited in a region of interest – *e.g.*, thin channels of PDMS-based microfluidic devices – by UV-induced *in situ* free-radical polymerisation of a mixture containing NIPAM, a spiropyran monomer, a crosslinker, and an initiator. Fig. 10B shows how three valves, separated by less than 2 mm from each other, can be opened independently by local irradiation with low-intensity (20 mW cm<sup>-2</sup>) blue light for less than 30 seconds. Although these valves could be opened by gentle heating as well, only the use of light allowed each valve to be addressed individually. Other original approaches to induce flow by means of light have been developed,<sup>234</sup> for example one in which channels are created in a single step in thin, flat sheets of poly(NIPAM–SP) gels by exposing them to blue light through a mask in the shape on the channel.<sup>232</sup>

In all of the above systems based on the unsubstituted (13 in Fig. 10C) spiropyran, reversibility is an issue: although blue light-induced ring closure (and so the valve opening) is fast, it takes more than one hour for the SP rings to reopen, for the gels to swell, and for the valves to close. To tackle this problem, Sumaru *et al.* investigated the effect of substituents on the kinetics of spontaneous ring opening.<sup>235</sup> Ring opening events occurring in polar solvents involve a transition state with a partial negative charge on the pyran oxygen atom – therefore, the electron-donating methoxy substituent was placed at the 6' position of the benzopyran moiety (14 in Fig. 10C) with the assumption that it would reduce the activation free energy of the reaction. Indeed, the ring-opening rate increased by a factor of three; conversely, installing an electron-withdrawing nitro group at the same position (16 in Fig. 10C) reduced the rate nearly 15 times. In addition, *any* type of substituent placed at the 8' position led to a higher reaction rate – these two effects combined led to a 20-fold increase of the reaction rate in the case of an 8'-OMe derivative (15 in Fig. 10C), as compared to its unsubstituted counterpart.<sup>235</sup> Therefore gels prepared from poly(NIPAM–SP–8'-OMe) exhibited excellent reversible swelling performance, with *both* the light-induced shrinking and spontaneous re-swelling to the original state completed within several minutes.

In the examples discussed above, spiropyran switching caused changes in hydration and the degree of swelling of a thermoresponsive polymer. Several photoinduced flow systems have also been developed which exploit different affinities of the switch to the solvent/solute molecules.<sup>236–240</sup> In one prominent example,<sup>238</sup> a molecularly imprinted polymer designed to bind tryptophan was prepared by polymerising a mixture of terminal alkenes containing a spiropyran derivative. The procedure was carried out under UV irradiation, which likely resulted in the formation of “binding sites” for the zwitterionic tryptophan in the proximity of the MC residues. Following polymerisation and extraction of the amino acid, the resulting materials were used as dialysis membranes. Permeability of tryptophan indeed depended on the state of the switch, with the diffusion through the MC-rich membrane faster by well over one order of magnitude.<sup>238</sup> Control experiments revealed that the membranes were tryptophan-specific – other molecules diffused slowly and with rates independent of the conformation of spiropyran – and also

confirmed the importance of the binding sites: a spiropyran polymer prepared in the absence of the template showed similar (and very low) permeability for tryptophan under both UV and visible light irradiation. This strategy was used to successfully develop a photoswitchable catalysis system, which comprised a spiropyran-functionalised polyacrylamide immobilising the enzyme  $\alpha$ -chymotrypsin;<sup>241</sup> while the diffusion of an amino acid-based substrate – and its access to the enzyme – was suppressed in SP-rich polymers, the system could be activated by UV light: under these conditions, the substrate readily diffused – and was converted into the product – through MC-rich copolymers. In another interesting example, commercial polyethersulfone (PES) ultrafiltration membranes were rendered photoresponsive by a grafting-from polymerisation process.<sup>242</sup> As expected, the hydrophobic SP isomer encouraged non-specific absorption of proteins, which, in turn, translated into lower flow rate of the buffer solution.

Finally, transport properties can be controlled through physical changes to the overall polymer structure.<sup>82,144</sup> For example, PTFE membranes coated with a poly(acrylamide-spiropyran) copolymer exhibited enhanced permeability towards water–methanol mixtures when irradiated with UV light – a property which could be correlated with UV-induced solution precipitation of this copolymer dissolved in the same mixture of solvents.<sup>140</sup> This “surface precipitation” behaviour was also utilised to control flow through glass filters functionalised with a similar copolymer.<sup>163,243</sup>

In addition to the systems presented here, light-controlled transport has been demonstrated using various biopolymers and nanoporous inorganic materials derivatised with spiropyran – these examples are covered in Sections 3.3, 3.7, and 5.2.

## 2.5. Photocontrol of polymers' mechanical properties (and mechanical control of polymers' optical properties)

Copolymers discussed in this section contain spiropyran as part of their polymer backbones. When the backbone is attached to the two different (that is, indoline and chromene) rings of the switch, the isomerisation process (which is associated with large structural changes of the spiropyran moiety) is expected to affect the overall structure of the polymer chains, and therefore the macroscopic properties of the polymer. Copolymers of this type were first prepared and studied by Smets *et al.*, who observed ~2% contraction in thin films of rubbery (glass transition temperature,  $T_g \approx -15$  °C) polyesters containing up to 1 mol% of the spiropyran units.<sup>165,244</sup> Upon storage in the dark, slow chain length recovery occurred and the process could be repeated multiple times.<sup>245</sup> The shrinking was thought to be entropically driven, with the planar MC moieties increasing both the mobility of the polymer chains and their ability to pack more efficiently.

Three decades later, a multidisciplinary team at UIUC considered the opposite – that is, the possibility to *induce* SP ring opening by applying mechanical force to polymer chains incorporating the chromophores in their backbones.<sup>167,169,170,246–249</sup> A hint that this type of behaviour would be possible was provided by earlier studies which showed<sup>80</sup> that small-molecule spiropyran

underwent ring-opening upon grinding, thereby demonstrating the unique feature of the switch of being a *mechanophore* (undergoes chemical transformation in response to a mechanical stimulus) that is additionally *mechanochromic* (exhibits colour change upon the application of mechanical force). To investigate the effect of mechanical force on the isomerisation of SP, the team first prepared a linear poly(methyl acrylate) (PMA; molecular weight,  $M_w \approx 170$  kDa) having precisely one SP unit near the center of the chain (at the position of greatest stress under chain elongation; Fig. 11).<sup>169</sup> The choice of the 5 and 8' positions as the attachment points was suggested by DFT calculations which predicted<sup>246</sup> that increasing the distance between these two points transmits the force efficiently to the C–O bond and leads to its rupture. Indeed, when an acetonitrile solution of the polymer was subjected to sonication, the colour of the solution changed from colourless to red, indicating the SP  $\rightarrow$  MC reaction (Fig. 11A). The process was reversible in that the solution turned transparent upon exposure to visible light. No such effects were observed for PMA

end-terminated<sup>171</sup> with SP, indicating that the isomerisation was indeed induced by stress, and not, for example, by temperature change.

The spiropyran mechanophore could also be incorporated into chains of bulk polymers.<sup>246</sup> Fig. 11B shows dogbone-shaped samples of elastomeric PMA prepared by SET-LRP using the bifunctional spiropyran **18** (Fig. 11C) as an initiator. When the samples were subjected to tensile loading, red colour – an indication of mechanochemical ring opening – emerged, and its intensity increased with increasing levels of strain. Samples moulded from control polymers – one lacking the polymer chain on the indole ring of spiropyran (prepared from **19** in Fig. 11C), the other one having both polymer chains attached to the same side of the spiro junction (prepared from **20** in Fig. 11C) – did not show any colour changes upon stretching, since neither presumably resulted in a significant force being transmitted to the sensitive C–O bond.

Similar behaviour was observed for SP-containing glassy PMMA prepared in the form of 100–500  $\mu\text{m}$  spheres (Fig. 11D).<sup>246</sup> Upon compression, an intense purple colour emerged as a result of tensile stress in the direction perpendicular to the loading direction, with the maximum tensile stress in the center of the bead. Importantly, intense colours, in all cases discussed here, appeared well before the samples failed at high strain levels, suggesting possible uses of these materials for detection and mapping of mechanical stress (in, *e.g.*, climbing ropes or bridges) prior to catastrophic failure.<sup>166,246</sup>

## 2.6. Photocontrol of metal ion complexation

In contrast to the SP isomer, the MC form has a tendency to bind different metal ions (in an MC:  $M^{n+}$  2:1 stoichiometry), with the interaction taking place through the MC's phenolate oxygen.<sup>250,251</sup> Although the binding strength of the individual MC moieties to metal ions is usually rather weak, the stability of the complex can be increased by pre-organising two or more MC groups – for example, on a polymer backbone (Fig. 12A). Despite the higher complexation constants, MC in such complexes can still be converted to SP upon exposure to visible light, thereby resulting in the expulsion of the metal ions. This behaviour is exemplified by a spiropyran-decorated PNIPAM as it interacts with  $\text{Pb}^{2+}$  ions.<sup>252</sup> As shown in Fig. 12B, the UV-Vis spectrum of this polymer shows an intense MC band at  $\lambda_{\text{max}} \approx 540$  nm due to negative photochromism. Addition of metal ions (in this case  $\text{Pb}^{2+}$ ) leads to the appearance of a new peak at  $\lambda_{\text{max}} \approx 430$  nm, attributed to an MC–metal ion complex.<sup>253,254</sup> This example is of further interest since combining the metal ion binding properties of the polymer with its thermoresponsive nature allows for quantitative removal of  $\text{Pb}^{2+}$  from water. This goal was achieved by (i) spontaneous binding of the metal ions by MC, and (ii) subsequent gentle heating above the LCST.<sup>252</sup> Irradiation of the resulting precipitate with visible light led to an  $\sim 50\%$  release of the  $\text{Pb}^{2+}$  ions from the solid state.<sup>252,255</sup> It is important to emphasise that the mild binding strength of MC to metal ions is essential for the photoswitchable binding and release: if the interaction energy was too weak, neither isomer of the switch would bind metal ions; if it was too strong, the binding (and ring-opening reaction) would be irreversible.<sup>124</sup>

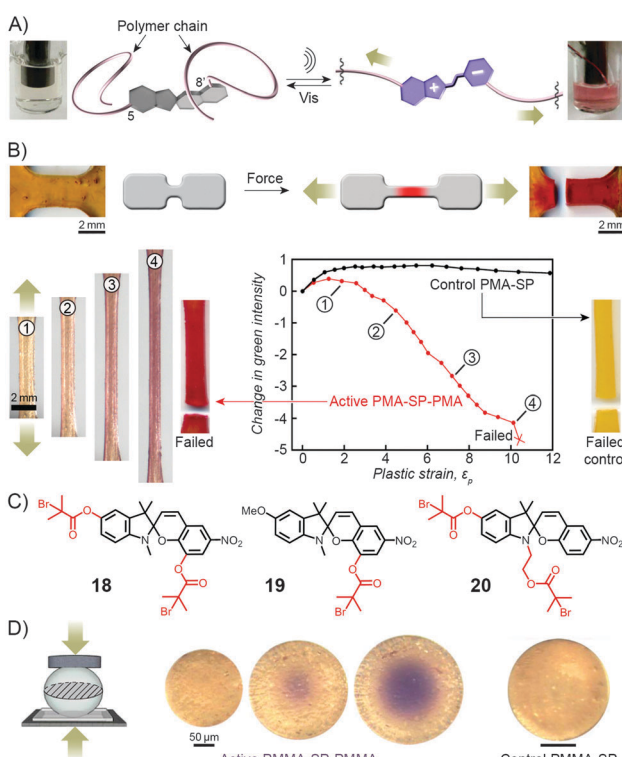
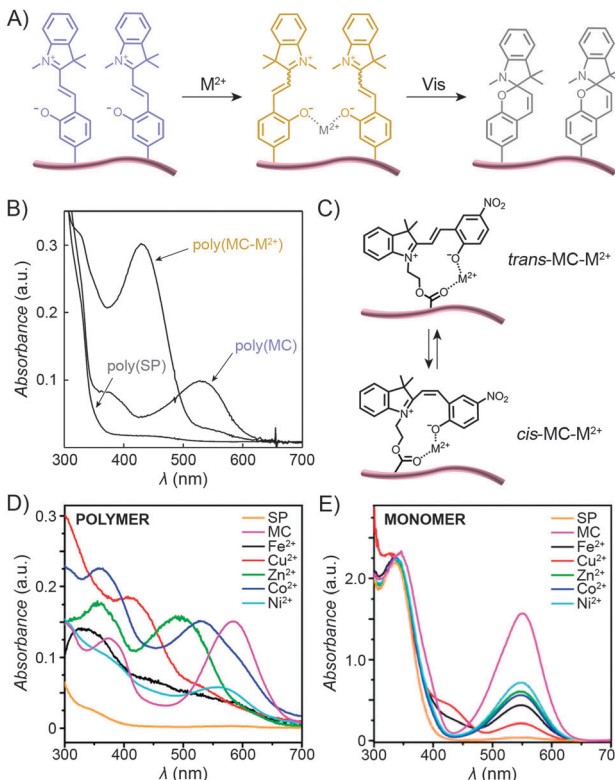


Fig. 11 Spiropyran as a mechanophore. (A) Effect of sonication on the colour of the solution of a spiropyran whose chromene and indoline moieties are functionalised with PMA chains (PMA-SP-PMA; prepared using precursor **18** in (C)). (B) Effect of tensile loading on a dogbone-shaped specimen moulded from a PMA-SP-PMA polymer (bottom left). For comparison, a control sample moulded from a polymer synthesised from a monofunctionalised spiropyran **19** failed without a colour change (bottom right). (C) Structural formulas of precursors of various spiropyran polymers used in the study of mechanoresponsiveness. (D) Colorimetric response of a glassy bead made of PMMA-SP-PMMA to compression (centre). Control bead prepared from a monofunctionalised spiropyran does not change colour upon compression (right). [Adapted with permission from ref. 169 (Copyright 2007 American Chemical Society) (A) and ref. 246 (Copyright 2009 Nature Publishing Group) (B–D).]





**Fig. 12** Light-controlled complexation of metal cations by spiropyran polymers. (A) Metal ions are bound by MC-polymers, and released following Vis-irradiation. (B) Optical spectra corresponding to the three states in (A). (C) Metal ions can be complexed by either *trans*- or *cis*-MC. (D) Optical properties of complexes formed between MC-polymers and metal ions are strongly dependent on the metal ion. (E) In contrast, no such diversity is seen when the same metal ions are complexed by a monomeric MC. [Adapted with permission from ref. 252 (Copyright 2004 Royal Society of Chemistry) (B) and ref. 258 (Copyright 2010 Royal Society of Chemistry) (D and E).]

The polymer backbone itself can also be modulated to enable selective detection of a specific metal ion – for example copolymers rich in sulfobetaine moieties give rise to an environment in which the pendant MC groups bind  $\text{Cu}^{2+}$  with high selectivity (over, *e.g.*,  $\text{Zn}^{2+}$ ,  $\text{Ni}^{2+}$ , and  $\text{Co}^{2+}$ ).<sup>256</sup> End-functionalised PMMAs have also been prepared:<sup>172</sup> addition of metal ions to these polymers induced the formation of 2 : 1 complexes thereby enabling selective and reversible dimerisation of polymer chains.<sup>225,257</sup>

If the MC unit is equipped with an additional metal ion-binding group, the resulting bidentate ligand can be used to form complexes of 1 : 1 stoichiometry. Locklin and co-workers prepared a polymer with a unique capability to bind and distinguish multiple divalent metal ions from each other.<sup>258</sup> In this design, MC was connected to a PMMA chain *via* an ester group – the latter serving as an additional coordinative group (Fig. 12C). Fig. 12D shows a collection of UV-Vis spectra of the polymer pre-irradiated with UV light and exposed to different metal ions, including  $\text{Fe}^{2+}$ ,  $\text{Cu}^{2+}$ ,  $\text{Zn}^{2+}$ ,  $\text{Co}^{2+}$  and  $\text{Ni}^{2+}$ . The spectra feature (i) bands centered at  $\lambda_{\text{max}} \approx 500$  nm, which can be assigned to *trans*-MC- $\text{M}^{2+}$ ; the different hypsochromic

shifts are thought to be due to varying degrees of deplanarisation of MC; and (ii) bands centered at  $\lambda_{\text{max}} \approx 400$  nm attributed to *cis*-MC- $\text{M}^{2+}$  complexes. This variety of optical responses can be contrasted to the behaviour of an analogous small-molecule MC, which lacked similar selectivity – for example, UV-Vis spectra of MC-bound  $\text{Zn}^{2+}$ ,  $\text{Co}^{2+}$ , and  $\text{Ni}^{2+}$  were all indistinguishable from each other (Fig. 12E) – thus confirming the critical role of MC immobilisation for inducing selectivity of binding. In a subsequent report, the same group demonstrated the possibility to selectively detect two metal cations simultaneously.<sup>259</sup> Meanwhile, Chan *et al.* reported a creative method to quantitatively detect  $\text{Cu}^{2+}$ , with sensitivities covering essentially the whole spectrum of physiological Cu ion levels.<sup>260</sup> The method is based on the combination of two types of polymer NPs, ~10–30 nm in diameter, both decorated with spiropyrans. Upon excitation, the first of these polymers, poly(2,5-dialkylphenylene-1,4-ethynylene) (PPE), emits blue light, and the other, PFBT, emits green while also quenching the PPE fluorescence (provided the two are in close proximity). As a result, aggregation of the NPs, driven by copper-induced MC dimerisation, can initiate the energy transfer, with an effectiveness – measured as the ratio of the green to the blue emission – proportional to the concentration of  $\text{Cu}^{2+}$ .<sup>260</sup>

In addition to sensing capabilities, metal cation binding to spiropyran polymers has other interesting implications. For instance, light-controlled complexation of  $\text{Zn}^{2+}$  ions resulted in reversible modulation of ionic conductivity.<sup>261</sup> While conductivity changes were small (<10%), a related polymer incorporating both spiropyran and crown ether moieties<sup>262,263</sup> (capable of reversibly binding  $\text{Li}^+$ ) provided light-controlled two-fold modulation of ionic conductivity.<sup>264</sup> The bound metal ions can also be chemically reduced, as shown for  $\text{Pd}^{2+}$  ions complexed by spiropyran polymers in the form of so-called honeycomb films.<sup>265</sup> Exposure of these Pd-rich films to a borohydride solution resulted in the formation of metallic palladium with a morphology reflecting that of the underlying honeycomb films.<sup>142</sup> The complexed  $\text{Pd}^{2+}$  could also serve as a catalyst for electroless plating of silver.<sup>266</sup> Notably, the latter two studies represent new approaches to creating nanostructured metallic surfaces.

## 2.7. Photocontrol of other polymer properties

In addition to binding metal ions, the MC isomer can also interact strongly with amino acids and cyanide anions, and the binding abilities of various spiropyran polymers could indeed be reversibly activated with UV light,<sup>267</sup> with the detection limit of  $\text{CN}^-$  down to the impressive 500 nM.<sup>268</sup> When the photoisomerisation process occurs at relatively low pH values, it is accompanied by proton capture/release, according to the equation  $\text{SP} + \text{H}^+ \xrightleftharpoons[\text{Vis}]{\text{UV}} \text{MCH}^+$ . Accordingly an ~10-fold increase in the solution concentration of the  $\text{H}^+$  ions was observed as the protonated merocyanine units were exposed to visible light.<sup>221</sup> Angiolini *et al.* took advantage of this light-regulated proton binding to construct a family of chiroptical switches based on polymers functionalised with both spiropyran and an optically

active pyrrolidinyl moiety linked to an azopyridine group. With the increasing basicity of the building blocks in the order SP < azopyridine < MC, proton shuffling between azopyridine and the SP-MC pair was enabled and observed both within copolymers incorporating spiropyran and azopyridine as parts of the same polymer chain,<sup>269</sup> and between poly(spiropyran) and poly(azopyridine) homopolymers.<sup>270,271</sup> The proton transfer occurred reversibly and resulted in pronounced changes in the circular dichroism (CD) spectra.

A variety of polyacrylates<sup>272–275</sup> and polysiloxanes<sup>276,277</sup> incorporating both SP and mesogenic units have been synthesised. Although the primary motivation was the development of reversible optical data storage,<sup>278–281</sup> other fascinating properties, such as transient birefringence<sup>98,282</sup> and second harmonic generation,<sup>283–285</sup> have also been observed in these systems. In another study, spiropyran-decorated polyacrylamide hydrogel was used to fill the empty spaces between regularly arranged polystyrene colloidal spheres, giving rise to so-called polymerised crystalline colloidal arrays (PCCAs).<sup>286</sup> The regular packing of the colloids resulted in the diffraction of incident light of a wavelength which was defined by the particle spacing. Photoisomerisation of spiropyran resulted in reversible contraction and expansion of the gel matrix – during which the crystalline arrangement of the colloidal spheres was retained. As a result, a reversible shift in the diffraction wavelength of as much as  $\sim 11$  nm was observed.<sup>286</sup> An as of yet unrealised challenge is the ability to control the electronic properties of conductive polymers using light. Several polymers have been synthesised for this purpose,<sup>141,287</sup> including ones with the spiropyran units incorporated into the polymer chain.<sup>288–290</sup> Finally, in an interesting application demonstrated recently,<sup>291</sup> a thin layer of a poly-spiropyran lying between solid surfaces and multilayer films grown by the layer-by-layer technique enabled an easy, light-induced detachment of these films from the underlying substrate – a task which could be difficult to realise otherwise.

### 3. Spiropyran-functionalised biopolymers

Functionalisation of Nature's macromolecules with artificial molecular photoswitches opens up the attractive possibility of influencing various biological processes using light. In the highly polar environments of biological systems, spiropyran exists in the MC form, and the isomerisation to SP can be accomplished with visible light; SP  $\rightarrow$  MC reisomerisation takes place spontaneously. The negative photochromism represents a major advantage by enabling the reversible switching to be accomplished *without* the use of UV – a stimulus which is (i) potentially harmful as far as the often sensitive biological systems are concerned; and (ii) induces fatigue to a much greater extent than visible light (consequently, many systems covered in this section have been reported to be “fully reversible”).

Functionalisation of various biomacromolecules with spiropyran is straightforward and can be accomplished in a single step using reagents 21 and 22 (Fig. 13A) – a spiropyran anhydride and an active ester, respectively. These molecules readily react

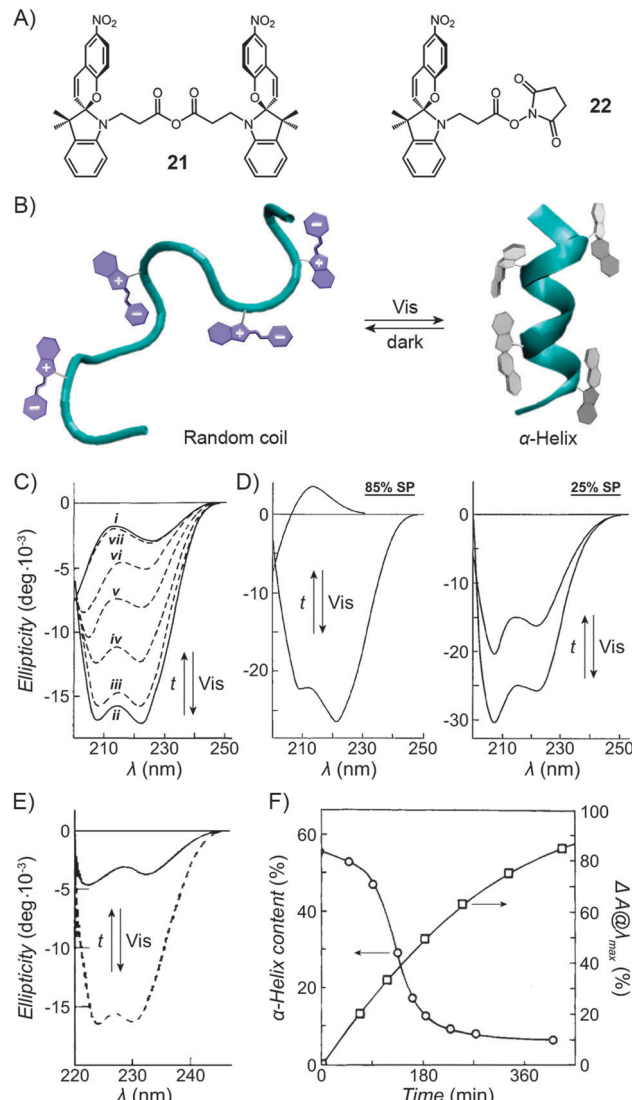


Fig. 13 Light-controlled folding of polypeptide chains. (A) Structural formulas of reactive spiropyran derivatives used for functionalisation of various biopolymers. (B) Schematic representation of light-controlled folding. (C) Changes in the CD spectra of MC-functionalised poly-L-glutamic acid as it is exposed to visible light (i  $\rightarrow$  ii), and during thermal equilibration (ii  $\rightarrow$  vii). (D) Effect of spiropyran content in poly-L-glutamic acid on the helix  $\leftrightarrow$  random coil transformation. (E) Photocontrol of poly-L-lysine conformation. (F) Dependence of the  $\alpha$ -helix content on the fraction of MC in a thermally equilibrating modified poly-L-lysine. Time = 0 represents a Vis-irradiated sample;  $\Delta A$  indicates the percentage of the MC state. While the SP decay follows first order kinetics, the helix content drops precipitously once enough MC has accumulated. [Adapted with permission from ref. 433 (Copyright 2009 American Institute of Physics) (B), ref. 295 (Copyright 1989 American Chemical Society) (C), ref. 301 (Copyright 1998 Elsevier) (D), ref. 304 (Copyright 1992 American Chemical Society) (E) and ref. 434 (Copyright 1995 American Chemical Society) (F).]

with free amino groups on the surfaces of biopolymers *via* amide bond formation, and have emerged as universal reagents for rendering biopolymers photoresponsive.

#### 3.1. Photocontrol of polypeptide conformation

Inspired by the elegance with which biological systems use photons to initiate biochemical processes, several groups have



investigated the structural properties of polypeptides decorated with spiropyran units.<sup>292</sup> First such photochromic polypeptides – spiropyran-functionalised poly-L-tyrosine<sup>293</sup> and poly-L-lysine<sup>294</sup> – were synthesised by Smets and co-workers, but no effects of photoswitching on conformational changes (Fig. 13B) were reported until two decades later when Ciardelli *et al.* studied the behaviour of spiropyran-decorated poly-L-glutamic acid.<sup>295</sup> Fig. 13C shows representative CD spectra of hexafluoropropanolic solutions of poly-L-glutamic acid having 41 mol% of the side chain -COOH groups functionalised with spiropyran. In this figure, i corresponds to a dark-adapted, MC-rich polypeptide, and the spectrum is typical of that of a random coil. By contrast, exposure to visible light generated a colourless (SP) solution with spectrum ii, whereby the two minima at 208 and 222 nm are characteristic of the  $\alpha$ -helix (the fraction of the chain adopting the helical conformation was estimated at 45%). The change was remarkably fast and took as little as 5 s of irradiation with  $\lambda = 525\text{--}575\text{ nm}$ .<sup>295</sup> Thermal relaxation to the original disordered conformation (ii  $\rightarrow$  vii) was significantly longer (e.g. 24 hours), but could be accelerated by placing different substituents on the spiropyran moiety.<sup>296</sup> The reversible helix  $\leftrightarrow$  random coil transformation could be repeated over many cycles, and was shown<sup>297</sup> to occur in a stepwise manner *via* an intermediate thought to be a solvated helix.

In addition to changes in the CD spectra, the folding process could be followed by viscosity measurements. A significant decrease in viscosity accompanying the MC  $\rightarrow$  SP isomerisation could not be rationalised by the isomerisation reaction alone; recall from Section 2.2 that the viscosities of spiropyran-decorated polymethacrylate solutions decreased by up to 50% upon visible light irradiation, whereas those of functionalised poly-L-Glu dropped by 250–300%.<sup>298</sup> In the present example, this enhanced effect was attributed to the conformational change, the  $\alpha$ -helix being much more compact than the random coil. Interestingly, such photoinduced conformational changes were also observed at the water-air interface.<sup>299,300</sup>

It is important to emphasise that the SP isomer does not, strictly speaking, stabilise the helical conformation – in fact, the native poly-L-Glu lacking any SP readily folds into an  $\alpha$ -helix under similar conditions – rather, the helical structure is *disrupted* by the MC isomer. This can be appreciated from Fig. 13D, where poly-L-glutamic acids decorated with 25 and 85 mol% SP both have  $\sim 85\%$  helical content. Upon thermal relaxation, however, the 85 mol% MC polypeptide adopted a completely disordered structure, whereas the 25 mol% MC one retained 55% of the helical content.<sup>301</sup> In other words, the fraction of the photoinduced  $\alpha$ -helix could be regulated by the degree of functionalisation of the side chain -COOH groups with spiropyran.

How exactly MC destabilises the  $\alpha$ -helical conformation has been a matter of some debate; however, strong MC–MC interactions involving the open form of the switch seem to play a key role. These interactions can be either attractive<sup>298</sup> or repulsive,<sup>302</sup> depending on whether the open form is in the zwitterionic (MC) or in the protonated ( $\text{MCH}^+$ ) state, respectively. In one elegant study, the unfolding process was shown, by means of UV-Vis spectroscopy,

to be accompanied by the formation MC dimers.<sup>301</sup> On the other hand, molecular dynamics simulations suggest the existence of hydrogen bonding interactions between the MC's phenolates and the unfunctionalised Glu's carboxylic acid groups.<sup>303</sup>

Photoinduced conformational changes are not limited to poly-L-Glu: for example, poly-L-lysine – another polypeptide with a tendency to adopt an  $\alpha$ -helical conformation – showed analogous behaviour upon the attachment of spiropyran moieties to the side chain -NH<sub>2</sub> groups (Fig. 13E).<sup>304,305</sup> However, it is important to note that structural properties of both poly-L-Glu and poly-L-Lys (and other polypeptides in general) are strongly environment-dependent<sup>306,307</sup> and that the reversible, light-induced conformational changes described above were observed only in selected solvents. Recently, a more general approach to controlling polypeptide conformations was introduced, which is based on a spiropyran-based crosslinker within a rationally designed peptide sequence.<sup>308</sup> This crosslinker acted as a reversible “hinge”, inducing different degrees of helicity (48% for the dark-adapted MC *vs.* 62% for the Vis-exposed SP) in an otherwise disordered polypeptide chain (12% helicity in the native peptide). Although the light-induced conformational changes were only moderate, the advantage of this approach is that it is expected to operate in a range of different environmental conditions.

### 3.2. Photocontrol of enzymatic activity

Enzymes whose catalytic activity can be modulated using light represent a highly attractive target as far as the control of the properties of biomacromolecules with external stimuli is concerned. Research in this field has been pioneered by Suzuki *et al.*, who demonstrated three different modes of photoregulating enzymatic activity – all based on immobilised spiropyrans (Fig. 14).<sup>309</sup> Initial studies based on this approach date back to as early as 1975 and deal with the enzyme  $\alpha$ -amylase<sup>310,311</sup> – an example which is here discussed as a case study.  $\alpha$ -Amylase, the enzyme hydrolysing  $\alpha$ -linked polysaccharides, was functionalised with excess of 21, and a solution of the resulting protein had a red colour indicating that the spiropyran was in the MC form. As could be expected, this modification significantly (by 64%) decreased the enzymatic activity as compared to the native  $\alpha$ -amylase; importantly, however, exposure to visible light (amylose-MC  $\rightarrow$  amylose-SP) reduced the activity by a further 18–36%.<sup>310,311</sup> While being rather small, this change can be appreciated given that only 2 out of  $\sim 900$  amino acid residues were modified with spiropyran. When left in the dark, the protein regained its original activity due to thermal SP  $\rightarrow$  MC re-isomerisation. It has been speculated that the hydrophobic nature of SP prevented the enzyme from interacting efficiently with its substrate – the hydrophilic amylose – resulting in decreased catalytic activity. A related enzyme  $\beta$ -amylase responded similarly, and the changes were much more pronounced: exposure to visible light reduced the activity by as much as 87%.<sup>312</sup>

In principle, however, the effect of switching on catalytic activity is difficult to predict *a priori*: modified  $\beta$ -glucosidase (another enzyme which hydrolyses polysaccharides), for example, was more active when its spiropyran residues were in the *closed* form.<sup>312</sup> A mechanism by which the MC groups deactivate their



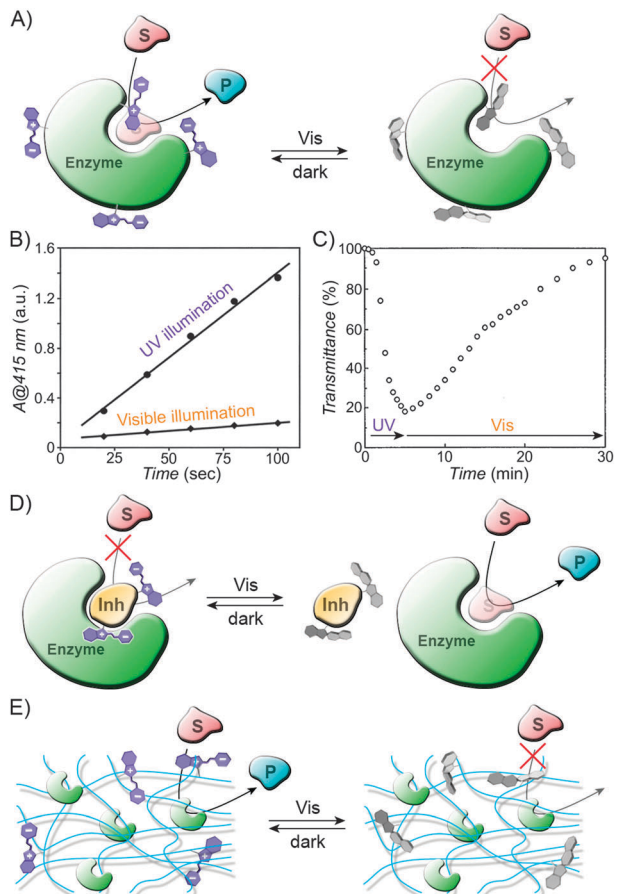


Fig. 14 Light-controlled catalysis using spiropyran-functionalised biomaterials. (A) Schematic representation of light-controlled catalysis using spiropyran-modified enzymes. Note that the MC  $\rightarrow$  SP isomerisation can either activate or deactivate the enzyme. (B) Effect of light on the catalytic activity of spiropyran-derivatised horseradish peroxidase. In this case, Vis-irradiation deactivated the enzyme. (C) The opposite trend was achieved with spiropyran-functionalised subtilisin. (D) Another approach to photoswitchable catalysis based on spiropyran-functionalised macromolecular inhibitors. (E) Light-controlled catalysis using enzymes bound to spiropyran-functionalised porous media. [Adapted with permission from ref. 320 (Copyright 1999 Elsevier) (B) and ref. 321 (Copyright 1999 Nature Publishing Group) (C).]

host enzymes might be based on intramolecular attractive MC–MC (or repulsive  $\text{MCH}^+–\text{MCH}^+$ ) interactions perturbing the active conformation of the protein – in fact, it has been shown by dynamic light scattering (DLS) that modified concanavalin A undergoes shrinkage upon SP  $\rightarrow$  MC isomerisation,<sup>313,314</sup> resulting in decreased binding<sup>315</sup> of the protein's monosaccharide substrates. Similarly,  $\alpha$ -chymotrypsin could be partially deactivated by converting the SP moieties on its surface to MC.<sup>312,316</sup> Other enzymes which were modified by the same approach and subsequently showed photoregulated catalytic properties include urease,<sup>317</sup> glucose oxidase (GOX),<sup>318,319</sup> and horseradish peroxidase (HRP).<sup>320</sup> This last example is worth highlighting because of the large changes in activity exhibited by the enzyme upon photoirradiation. HRP equipped with 8–9 spiropyran groups per protein molecule readily catalysed the oxidation of a model compound when the switch was in the MC

form, whereas exposure to visible light reduced the reaction rate by as much as 92% (Fig. 14B).<sup>320</sup> An even more impressive change was facilitated by an approach based on the light-induced precipitation of the enzyme from the solution. To achieve this goal, Ito and co-workers prepared a construct comprising the enzyme subtilisin and a photoswitchable random copolymer pre-synthesised from (i) methacrylic acid, (ii) methyl methacrylate, and (iii) a spiropyran-appended methacrylate.<sup>321</sup> The resulting *hybrid subtilisin* carried as many as  $\sim$ 30–80 spiropyran moieties per protein molecule, which provided a unique hybrid system with dramatic photo-responsiveness. For example, the hybrid formed well-defined solutions in toluene, from which it could be quantitatively precipitated upon exposure to UV light (Fig. 14C), thus effectively shutting down its catalytic activity in a transesterification reaction. Notably, the catalytic efficiency of the hybrid enzyme did not change after three precipitation–solubilisation cycles.<sup>321</sup>

The second strategy to manipulate enzymatic activity with light is based on *photoswitchable inhibitors* – that is, inhibitors whose affinities to native enzymes depend on the light to which they are exposed (Fig. 14D).<sup>322</sup> For example, ovomucoid, a protein also known as *trypsin inhibitor*, was functionalised with spiropyran using the generic reagent 21.<sup>323</sup> The photoinhibition effect of the modified ovomucoid towards native trypsin – defined as the ratio of the amount of trypsin inhibited by unit mass of the inhibitor under visible light *vs.* in the dark – depended on the degree of functionalisation with SP; it was established that the highest effect was exhibited by ovomucoid having 2 of its 10 amino groups modified with spiropyran. Specifically, this modified inhibitor showed a photoinhibition effect of 0.72, indicating that the inhibitor functionalised with MC interacted with trypsin more strongly than when appended with SP.<sup>323</sup> This difference has been attributed to the electrostatic stabilisation of the enzyme–(inhibitor-MC) binding (the activity of the inhibitor decreased with increasing ionic strength of the solution).

Finally, photoswitchable catalysis can be achieved using *native enzymes* which have been non-covalently associated with photoswitchable membranes (Fig. 14E). Such photoresponsive environments can be easily prepared by modifying inexpensive biomacromolecules such as collagen fibrils and agarose gels with 21. Suzuki *et al.* were the first to show that various enzymes embedded in such membranes display light-dependent activities, despite not being chemically attached to the SP species. Generally, these different systems all showed that the rate of the catalytic reaction (*e.g.* urease-catalysed urea hydrolysis; lactate dehydrogenase-catalysed lactate oxidation) was *decelerated* upon exposure of the MC-gels (negative photochromism) to visible light. The changes, however, were small: the activity of trypsin,<sup>324</sup> lactate dehydrogenase,<sup>325</sup> and urease<sup>326</sup> – all embedded in spiropyran-functionalised collagen – dropped by 22%, 37%, and  $\sim$ 50%, respectively. Similarly, the rate of hydrolysis catalysed by trypsin associated with a spiropyran-agarose gel decreased by 33%.<sup>327</sup> The differences in reaction rates could be attributed to environment-dependent diffusion coefficients of the reaction substrates: MC-rich media can be hydrated more readily



than their SP counterparts, thus enabling efficient transport of solutes and their delivery to the enzymes (it has been shown, for example, that urea hydrolysis catalysed by a spiropyran–collagen gel is a diffusion-limited process<sup>328</sup>). In certain cases, however, the visible light-decreased reactivities could not be accounted for by the diffusion effects: *e.g.* both lactate and NAD – substrates for lactate dehydrogenase – diffused *faster* through SP- than through MC-collagen membranes (presumably due to their attractive interactions with the MC groups). It was speculated that the hydrophobic microenvironment around the lactate dehydrogenase imposed by the SP moieties may directly destabilise the enzyme.<sup>325</sup>

Whether an enzyme-catalysed reaction will be accelerated or suppressed by visible light depends also on the nature of the reaction. A chymotrypsin-catalysed plastein synthesis – a process during which peptide bonds *form* as opposed to being hydrolysed – proceeded more efficiently in SP-rich agarose gels.<sup>329</sup> The authors hypothesised that the hydrophobic microenvironment promoted a reaction in which water molecules are consumed.<sup>329</sup> In a remarkable example supporting this reasoning, the direction of a reaction – esterification *vs.* ester hydrolysis – could be controlled by the state of spiropyran.<sup>330</sup> Specifically, a Vis-irradiated spiropyran-agarose gel promoted esterification of *N*-acetyl-L-tyrosine with ethanol, whereas in the dark, the respective ester was hydrolysed. In an elegant demonstration of this behaviour, this ester could reversibly be formed and subsequently quantitatively hydrolysed upon exposure to visible light and dark adaptation, respectively, over several cycles.<sup>330</sup>

### 3.3. Photocontrol of transport through biopolymers

In the last mode of light-controlled catalysis discussed above,<sup>325</sup> the rate of diffusion through spiropyran-functionalised gels depended on the state of the switch. Another example of such behaviour was found during studies on cytochrome *c* (Cyt *c*), which interacted more strongly with the SP isomer of spiropyran immobilised on an agarose gel, such that ~46% of the protein bound under visible light could subsequently be released in the dark.<sup>331</sup> While the interactions with SP/MC alone are not selective enough as far as *mixtures* of proteins are concerned, co-functionalisation of the stationary media with the photoswitchable groups *and* specific enzyme inhibitors at the same time could greatly increase binding selectivities of selected proteins, which, in combination with the light responsiveness, has become the basis of a technique called *light-enhanced affinity chromatography*. The principle of this technique is based on the empirical observation<sup>332,333</sup> that the strength of an enzyme's interaction with immobilised inhibitors depends on whether the nearby photoswitch molecules are in the SP *vs.* the MC form. For example, trypsin interacted strongly with spiropyran-functionalised agarose gel appended with the *soybean trypsin inhibitor* in the dark (whereby spiropyran existed in the MC state due to negative photochromism), but could be released upon exposure to visible light. The potential of this technique was demonstrated by the purification of crude trypsin from bovine pancreas: light-induced elution from a column packed with the

modified agarose gel led to 21-fold purification of the enzyme.<sup>333</sup> Notably, the opposite binding pattern was observed when the spiropyran-agarose gel – now co-functionalised with aspartate residues – interacted with the enzyme asparaginase. While the enzyme bound strongly to the visible light-irradiated, SP-rich gel, it was readily released in the dark, leading to 90-fold purification of the crude enzyme.<sup>332</sup> It is worth emphasising that asparaginase interacted with the aspartate residues, and not with the photo-switch – in fact, no binding was observed between the enzyme and a spiropyran gel lacking any aspartates. Instead the mode of action of the switch was thought to involve reversible modulation of the ionic strength in the proximity of the enzyme–ligand interaction site.

### 3.4. Photocontrol of DNA hybridisation

The ability to reversibly unwind the DNA double helix using light could be used to phototrigger a variety of biological processes. A rationale behind using spiropyran as a building block for photoswitchable DNA is that its MC isomer bears much more structural resemblance to the DNA bases than the SP form. Consequently, one might expect a preferential ability of MC to participate in  $\pi$ – $\pi$  stacking interactions with the DNA bases, and consequently to increase the stability of the double helix. This hypothesis was verified in a study based on a spiropyran-terminated homothymidine (T<sub>8</sub>). Indeed, the melting temperature of this oligonucleotide increased from 18.0 °C to 21.6 °C upon SP  $\rightarrow$  MC isomerisation,<sup>334</sup> suggesting that within this narrow temperature window, reversible, light-induced duplex formation/melting was possible. Functionalisation of long-chain DNA was also reported, whereby control of the extent of functionalisation with SP was demonstrated – again, efficient isomerisation of the switch was observed.<sup>335</sup> Recently, more sophisticated spiropyran-functionalised DNA molecules were synthesised, incorporating the photoswitch at the center of the chains. Within this context, spiropyran was found to be resistant to UV irradiation.<sup>336</sup> The authors hypothesised that this lack of responsiveness was due to quenching of the triplet state of spiropyran by neighbouring DNA bases.

### 3.5. Photocontrol of volume phase transitions in thermoresponsive polypeptides

Elastin-like polypeptides (*e.g.* (VPGVG)<sub>*n*</sub> polymers) show behaviour analogous to that of thermoresponsive polymers (*cf.* Sections 2.1 and 2.3) in that they precipitate from aqueous solutions concurrent to a temperature increase. The temperature at which the transition occurs is referred to as the *inverse transition temperature* (*T<sub>t</sub>*; compare with LCST).<sup>337</sup> To investigate the possibility of modulating phase transitions in elastin-like polymers using light, Rodríguez-Cabello and co-workers prepared a random copolymer [(VPGVG)<sub>0.74</sub>(VPGEVG)<sub>0.26</sub>]<sub>*n*</sub>, and functionalised the side chain –COOH groups with spiropyran moieties *via* esterification.<sup>338</sup> The dark-adapted photostationary state of the resulting polymer contained approximately equal fractions of SP and MC, and the polypeptide had a *T<sub>t</sub>*  $\approx$  13.5 °C, a value which could be decreased to  $\sim$ 10 °C and increased to  $\sim$ 20 °C upon exposure to visible and UV light, respectively. Subjecting a solution of this polymer to

alternate cycles of visible and UV light irradiation at  $T = 14\text{ }^{\circ}\text{C}$  increased the population of SP and MC, respectively, to the extent that the polymer reversibly precipitated and redissolved. Remarkably, these drastic solubility changes could be achieved with a polymer equipped with as little as 2.3 spiropyran groups per 100 amino acid residues.

### 3.6. Photocontrol of protein folding

A fascinating idea of employing the reversible  $\text{SP} \leftrightarrow \text{MC}$  isomerisation for triggering conformational changes of nearby protein molecules was investigated by Akiyoshi *et al.*<sup>339</sup> These researchers prepared nanoparticles of gels (“nanogels”) made of the polysaccharide pullulan functionalised with spiropyran. An intentionally misfolded protein – citrate synthase (CS) – was then interfaced with the nanogels, and the rate of its refolding to the native conformation, estimated by the rate of recovery of the enzyme activity, was probed under different types of irradiation. Specifically, denatured CS exhibited 32% of the native enzyme activity when no nanogels were added. Upon the addition of a nanogel containing both the SP and the MC forms of the switch, CS activity increased to 61%. Interestingly, however, when the protein was first incubated with the same SP + MC gel for a short time, and then exposed to visible light which gave rise to an all-SP nanogel, 81% of the native CS activity was regained. Clearly, the MC  $\rightarrow$  SP isomerisation induced extra refolding in a process perhaps reminiscent of the mode of action of the natural chaperones, which undergo ATP-driven conformational changes thereby refolding misfolded proteins bound in their cavity. Unfortunately, only one switching cycle was reported, and the question of if and how the amount of refolded protein would increase by repeated UV-Vis cycling remains. Nevertheless, this study represents an important step toward a rational development of synthetic machinery with chaperone-like activity.

### 3.7. Photocontrol of transport through natural nanopores

The large change in polarity accompanying the  $\text{SP} \leftrightarrow \text{MC}$  isomerisation is critical in the design of light-actuated nanovalves.<sup>340,341</sup> Such “smart” nanovalves are based on a natural channel protein found in *Escherichia coli* known as the mechano-sensitive channel of large conductance (MscL). In the bacteria, the valves are embedded within the membranes and, under normal conditions (that is, no significant difference in osmotic pressure on the two sides of the membrane), the native MscL is “closed” – as a consequence of hydrophobic interactions between non-polar amino acid residues located inside the channel. It has been found, however, that substituting a single, strategically positioned hydrophobic glycine residue with polar amino acids leads to increased hydration of the pore, and consequently increased channel mechanosensitivity.<sup>342</sup> Based on this knowledge, Feringa, Meijberg, and co-workers prepared an MscL mutant wherein the Gly residue was substituted with cysteine, and then post-synthetically modified the resulting protein using a cysteine-selective alkylating agent comprising an iodoacetate group and a spiropyran moiety.<sup>340</sup> As predicted, the reversible hydrophobic  $\leftrightarrow$  hydrophilic isomerisation of spiropyran which was thus installed

within the channel enabled opening and resealing of the channel, respectively. The utility of these nanovalves was demonstrated by performing light-controlled transport of a fluorescent dye across a membrane incorporating the modified nanopores.

### 3.8. Spiropyran as a probe for the analysis of biological microenvironments

We saw in Section 2.3 how the open form of spiropyran could act as a colorimetric sensor of the polarity of its microenvironment in the context of phase transitions in thermo-responsive polymers (*cf.* Fig. 9E). Importantly, environment-dependent properties of the switch can also be employed in order to tackle meaningful biological questions. Imanishi *et al.* synthesised several spiropyran-functionalised oligopeptides, all with the sequence corresponding to the shortest active fragment of *melittin*, and equipped them with the photoswitch at different positions of the sequence (*melittin* is the active component of honey bee venom, and it is responsible for cell membrane lysis). These different peptides were exposed to UV light, and the rate of thermal MC  $\rightarrow$  SP re-isomerisation in the presence of lamellar vesicles (mimicking cell membranes) was followed spectroscopically.<sup>343</sup> The isomerisation rate was shown to be dependent on the location of the photoswitch, ranging from fast decay of the MC signal when the probe was at the C-terminus of the peptide, to an indefinite stabilisation of the coloured form for the N-terminus-functionalised peptide (negative photochromism). Placing the MC probe at the center of the peptide sequence resulted in an intermediate decay rate. These results indicate that the C-terminus of the peptide was located in the hydrophobic part of the vesicles, whereas the N-terminus was exposed to the aqueous environment. In an interesting extension of this study, light-stimulated lysis of membranes incorporating spiropyran-containing *melittin* fragments was demonstrated.<sup>344</sup>

Similarly, Mihara *et al.* developed a technique called photochromism-based assay, which is based on spiropyran-functionalised polypeptides having specific protein-binding sequences. Again, the peptides were pre-exposed to UV light, and, the rate of MC  $\rightarrow$  SP re-isomerisation was followed by measuring the decay of fluorescence due to the MC isomer.<sup>345</sup> Attractive interactions with the target protein molecules were evidenced by an emission decay rate *different* from that of the same peptide in a protein-free solution. These differences could stem either from the different dielectric constant of the new microenvironment around the switch, or from the steric hindrance imposed by the target protein molecule. Based on how a given protein affected the emission behaviour of eight different spiropyran-containing polypeptides, it was assigned a specific “barcode”, by which it could then be recognised. Using this strategy, six different proteins could unambiguously be identified. The same authors also described a closely related method: the chromism-based assay (CHROBA), which has been useful in detecting the phosphorylation activity of kinases.<sup>346</sup> The assay is similarly based on spiropyran-functionalised polypeptides – in this case substrates for specific kinases. For example, one such peptide contained the so-called Kemptide



sequence (LRRASLG-NH<sub>2</sub>) – a kinase A-specific substrate – having spiropyran covalently attached to its C-terminus (S indicates the serine residue which can be phosphorylated). Following phosphorylation (or lack thereof), this peptide was incubated with polyelectrolytes – poly(L-lysine), poly(L-arginine), and/or poly(L-aspartic acid) (Fig. 15). Since each phosphorylation event entails the introduction of two negative charges (at near-physiological pH), phosphorylated peptides are expected to interact differently with the polyelectrolytes: specifically, their binding with poly(lysine) and poly(arginine) should be stronger, whereas with poly(aspartic acid) – weaker upon phosphorylation. Association with a polyelectrolyte is, in turn, expected to *suppress* the rate of spontaneous SP  $\rightarrow$  MC isomerisation (solutions are pre-exposed to visible light), now taking place in a viscous microenvironment of the polyelectrolyte.<sup>347</sup> This isomerisation could be followed fluorometrically or even colorimetrically<sup>348</sup> – that is, visual inspection of the samples allows one to discriminate the original, non-phosphorylated substrates from the modified ones, or, in other words, to detect the presence of a given kinase (e.g. it was established that the lower limit for the detection of kinase A is  $\sim 0.1\text{--}1.0\ \mu\text{g mL}^{-1}$ ). A significant advantage of CHROBA over traditional phosphorylation assays is that it avoids the need to use immobilised protein substrates or laborious isolation steps.

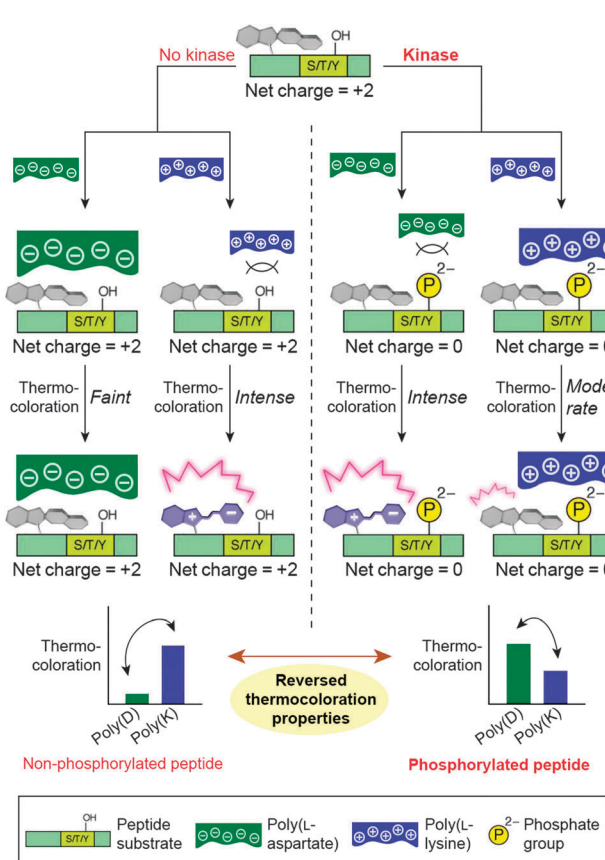


Fig. 15 "Chromism-based assay" for the detection of phosphorylation activity. See text for explanation. [Adapted with permission from ref. 348 (Copyright 2006 Royal Society of Chemistry).]

## 4. Spiropyran-functionalised inorganic nanoparticles

Decades of research in the modification of planar inorganic surfaces with organic ligands provide important lessons as far as modification of nanostructured particles is concerned. In principle, the choice of the ligand monolayer depends on the chemistry, but not the curvature of the solid substrate – that is, the same chemical functionalities can be used for the modification of planar and nanostructured surfaces. Accordingly, gold NPs have been functionalised with spiropyran-terminated thiols,<sup>349,350</sup> silica shells of upconverting nanocrystals (UNCs) were modified with a spiropyran-terminated silane, and so on. An attractive alternative to the above place-exchange methods is provided by "post-synthetic" modification of SAMs – a strategy particularly useful in the case of chemically sensitive NPs. For example, alkyne-terminated CdSe quantum dots underwent further modification *via* the copper-catalysed [3+2] cycloaddition – *e.g.* with an azide-appended small-molecule spiropyran.<sup>351,352</sup>

### 4.1. Photocontrol of nanoparticle fluorescence

The ability of spiropyran to switch between an optically transparent SP and a strongly absorbing, fluorescent MC form enables the reversible control of FRET; several examples of modulating the fluorescence of *organic* fluorophores<sup>353</sup> have been covered in Section 2.1. This concept can be extended to inorganic fluorescent NPs by functionalising their surfaces with spiropyran molecules,<sup>9</sup> and has to date been demonstrated for four different classes of such materials: CdSe-ZnS core-shell quantum dots (QDs), gold clusters, carbon nanodots, and rare-earth nanophosphors. In all of these cases, the inherent fluorescence of the NP cores can effectively be "turned off" and "on" as a consequence of the reversible isomerisation of the photoswitch. It is worth recalling, however, that the excitation wavelength should be adjusted such that it does not induce the SP  $\rightarrow$  MC or MC  $\rightarrow$  SP photochemical isomerisation.

Fortunately, quantum dots can be excited with a wide spectrum of wavelengths, such that those fulfilling the above condition can easily be identified. Medintz and co-workers were the first to interface CdSe-ZnS core–shell QDs with spiropyran, employing a rather complex immobilisation approach based on decorating the ZnS shells with a pentahistidine sequence appended to the C-terminus of the maltose binding protein, which had been modified with spiropyran using an active ester similar to 22 in Fig. 13.<sup>354</sup> The number of switch units per protein molecule could be varied between 1 and 5, thereby allowing placement of various numbers of spiropyran moieties on each QD, and ultimately control of FRET efficiency (*e.g.*  $\sim 25\%$  and  $\sim 60\%$  for proteins carrying 1 and 5 spiropyran units, respectively). The same NPs were subsequently functionalised with spiropyran using a simpler approach based on thiolate self-assembled monolayers (SAMs).<sup>175</sup> When covered with the SP isomer and excited with  $\lambda = 420\text{ nm}$ , these 5 nm NPs emitted green light, as shown in Fig. 16A, left. Exposure to only 5 seconds of UV, however, activated FRET and the excited solution assumed a red colour typical of MC emission

(Fig. 16A, right). The process is reversible and NPs' emission can be restored using visible light (Fig. 16B).

Fig. 16C provides an elegant manifestation of the importance of the overlap<sup>355</sup> of MC's absorption and the nanocrystals' emission for effective FRET. One can see that for any given number of MC per NP, FRET is *most* efficient for the largest, 6 nm QDs. This seemingly counter-intuitive result can be understood by taking into account the maximum emission wavelengths of the differently sized QDs:  $\lambda_{\text{em}} \approx 523$  nm for 4 nm NPs,  $\lambda_{\text{em}} \approx 546$  nm for

5 nm NPs, and  $\lambda_{\text{em}} \approx 578$  nm for 6 nm NPs (compare with MC absorption at  $\sim 580$  nm). Hence, MC absorption coincides with the emission of the QDs that are 6 nm in diameter (it is worth emphasising that as little as 10% surface coverage of the 6 nm NP with the MC groups can reduce as much as  $\sim 50\%$  of the original emission intensity). On the other hand, the poor overlap of MC absorption with the emission of the 4 nm QDs is reflected by only mediocre FRET values of these small NPs.

Analogous results were reported for spiropyran-functionalised fluorescent gold nanoclusters.<sup>349</sup> The emission of these dots, comprising on average only eight gold atoms each ( $\lambda_{\text{max}} \approx 480$  nm), partially overlapped with the absorption spectrum of the open form of spiropyran. As a result, fluorescence of  $\text{Au}_8$  decorated with a spiropyran thiol could efficiently (by  $\sim 90\%$ ) and reversibly be quenched upon irradiation with UV light. The same methodology has been applied to spiropyran-modified 3 nm carbon nanodots,<sup>356</sup> with a blue emission at  $\lambda_{\text{max}} \approx 510$  nm (Fig. 16D, left). Following UV exposure, efficient FRET occurred, and the dots emitted red light (Fig. 16D, right). As Fig. 16E shows, blue emission intensity decreased by  $\sim 80\%$  even after ten cycles of switching. Finally, Yan *et al.* reported a very interesting example of selective silencing of only one emission channel of *dual-emissive* NPs (Fig. 16F).<sup>357</sup> These researchers synthesised a trimethoxysilyl-terminated spiropyran and used it to functionalise silica-coated  $\text{NaYF}_4:\text{Yb},\text{Er}@\text{CaF}_2$  UNC (‘‘rare-earth nanophosphors’’) (Fig. 16G, inset). The fluorescence spectrum of as-prepared UNCs is shown in Fig. 16G: when excited with a near-infrared (980 nm) laser, they show two sharp bands centered at  $\sim 540$  nm and  $\sim 660$  nm, corresponding to green and red emission, respectively. Upon exposure to UV,  $\text{SP} \rightarrow \text{MC}$  isomerisation takes place, and the resulting MC absorption strongly overlaps with the green emission channel of the UNCs; consequently, green emission is quenched by as much as 94% (Fig. 16H; note that, interestingly, MC's own emission coincides with the red emission channel of the UNCs). The system was remarkably reversible, with barely any degradation observed after ten switching cycles.<sup>357</sup>

#### 4.2. Photocontrol of nanoparticle solubility

Control of the stability of colloidal suspensions using light can be achieved by decorating the particle surfaces with monolayers of spiropyran. Typically, the non-polar character of the SP isomer ensures good solubility of SP-coated particles in apolar solvents; these suspensions can then be destabilised – and the particles flocculated – upon generation of the polar MC isomer by exposure to UV light. In addition, aggregation can also take place due to attractive MC–MC and MC–SP interactions between moieties located at different particles. Seminal reports on the photocontrol of colloidal stability were published in the mid-nineties by Ueda and co-workers, who worked with spiropyran-functionalised 150 nm silica particles.<sup>108,358,359</sup> They found, for example, that such (transparent) suspensions in  $\text{CCl}_4$  were relatively stable under ambient light, but when exposed to UV, red solids rapidly precipitated. These initial studies highlighted the importance of the solvent on the particles' behaviour: when the medium was too hydrophobic

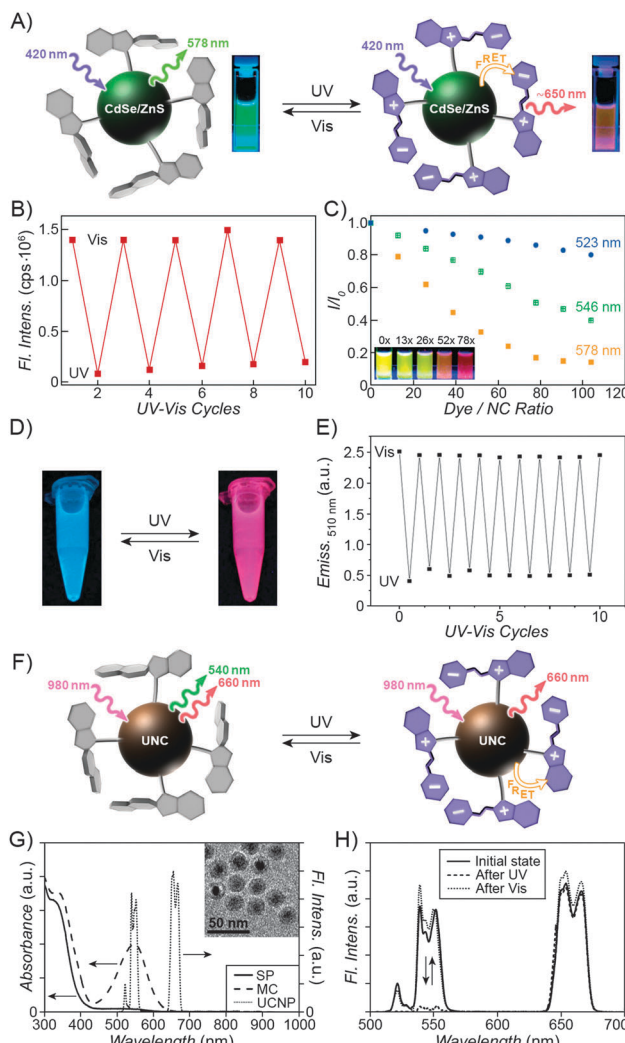


Fig. 16 Light-controlled modulation of fluorescence of inorganic nanoparticles. (A) Reversible FRET between a green-emitting core and an MC shell in spiropyran-coated quantum dots. (B) Reversible quenching of the quantum dots' emission at 546 nm. (C) Dependence of fluorescence quenching efficiency on the overlap of quantum dots' emission and MC absorption. Inset: fluorescence emission as a function of spiropyran loading. (D) Dual-emissive spiropyran-modified carbon nanodots. (E) Reversible quenching of carbon nanodots' emission at 510 nm. (F) Selective quenching of only one emission wavelength of dual-emissive upconverting nanocrystals. (G) Absorption spectra of SP and MC along with the emission spectrum of UNCs. (H) Selective, reversible quenching of the green emission of the UNCs. [Adapted with permission from ref. 175 (Copyright 2005 American Chemical Society) (A–C), ref. 356 (Copyright 2013 Royal Society of Chemistry) (D and E), and ref. 357 (Copyright 2012 Wiley-VCH) (G and H).]



(e.g. cyclohexane), NPs quickly sedimented irrespective of irradiation, whereas other solvents (e.g.  $\text{CHCl}_3$ ) stabilised NPs decorated with both isomers of the switch equally well (compare with Fig. 17D).

More recently, Bell *et al.* worked with similar systems comprising  $\sim 300$  and  $\sim 900$  nm silica spheres functionalised with spiropyran polymers synthesised *via* surface-initiated ATRP (Fig. 17A).<sup>49,360</sup> Exposing the relatively stable toluene suspension of these particles to UV resulted in rapid precipitation of red solids, and SEM confirmed the presence of aggregates (Fig. 17B and C).<sup>125</sup> Again, the behaviour was strongly solvent-dependent, as evidenced by rates of sedimentation under UV or Vis light – for example, while the strong effect of light on solubility was observed in toluene (specifically, the sedimentation rate was enhanced  $\sim 335$  times in the presence of UV), particles decorated with either SP or MC sedimented rapidly in *o*-xylene, and could efficiently be stabilised in THF irrespective of the isomer (Fig. 17D). These light-controlled dispersibility changes imply that in a biphasic system comprising a polar and an apolar solvent, the particles might be able to undergo a reversible phase transfer. A realisation of this remarkable concept has recently been reported using  $\sim 400$  nm diameter  $\text{SiO}_2$  spheres which have been chemically functionalised with a spiropyran polymer.<sup>102</sup> The behaviour of this system is shown in Fig. 17E and F; in pure toluene, UV irradiation caused an almost colourless suspension of the particles to turn purple and quickly sediment (Fig. 17E). The presence of the additional aqueous phase allowed this precipitate to be effectively resuspended (Fig. 17F). In both cases, exposure to visible light regenerated the original toluene suspension *via* simple resuspension or phase transfer for the one- and two-phase systems, respectively. Notably, at intermediate stages of irradiation the silica spheres behaved as “colloidal surfactants” able to stabilise water–toluene emulsions.<sup>102</sup>

What are the implications of reversible, light-controlled self-assembly of nanoparticles? In one interesting example, Louie *et al.* showed that light-induced aggregation of spiropyran-coated magnetic iron oxide NPs could modulate the spin–spin (T2) relaxation time of adjacent water protons.<sup>361</sup> Surface chemistry of these NPs was tailored so as to induce negative photochromism and ensure good water solubility of the particles in the dark. Indeed, DLS showed that aggregation commenced upon exposure to visible light, and it entailed reduction in the T2 relaxation time from  $\sim 37$  to  $\sim 25$  milliseconds – results which are of potential interest for the development of new types of “smart” MRI contrast agents.

As first demonstrated by Ueda’s studies on silica colloids, aggregation properties of SP/MC-coated particles depend strongly on the polarity of the medium. In solvents stabilising *both* isomers the NPs display good solubility, yet aggregation can still be induced upon the addition of metal ions – provided the switch is present in the MC form (compare Section 2.6). This property inspired Wang, Jiang *et al.* to develop a series of logic gates whose key components were spiropyran-functionalised gold NPs in combination with metal ions.<sup>350</sup> One such logic gate capable of performing an AND operation is shown in Fig. 17G. Neither UV

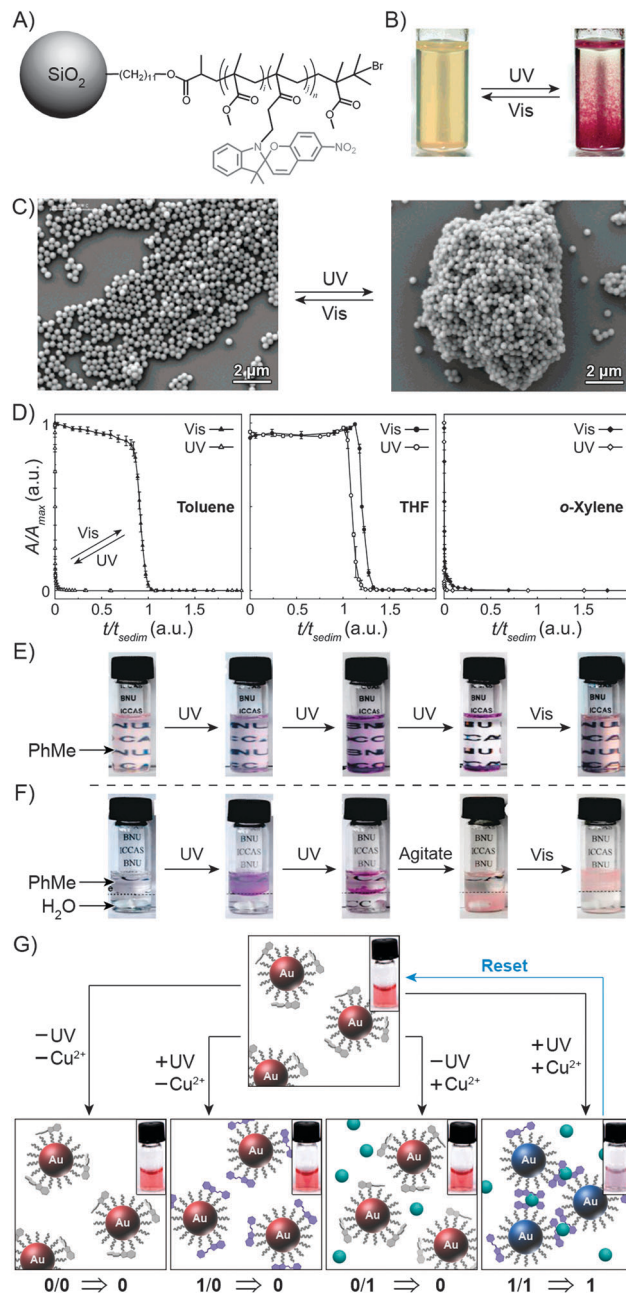


Fig. 17 Spiropyran enables light-controlled aggregation of nanoparticles. (A) Structural formula of a photoresponsive copolymer used to functionalise silica colloids. (B) Light-controlled aggregation of spiropyran-coated silica. (C) SEM images of photoresponsive silica colloids under visible (left) and UV (right) light irradiation. (D) Solvent-dependent behaviour of spiropyran-functionalised silica particles. (E) Light-controlled precipitation of silica colloids from toluene. (F) Light-controlled phase transfer of silica colloids between toluene and water. (G) Dual-controlled aggregation of spiropyran-functionalised gold NPs. [Adapted with permission from ref. 125 (Copyright 2006 American Chemical Society) (B–D), ref. 102 (Copyright 2010 American Chemical Society) (E and F) and ref. 350 (Copyright 2011 Wiley-VCH) (G).]

light nor  $\text{Cu}^{2+}$  alone affects the state of the NPs dissolved in ethanol; however, when *both* of these “inputs” are present, aggregation commences, resulting in the colour change



(Fig. 17G, bottom right). Importantly, the NP aggregates could be disassembled (and the gate allowed to “reset”) upon exposure to visible light, which re-isomerised MC back to SP. Similarly, OR and INHIBIT logic gates were realised by using other metal ions and EDTA, respectively, as additional components.<sup>350</sup> In addition to metal cations, MC-coated NPs can also interact with amino acids, which suppress the MC  $\rightarrow$  SP re-isomerisation rate.<sup>362</sup>

## 5. Spiropyran-functionalised solid surfaces

Having discussed spirocyclic-functionalised polymers, biopolymers and inorganic NPs, we conclude with inorganic solid-state materials having their surfaces covalently modified by spirocyclics. Similar to inorganic NPs, the surface modification strategy is dictated by the chemical composition of the solid substrate. However, UV-Vis spectroscopy, which is routinely used to monitor the SP-MC isomerisation in solution, is hardly applicable<sup>48,363,364</sup> to single layers of molecules on solid substrates because of the very short optical pathways. This forces one to resort to other tools as discussed below in Section 5.1. Conversely, immobilisation on solid surfaces offers one the unique opportunity to study the isomerisation process using *force microscopy* techniques, and several meaningful conclusions from such studies follow. Picraux *et al.* employed interfacial force microscopy to probe isomerisation within diluted monolayers of spirocyclics on glass.<sup>365</sup> Studies performed in air showed an increase in the dipole moment upon UV irradiation, with the dipoles pointing towards the surface (consistent with the mode of attachment of the switch to the substrate). Reversible changes in the dipole moment were observed upon alternating UV and Vis irradiation, and the gradual decay of the difference could be attributed to the fatigue effects. Measurements carried out on the same monolayers in a polar liquid, on the other hand, provided evidence for a partial positive charge of the open-ring isomer (due to  $\text{MCH}^+$ ). Depending on whether the tip was negatively (bare silica) or positively (amine-coated silica) charged, the long-range force was attractive or repulsive, respectively.<sup>365</sup> In another elegant study, Kimura and co-workers went a step further and immobilised spirocyclic on *both* the AFM tip and the substrate.<sup>366</sup> Adhesion forces between the tip and the surface increased substantially (by  $\sim 50\%$ ) under *in situ* UV irradiation in ethanol, which could be attributed to direct MC-MC interactions. In toluene, however, no differences were seen under UV *vs.* Vis radiation – as expected from the low stability and fast re-isomerisation of the MC isomer in the non-polar medium.<sup>366</sup>

### 5.1. Photocontrol of surface wettability

Perhaps the most obvious manifestation of the surface polarity switching is the change in wetting properties.<sup>367</sup> The MC isomer, being more polar than SP, would be expected to increase the wettability of spirocyclic-functionalised surfaces by polar solvents upon exposure to UV light. Fig. 18A shows this phenomenon for water droplets lying on glass substrates

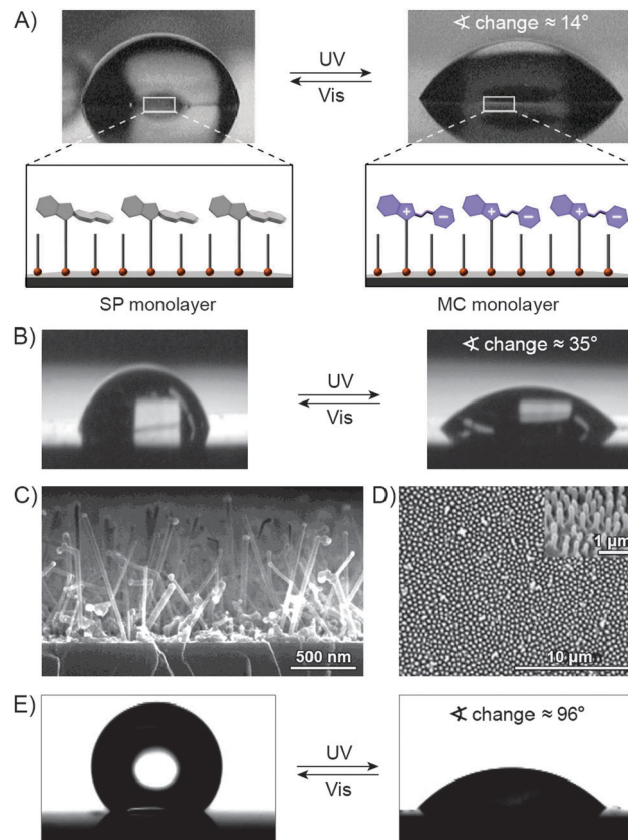


Fig. 18 Photocontrolled wetting of spirocyclic-functionalised surfaces. (A) Wettability change of spirocyclic-functionalised glass. (B) Photoinduced change in the contact angle of an aqueous solution of  $\text{Co}^{2+}$  on spirocyclic-functionalised silicon. (C) SEM image of a spirocyclic-functionalised rough Si surface. (D) SEM image of a spirocyclic-functionalised array of polymer nanorods. (E) Wettability change of a spirocyclic-functionalised nanostructured surface. [Adapted with permission from ref. 78 (Copyright 2002 American Chemical Society) (A), ref. 90 (Copyright 2008 Royal Society of Chemistry) (B), ref. 370 (Copyright 2004 American Chemical Society) (C), ref. 373 (Copyright 2010 Royal Society of Chemistry) (D) and ref. 372 (Copyright 2012 Wiley-VCH) (E)].

decorated with mixed monolayers comprising spirocyclic-terminated silanes diluted with shorter, “dummy” silanes.<sup>78</sup> The dilution with background ligands, while decreasing the surface concentration of spirocyclic, *enhanced* wettability change by virtue of promoting efficient isomerisation, increasing contact angle variation from  $\sim 5^\circ$  to  $\sim 13^\circ$ . Still, the change seen in Fig. 18A is much smaller than what one might expect from a hydrophobic-to-zwitterionic change in the character of the photoswitch. Some clues of why this may be come from the employment of diverse experimental techniques to study on-surface isomerisation processes. For example, Brewster angle reflectometry,<sup>109</sup> X-ray photoelectron spectroscopy,<sup>48</sup> and atomic force microscopy<sup>365,368</sup> all suggest that the yield of ring opening is far from quantitative ( $\sim 10\text{--}20\%$ ), even within diluted monolayers very similar to those from Fig. 18A.<sup>109</sup> On the other hand, sum frequency generation (SFG) vibrational spectroscopy proved invaluable in probing the orientation of the photoswitch with respect to the underlying surface.<sup>369</sup> When *p*-polarised beams



are used for the SFG measurements, the method is sensitive to vibrational modes perpendicular with respect to the underlying surface. The authors identified symmetric and antisymmetric stretching modes of the spiropyran's nitro group as diagnostic of the isomerisation process, and concluded that in the open form, the  $\text{NO}_2$  group points away from the surface. This orientation of the molecule hinders the negatively charged oxygen atom away from the environment, and as a consequence, MC-functionalised surfaces retain much of the hydrophobic character of the SP-decorated ones<sup>369</sup> – in agreement with the high values of the water contact angles before and after UV irradiation.

Research in the field of photoswitchable surfaces is motivated in part by the quest for new, efficient ways to direct the motion of liquids in thin channels of the ever-shrinking microfluidic devices. The photoswitchable wettability change shown in Fig. 18A was sufficient to raise the water level in 500  $\mu\text{m}$ -thick glass capillaries functionalised with the same monolayer by 2.8 mm – an interesting demonstration dubbed “photocapillarity”,<sup>78</sup> – but was not large enough to induce a reverse effect upon MC  $\rightarrow$  SP re-isomerisation. A general condition for a droplet to move<sup>33</sup> along a spiropyran-functionalised surface is that the advancing contact angle on an MC-rich surface be smaller than the receding contact angle on an SP-rich one – which, in principle, requires a significant difference in the advancing contact angles on surfaces coated with the two isomers. Accordingly, different approaches have been undertaken in an effort to increase contact angle variation. Locklin *et al.* reported that simply the addition of metal salts to a water droplet lying on a spiropyran-functionalised surface can increase contact angle difference from  $\sim 15^\circ$  to  $\sim 35^\circ$ , as shown in Fig. 18B for a  $\text{Co}^{2+}$  salt.<sup>90</sup> The reason is that under these conditions, the isomerisation takes place between SP and the MC- $\text{Co}^{2+}$  complex as opposed to a free MC – the complex having a more hydrophilic character than the uncomplexed MC. A disadvantage of this approach is that it requires the presence of a dissolved metal salt in the droplet.

An alternative strategy to amplify the change in contact angle is based on the immobilisation of spiropyran onto *rough* surfaces,<sup>370–373</sup> and takes advantage of the well-known lotus effect.<sup>374</sup> SEM images of some such surfaces are shown in Fig. 18C and D, whereby the roughness originates from arrays of silicon nanowires and polymeric nanorods, respectively. It is generally assumed<sup>375</sup> that while the pronounced water-repellent properties of nanostructured *hydrophobic* surfaces originate from the air trapped in the nanopores, the enhanced wettability of the *hydrophilic* ones can be attributed to water penetrating the pores by the capillary action. Fig. 18E demonstrates such enhanced wettability change on porous silicon substrates, with the water contact angle decreasing – reversibly<sup>372</sup> – by as much as  $96^\circ$ . A record value of  $118^\circ$  was reported in a conceptually different system based on a poly(NIPAM-SP) (*cf.* Sections 2.1 and 2.3) copolymer.<sup>373</sup> In the dark, the polymer was rich in the  $\text{MCH}^+$  units and readily hydrated; exposure to visible light, however, generated SP, triggering dehydration of the polymer. The authors then systematically investigated the

effect of substrate morphology, and showed that the transition from flat to microstructured to nanostructured surface increased contact angle difference from  $\sim 24^\circ$  to  $\sim 79^\circ$  to  $\sim 118^\circ$ .<sup>373</sup>

## 5.2. Photocontrol of transport through porous media

The photoswitchable systems discussed in this section are based on inorganic porous materials functionalised with monolayers of spiropyrans, and are complementary to the systems based on organic polymers covered in Section 2.4. Perhaps the simplest of such porous materials is commercial silica gel, which can be readily functionalised with desired monolayers. For example, Kimura *et al.* attached their “crowned spiropyrans” (see Section 2.6) to silica and used the resulting particles as the stationary phase for the separation of alkali metal ions.<sup>376</sup> The binding ability of these modified crown ethers towards metal ions is enhanced by the UV-induced generation of the phenolate group – with the enhancement being metal-dependent. For example,  $\text{Li}^+$  and  $\text{K}^+$  could readily be separated when the chromatography column was exposed to UV light, but virtually no separation was achieved under visible light.<sup>376</sup> A similar setup was employed by Zharov and co-workers, who prepared pads made from densely packed monodisperse,  $\sim 170$  nm silica spheres. These pads were  $\sim 5$   $\mu\text{m}$ -thick (Fig. 19A) and the colloidal spheres comprising them had been derivatised with spiropyran monolayers.<sup>377</sup> The authors monitored the flux of a positively charged redox probe –  $[\text{Ru}(\text{NH}_3)_6]^{3+}$  – by measuring the voltammetric limiting current, with the assumptions that the current is proportional to the flux under steady-state conditions, and that the SP  $\rightarrow$   $\text{MCH}^+$  isomerisation would reduce the flux as a result of the electrostatic repulsion between the positively charged probe and the like-charged porous medium. At a low (1.8) pH, however, the switch existed in the  $\text{MCH}^+$  form irrespective of irradiation, whereas photoisomerisation at pH 6.6 took place between two neutral states (SP  $\leftrightarrow$  MC) – as a consequence, only a minor (albeit reversible; *cf.* Fig. 19B) effect of light on the flux was observed.

Another study from the same group has demonstrated that efficient switching between the neutral SP and the positively charged  $\text{MCH}^+$  states can enable high selectivities of transport of a positively charged probe  $[\text{Fe}(\text{bpy})_3]^{2+}$ . In this case, the setup was based on the glass nanopore electrode, which comprised a Pt disk electrode embedded at the bottom of a conical pore (Fig. 19C). The electrode was immersed in an acidic acetonitrile solution. In order to reach the electrode, the solution molecules had to diffuse through the nanopore orifice whose diameter was in the range of 30–180 nm.<sup>378</sup> The voltammetric response of the channel with the narrowest (30 nm) orifice is shown as a black trace in Fig. 19D and corresponds to diffusion-limited current. This current decreased with UV irradiation (pink trace after 5 minutes), until it was reduced to background levels (red trace after 20 minutes of UV) – under these conditions, the local concentration of the  $\text{MCH}^+$  groups immobilised at the pore orifice was sufficiently high so as prevent any of the like-charged  $[\text{Fe}(\text{bpy})_3]^{2+}$  from crossing the orifice and reaching the electrode. At the same time, visible light (5 min) induced regeneration of the neutral SP, with the faradaic current



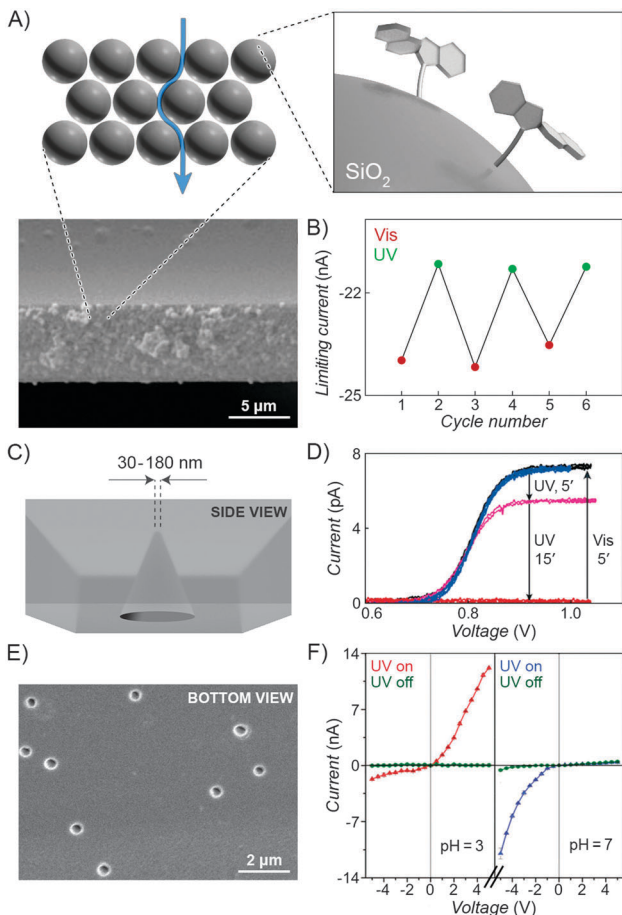


**Fig. 19** Light-controlled transport through porous materials. (A and B) Effect of irradiation on the flux of a charged redox probe through densely packed, spiropyran-functionalised colloidal spheres. (C) Schematic representation of a conical nanopore with spiropyran-functionalised interior. (D) Light-controlled transport through a conical nanopore. Formation of the positively charged  $\text{MCH}^+$  inhibits the flux of a positively charged probe. (E) SEM image showing multiple spiropyran-functionalised nanopores. (F) Ionic current rectification modulated by pH and light. [Adapted with permission from ref. 377 (Copyright 2010 Springer) (A and B), ref. 378 (Copyright 2006 Royal Society of Chemistry) (D) and ref. 379 (Copyright 2012 Wiley-VCH) (E and F)].

reaching the original values (blue trace), and the sequence could be repeated over at least several cycles. This mechanism of transport control based on repulsive electrostatic interactions is supported by three experimental observations, where no light-induced current modulation was observed (i) using small nanopores lacking the spiropyran coating, (ii) using large-diameter ( $4 \mu\text{m}$ ) pores functionalised with spiropyran, and (iii) using small nanopores functionalised with spiropyran in the presence of high concentrations of a strong electrolyte, which screened the surface charge originating from  $\text{MCH}^+$ .<sup>378</sup> In another system, similarly shaped nanochannels functionalised with spiropyran monolayers were shown to act as light- and pH-operated nanofluidic diodes.<sup>379</sup> Depending on whether the surface of nanochannels was positively or negatively charged, they were anion- or cation-selective, respectively. In addition, the conical shape of such charged nanochannels enabled preferential flow of

ions in one direction (from the tip to the base) – that is, absolute values of ionic current at the applied voltage =  $+n$  vs.  $-n$  V were different, resulting in current rectification. Zhai *et al.* functionalised the interiors of conical ( $\sim 350 \text{ nm}$  base – Fig. 19E – and  $\sim 12 \text{ nm}$  tip) nanochannels with a spiropyran monolayer and showed that ionic current under visible light (neutral SP) was, in fact, negligible and independent of pH (Fig. 19F, green traces). When the system was exposed to UV light at pH 3, however, a high current rectification ratio of  $\sim 7$  was observed (Fig. 19F, red trace), which could be attributed to the positively charged  $\text{MCH}^+$  moieties on the channel walls. Interestingly, UV irradiation at pH 7 resulted in an even higher value of rectification ( $\sim 30$ ), with the current flowing in the opposite direction (indicating that cations are the majority carriers). This behaviour could be rationalised by the fact that although the zwitterionic MC groups carry zero net charge, the negatively charged oxygen atoms are more exposed to the solution compared with the positively charged nitrogen atoms (which act as a point of attachment to the nanopore surface).

A conceptually different approach to control transport properties has enabled Smirnov *et al.* to construct light-activated “burst” valves.<sup>380,381</sup> These researchers used mixed monolayers comprising spiropyran and hydrophobic molecules to functionalise nanoporous alumina membranes. In the “off” (SP) state, no transport through the membranes was observed simply because water did not wet the strongly hydrophobic, narrow ( $\sim 20 \text{ nm}$ ) nanopores. Exposure to UV light, however, generated MC and triggered the admission of water to the nanopores and the consequent flow. However, capillary forces prevented the dewetting of the nanopores upon subsequent MC  $\rightarrow$  SP re-isomerisation – therefore, these “burst” valves could be opened, but not resealed using light.<sup>380</sup> Other porous materials which have been functionalised with spiropyran include zeolite L<sup>382</sup> and mesoporous silica.<sup>383–385</sup> The latter material has enabled “on-demand” release of encapsulated dyes upon exposure to UV light.<sup>385</sup>

### 5.3. Photocontrol of binding to surfaces

As discussed in Section 2.6, MC can bind different metal ions with varying strengths, and the distinctive optical properties of the resulting complexes are key to the development of sensing devices. The spiropyran-based systems are unique in their need to be pre-activated with UV light in order to bind metal cations,<sup>386,387</sup> and particularly attractive in that once they have performed their sensing function, they can be “reset” using visible light, to be reused again later. These characteristics have led Diamond *et al.* to propose the concept of *remotely activatable* colorimetric sensors,<sup>388</sup> which are normally in their “passive” state, but can be “turned on” at will – when the measurement is required.<sup>389</sup> This ability to activate and deactivate sensors “on demand” can significantly increase their lifetime. In order to develop practical sensing devices, however, it is necessary to immobilise spiropyrans onto solid supports. Fig. 20A, for example, shows spiropyran-functionalised glass slides that, having been pre-activated with UV, were exposed to



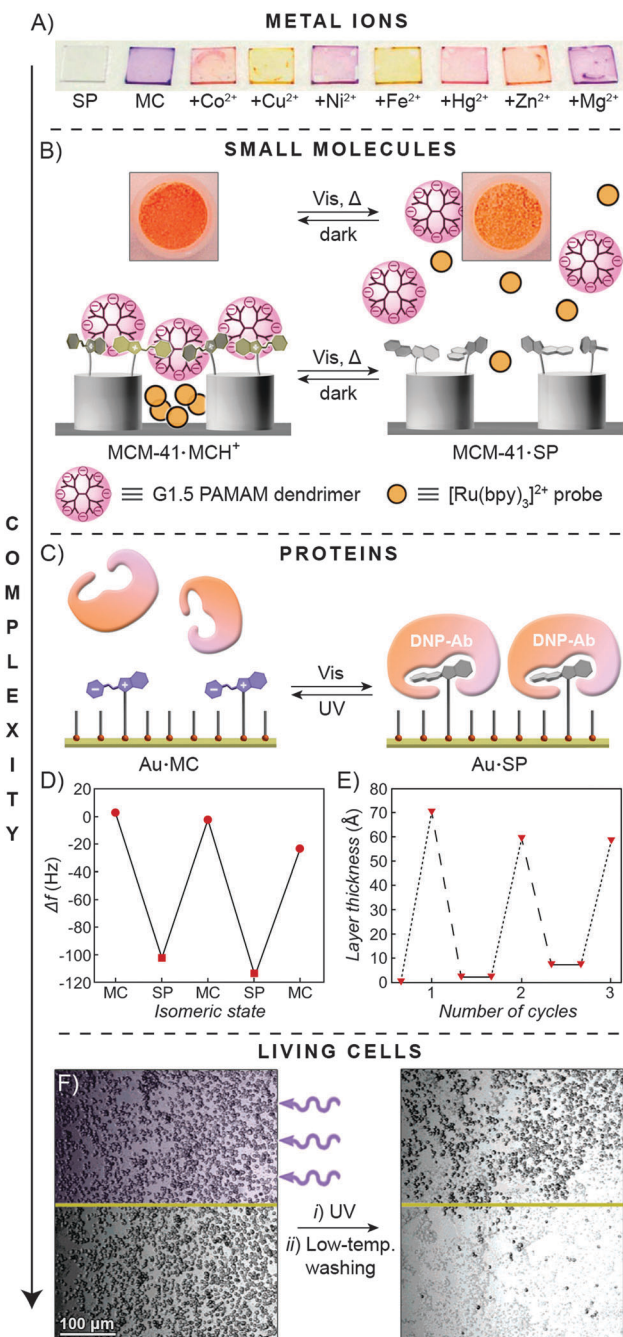


**Fig. 20** Light-controlled adsorption to spiropyran-functionalised surfaces. (A) Glass slides functionalised with a spiropyran polymer brush before (SP) and after (MC) irradiation with UV light, and after exposure of the latter to a series of metal ions. (B)  $\text{MCH}^+$   $\rightarrow$  SP transformation cancels out the electrostatic interactions between the positively charged surface of a mesoporous material and negatively charged dendrimers, triggering dye release. (C) Light-controlled adsorption of the anti-DNP antibody onto a spiropyran-functionalised surface. (D) Following reversible adsorption of the anti-DNP Ab using quartz crystal microbalance analysis. (E) Following reversible adsorption of the same antibody onto an SP-functionalised surface by means of surface plasmon resonance. Dotted lines = addition of the anti-DNP Ab. Dashed lines = exposure to UV followed by rinsing. (F) Site-selective cell release from areas not exposed to UV. [Adapted with permission from ref. 435 (Copyright 2008 Royal Society of Chemistry) (A), ref. 394 (Copyright 2007 Wiley-VCH) (B), ref. 397 (Copyright 1997 American Chemical Society) (D), ref. 398 (Copyright 1999 American Chemical Society) (E) and ref. 403 (Copyright 2005 American Chemical Society) (F).]

a series of divalent metal cations, giving rise to differently coloured complexes. Metal cations can then be released from the surfaces and recaptured over multiple cycles using visible and UV light, respectively.<sup>390</sup> Interestingly, capturing of metal ions on the surfaces of MC-decorated *electrodes* could be followed by electrochemical reduction – giving rise to the corresponding metallic NPs, as was shown for silver<sup>391,392</sup> and cobalt.<sup>393</sup> Although the resulting metallic layers could not be released upon exposure to visible light, they readily redissolved upon electrooxidation. This method has enabled high-resolution patterning of electrode surfaces, with the smallest feature sizes on the order of only a few micrometers.<sup>392,393</sup>

On the other hand, immobilised  $\text{MCH}^+$  groups can interact electrostatically and bind various negatively charged molecules. These interactions were explored for the construction of a light-activated release system shown in Fig. 20B.<sup>394</sup> In this design, mesoporous silica MCM-41 was surface-functionalised with  $\text{MCH}^+$ , which bound negatively charged generation 1.5 poly(amidoamine) (PAMAM) dendrimers from solution. With their fairly large molecular sizes ( $\sim 2.8$  nm), the dendrimers acted as “stoppers” for MCM-41’s nanopores (diameter  $\sim 2.1$  nm) pre-loaded with an optically active  $[\text{Ru}(\text{bpy})_3]^{2+}$  “cargo” (Fig. 20B, left). The release of the probe could be triggered upon exposing the system to visible light, which generated the SP isomer and cancelled the attractive interactions between the surfaces and the dendritic “plugs” (Fig. 20B, right). To increase the specificity of binding beyond electrostatic interactions, Willner *et al.* performed electropolymerisation of 4-thioaniline anchored to the surfaces of gold NPs co-functionalised with spiropyran, in the presence of a small-molecule template *N,N'*-bis(3-sulfatopropyl)-4,4'-bipyridinium. The affinity of the resulting NP “sponges” to the template molecule could be controlled using both optical and electrical stimuli.<sup>395</sup> Larger molecules can also be reversibly adsorbed onto surfaces – the same authors found that spiropyran bearing two  $\text{NO}_2$  groups (dinitrospiropyran) can act as an antigen for the anti-dinitrophenol (anti-DNP) antibody (AB) when it exists in the closed – but not in the open – form (Fig. 20C). Accordingly, gold surfaces functionalised with dinitrospiropyran monolayers could capture and release this specific AB,<sup>396</sup> and the reversibility of the process was confirmed by quartz crystal microbalance analysis (Fig. 20D)<sup>397</sup> as well as by surface plasmon resonance (Fig. 20E)<sup>398</sup> and impedance<sup>399</sup> spectroscopies.

The complexity of the species whose reversible adsorption onto spiropyran-decorated surfaces has been demonstrated ranges from metal ions through small molecules through proteins, all the way to living cells. Higuchi and co-workers investigated interactions between mesenchymal stem cells and glass plates coated with a PMMA-based copolymer comprising spiropyran as a function of UV light.<sup>400</sup> Irradiation with low-intensity UV light released  $\sim 90\%$  of the cells originally adhering to the surface, almost all of which remained alive. Control experiments with analogous surfaces lacking spiropyran confirmed that the release was indeed due to the generation of MC as opposed to the direct interaction of the cells with UV light. It is interesting to point out that the same trend was observed in

experiments aimed at investigating interactions at a single molecule level; in a recent study,<sup>401</sup> AFM tips functionalised with fibronectin – a protein involved in mediating cell adhesion – were interfaced with spiropyran-decorated polymers, and the adhesion forces were measured under UV and visible irradiation. As expected, the adhesion force of the protein to the SP-rich surfaces was higher (by ~50%) than to the MC-rich ones.

Interestingly, surfaces exhibiting the opposite effect – that is, adhesion of cells to the UV-irradiated locations – have also been developed. This design is based on previous studies<sup>402</sup> which found that the adhesion of cells to the thermoresponsive PNIPAM is dramatically reduced upon dehydration of the polymer (that is, above the LCST). With the possibility to modulate the LCST of poly(NIPAM-SP) using light (compare Sections 2.1 and 2.3), Sumaru *et al.* employed this photoresponsive copolymer as the key component of “photoresponsive cell culture surfaces” (PRCS).<sup>403–405</sup> The behaviour of a PRCS is demonstrated in Fig. 20F, whereby the upper half of the sample was exposed to UV light. Subsequent washing at a lower temperature  $T$ , such that  $LCST_{poly(NIPAM-MC)} < T < LCST_{poly(NIPAM-SP)}$ , removed CHO-K1 cells selectively from the non-irradiated area. An important advantage of using light to promote/inhibit cell adhesion is that it enables patterning of surfaces with cells with high spatial precision.<sup>403,405</sup>

#### 5.4. Photocontrol of electrochemical properties

Light-induced adsorption of various species onto surfaces as discussed in the previous section results in decreased contact of solution molecules with the surface. This has some interesting implications: consider, for example, the possibility of employing light to affect the communication of solubilised redox probes with the surfaces of *electrodes* – such control could be used as a way to *modulate the electrode potential using light*. A variety of such “smart electrodes” based on spiropyran-functionalised surfaces have been developed by Willner and co-workers, and are the focus of this section.

The binding of the anti-DNP antibody to SP-functionalised electrodes insulates the electrochemically active surface from the molecules in the solution. An example is shown in Fig. 21B, where the originally high amperometric signal, corresponding to reversible  $[Fe(CN)_6]^{3-}/[Fe(CN)_6]^{4-}$  conversion on an MC-decorated electrode, gradually decreased upon exposure to visible light in the presence of the anti-DNP AB. A near-complete loss of electrochemical activity was observed after 16 min of irradiation. The activity of thus-generated AB-insulated SP-electrode was partially restored upon subsequent irradiation with UV – a process which regenerated a surface coated with the MC isomer, to which the anti-DNP AB did not bind.<sup>406</sup> Similarly, reversible passivation of electrodes with the same AB controlled the rate of oxidation of catechols to quinones.<sup>407</sup>

Light-controlled electrode insulation could also be transduced into *amplified* amperometric responses. Here, the electrodes were reversibly protected from molecules acting as electrocatalysts for a model reaction. An example of this concept is provided by the same SP-functionalised electrodes interfaced with ferrocene-modified GOX.<sup>397</sup> Trace (i) in Fig. 21C indicates high electrocatalytic current resulting from the efficient GOX-catalysed oxidation of glucose

enabled by an effective communication between the enzyme and the SP-coated electrode. Addition of the anti-DNP antibody blocked the access to the electrode and suppressed the catalytic process (Fig. 21C, trace (ii)). When the AB was introduced to the same system having the electrode coated with the MC isomer, minute changes in the electrocatalytic current were seen (trace (iii) vs. (iv) in Fig. 21C). Moreover, the process showed good reversibility – the current at 0.4 V oscillated between ~0.5  $\mu$ A

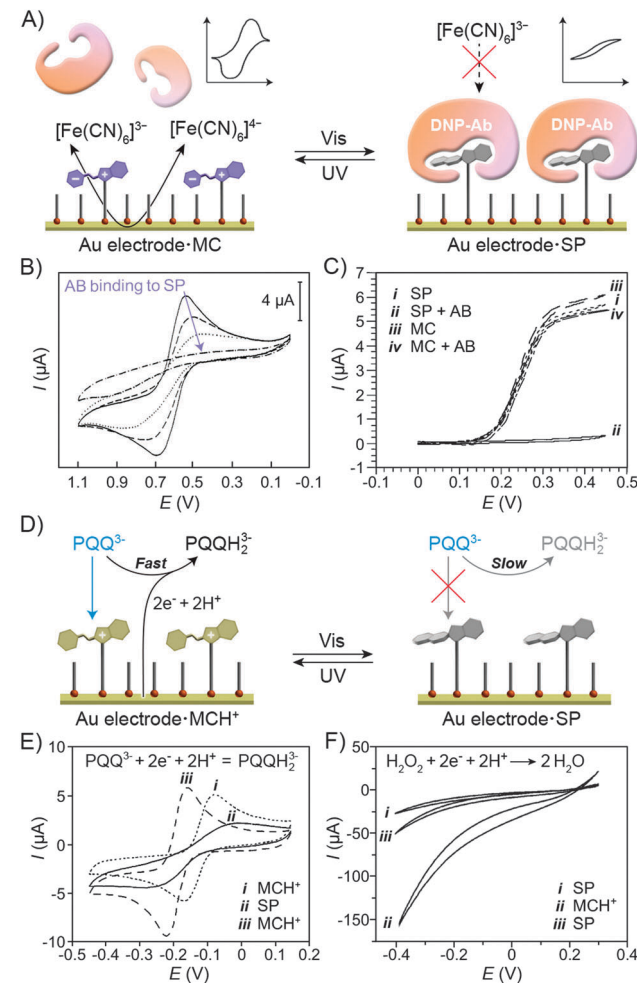


Fig. 21 Modulation of electrochemical properties of electrodes using light. (A) Reversible electrode insulation from redox-active molecules in the solution. (B) Gradual changes (see the arrow) in cyclic voltammograms of an SP-functionalised electrode in the presence of  $[Fe(CN)_6]^{3-}$  following the addition of the anti-DNP Ab. (C) Electrocatalytic currents for glucose oxidation in the presence of an SP/MCH<sup>+</sup>-coated electrode in the presence and in the absence of the anti-DNP Ab. (D) Photocontrol of the Frumkin effect: negatively charged species are attracted to the MCH<sup>+</sup>-functionalised electrode, facilitating the redox reactions (left). No such acceleration takes place on a neutral electrode (right). (E) Cyclic voltammograms of a spiropyran-functionalised electrode in the presence of PQQ before (i) and after (ii) exposure to visible light, and after thermal treatment (iii). (F) Electrocatalytic current for  $H_2O_2$  reduction in the presence of (i) SP- and (ii) MCH<sup>+</sup>-coated electrodes, and after exposure of the latter electrode to visible light (iii). [Adapted with permission from ref. 406 (Copyright 1994 Royal Society of Chemistry) (B), ref. 397 (Copyright 1997 American Chemical Society) (C), ref. 411 (Copyright 1995 Wiley-VCH) (E), ref. 416 (Copyright 2007 American Chemical Society) (F).]



and 5  $\mu$ A upon treatment with UV and Vis light. Unfortunately, the UV-released AB remained adsorbed on the electrode surface following the SP  $\rightarrow$  MC isomerisation, and had to be washed off in order for high electrocatalytic activity to be regained.<sup>408</sup>

The second mode of regulating the properties of electrodes using light explores the so-called Frumkin effect<sup>409</sup> – that is, the dependence of electrochemical reaction kinetics on the surface charge of the electrodes. With their ability to switch surface charge upon exposure to light, spiropyran-decorated electrodes provide an ideal platform for studying the Frumkin effect. Pyrroloquinoline quinone (PQQ<sup>3-</sup>), for example, is a widely used redox probe bearing three negative charges at pH 7; as such, it is expected to exhibit attractive electrostatic interactions with MCH<sup>+</sup>-decorated electrodes, resulting in efficient interfacial electron transfer,<sup>410</sup> as manifested, for example, by the dashed and dotted lines in Fig. 21E. Electrochemical reduction of PQQ<sup>3-</sup> is blocked, however, after exposing the electrode to visible light, as the resulting SP-coated electrode loses its ability to electrostatically interact with the probe (solid line in Fig. 21E).<sup>411</sup> The electrochemical activity could be restored by thermal regeneration of the open-ring isomer. Interestingly, the positive surface charge of the MCH<sup>+</sup>-coated electrodes allowed for the selection of substrates from the solution based on their net charge. For example, electrooxidation was accomplished selectively on the negatively charged (3,4-dihydroxyphenyl)acetate in the presence of the positively charged protonated dopamine.<sup>407</sup> When functionalised with the SP isomer, however, the electrode did not discriminate between these two catechols.

Apart from charged redox-active substrates, the light-controlled Frumkin effect has also been demonstrated for charged (i) electron transfer mediators, (ii) cofactors, (iii) enzymes, and (iv) catalytic NPs. First, glucose oxidase (GOX) reconstituted on the electrode surface was used to catalyse oxidation of glucose to gluconic acid in the presence of a positively charged electron relay.<sup>412</sup> When the electrode was co-functionalised with MCH<sup>+</sup> moieties, the reaction was significantly slowed down on account of electrostatic repulsions between the electron transfer mediator and the like-charged surface. Isomerisation to SP increased the electrocatalytic current by over ten fold.<sup>412</sup> Second, PQQ covalently attached to the electrode surface acted as an electrocatalyst for the oxidation of nicotinamide adenine dinucleotide phosphate (NADPH). This reaction required the presence of the Ca<sup>2+</sup> “cofactor”, whose complexation by PQQ could be regulated by the state of spiropyran co-adsorbed with PQQ as a mixed SAM.<sup>319,410</sup> While the SP isomer did not affect the reaction kinetics, Ca<sup>2+</sup> was repelled from the MCH<sup>+</sup>-decorated monolayer and, as a consequence, the electrocatalysed oxidation was slowed down.

Third, the same principle was used to control the interaction of the positively charged enzyme Cyt *c* with spiropyran-functionalised electrodes. Under visible light, efficient electron transfer between the SP-coated electrode and Cyt *c* took place, enabling inter-protein electron transfer to cytochrome *c* oxidase (COX), which catalysed the oxygen reduction reaction (ORR).<sup>413</sup> The ORR was nearly completely shut down, however, upon

isomerisation to the MCH<sup>+</sup>-electrode. The reversible reduction of Cyt *c* was also coupled to a bioelectrocatalysed reduction: here, the reduced Cyt *c* was used to activate lactate dehydrogenase towards the reduction of lactate to pyruvate.<sup>414</sup> The opposite effect – that is, attraction of a negatively charged protein to an MCH<sup>+</sup>-electrode – has also been described and is exemplified by UV light-accelerated glucose oxidation catalysed by the negatively charged GOX appended with a ferrocene relay unit.<sup>415</sup> Fourth, 20–30 nm platinum NPs have been employed as electrocatalysts for the reduction of H<sub>2</sub>O<sub>2</sub> (Fig. 21F). Stabilised with the citrate anions, these NPs carried substantial negative charge, favouring their interaction with the positively charged MCH<sup>+</sup>-coated electrodes. Consequently, enhanced electrocatalytic current was observed under UV irradiation (Fig. 21F).<sup>416</sup>

### 5.5. Photocontrol of other surface properties

Other creative implications of isomerisation of immobilised spiropyrans are being reported; Thomas *et al.*, for example, investigated contact electrification between steel and spiropyran polymers.<sup>417</sup> In these experiments, steel spheres were rolled on spiropyran-functionalised surfaces, and the charges developing on the spheres were monitored. The most interesting result was found for a copolymer of spiropyran methacrylate and 4-fluorostyrene: while the spheres charged positively on poly(SP), the direction of charge transfer on poly(MC) was reversed. In an elegant experiment, the authors UV-irradiated a positively charged (+160 pC) sphere rolling on poly(SP) and observed a gradual decrease of charge down to -160 pC within 100 s of irradiation. Finally, some efforts have been devoted to the concept of aligning liquid crystal molecules using the underlying spiropyran-functionalised surfaces;<sup>418–420</sup> however, experimental realisation of the concept has yet to be demonstrated.<sup>421</sup>

## 6. Conclusions and outlook

Reversible isomerisation of spiropyrans was first reported as early as 1952.<sup>422</sup> Six decades later, a resurgence of interest in this molecular switch has been prompted by advances in controlled polymerisation reactions and other synthetic methods, the ever-improving capabilities of high-resolution imaging and spectroscopy techniques, and – most of all – an emerging focus on dynamic materials. This review has discussed a variety of dynamic materials resulting from covalent immobilisation of spiropyran onto the following types of organic and inorganic supports: polymer chains, biomacromolecules, inorganic nanoparticles, and solid surfaces. The resulting materials often have fascinating properties whereby the support affects the properties of the switch, and – more importantly – *vice versa*: spiropyran isomerisation can control the emission of quantum dots, folding of polypeptides, and the dimensions of polymeric micelles, among many other properties. Potential applications are well within reach and include reusable sensors, high-resolution imaging in biological samples and the detection and mapping of mechanical stresses.

What more can we expect in the decade to come? The superb fatigue resistance of properly immobilised spiropyrans<sup>127</sup> can



enable the realisation of information storage devices and holographic optical materials.<sup>423,424</sup> In this context, the strong dependence of the isomerisation kinetics on the microenvironment is particularly attractive, as it can allow for tuning of the information storage time.<sup>425</sup> An ambitious challenge that has yet to be addressed is the reversible control of the remarkable physical properties of graphene by means of isomerisation of surface-immobilised spirobifluorophanes. The development of such hybrid materials could take advantage of earlier studies<sup>426–428</sup> in which spirobifluorophane was covalently attached to the surfaces of carbon nanotubes. Another direction is the development of materials which are responsive to multiple external stimuli in an orthogonal fashion. Here, the state-of-the-art is represented by a triblock copolymer designed to self-assemble in response to (i) light, (ii) pH, (iii) metal ions, and (iv) thermal treatment (“quadrupole responsiveness”).<sup>162</sup> But, arguably, the most room for creativity lies in the derivatisation of biological systems. Here, studies aimed at structural modification of the parent spirobifluorophane to increase its stability in aqueous media are ongoing.<sup>429</sup> Of particular importance is the ability to place the spirobifluorophane units at precise locations within the protein structures. In one elegant example, the chaperonin GroEL was equipped with spirobifluorophane groups selectively at the portal regions; this functionalisation enabled self-assembly of individual GroEL units into one-dimensional supramolecular polymers.<sup>430</sup> Spirobifluorophane has several important advantages over the structurally simpler azobenzene (whose applications in biological systems are also emerging<sup>431,432</sup>) – most notably, isomerisation can be accomplished using NIR light and its yield can be near-quantitative in both directions. The ultimate goal would be to use light in order to control various biological processes within living organisms in a spatiotemporal fashion.

## Abbreviations

AB	Antibody
AIBN	Azobisisobutyronitrile
ATRP	Atom transfer radical polymerisation
bpy	Bipyridyl
CD	Circular dichroism
CHROBA	Chromism-based assay
COX	Cytochrome <i>c</i> oxidase
CS	Citrate synthase
Cyt <i>c</i>	Cytochrome <i>c</i>
DLS	Dynamic light scattering
DNP	2,4-Dinitrophenyl
FRET	Fluorescence resonance energy transfer
GOX	Glucose oxidase
HRP	Horseradish peroxidase
LCST	Lower critical solution temperature
MC	Mero (“open”) form of spirobifluorophane
MMA	Methyl methacrylate
MscL	Mechanosensitive channel of large conductance
MTHF	2-Methyltetrahydrofuran
NAD	Nicotinamide adenine dinucleotide

NBD	Nitrobenzoxadiazolyl
NIPAM	<i>N</i> -Isopropylacrylamide
NIR	Near-infrared
NP	Nanoparticle
ORR	Oxygen reduction reaction
PAMAM	Poly(amidoamine)
PDEGMMA	Poly(2-(2-methoxyethoxy)ethyl methacrylate)
PDMA	Poly( <i>N,N</i> -dimethylacrylamide)
PDMAEMA	Poly(2-(dimethylamino)ethyl methacrylate)
PEG	Poly(ethylene glycol)
PES	Polyethersulfone
PFBT	Poly(fluorenyl- <i>co</i> -benzothiadiazole)
PMA	Poly(methyl acrylate)
PMMA	Poly(methyl methacrylate)
PNIPAM	Poly( <i>N</i> -isopropylacrylamide)
PPE	Poly(2,5-dialkylphenylene-1,4-ethynylene)
PQQ	Pyrroloquinoline quinone
PRCS	Photoresponsive cell culture surface
PTFE	Polytetrafluoroethylene
PULSAR	Photoactuated unimolecular logical switching-attained reconstruction
QD	Quantum dot
SAM	Self-assembled monolayer
SEM	Scanning electron microscopy
SET-LRP	Single-electron transfer living radical polymerisation
SFG	Sum frequency generation
SP	Spiro (“closed”) form of spirobifluorophane
THF	Tetrahydrofuran
UNC	Upconverting nanocrystal
UV	Ultraviolet light
Vis	Visible light

## Acknowledgements

This work was supported by the Israel Science Foundation (grant no. 1463/11). The author acknowledges Dr S. Das and Mr K. Livanov for performing the initial literature search, and Dr E. M. Schuster for critical reading of the manuscript.

## References

- 1 *Stress Response in Microbiology*, ed. J. M. Requena, Calster Academic Press, Norfolk, UK, 2012.
- 2 M. Stevens and S. Merilaita, *Philos. Trans. R. Soc. London, Ser. B*, 2009, **364**, 423–427.
- 3 J. Aizenberg, A. Tkachenko, S. Weiner, L. Addadi and G. Hendl, *Nature*, 2001, **412**, 819–822.
- 4 M. Ballerini, N. Calibbo, R. Candeleir, A. Cavagna, E. Cisbani, I. Giardina, V. Lecomte, A. Orlandi, G. Parisi, A. Procaccini, M. Viale and V. Zdravkovic, *Proc. Natl. Acad. Sci. U. S. A.*, 2008, **105**, 1232–1237.
- 5 M. Fialkowski, K. J. M. Bishop, R. Klajn, S. K. Smoukov, C. J. Campbell and B. A. Grzybowski, *J. Phys. Chem. B*, 2006, **110**, 2482–2496.



6 A. Grinthal and J. Aizenberg, *Chem. Soc. Rev.*, 2013, **42**, 7072–7085, DOI: 10.1039/c3cs60045a.

7 M.-M. Russew and S. Hecht, *Adv. Mater.*, 2010, **22**, 3348–3360.

8 C. Roche and V. Percec, *Isr. J. Chem.*, 2013, **53**, 30–44.

9 R. Klajn, J. F. Stoddart and B. A. Grzybowski, *Chem. Soc. Rev.*, 2010, **39**, 2203–2237.

10 S. Das, P. Ranjan, P. S. Maiti, G. Singh, G. Leitus and R. Klajn, *Adv. Mater.*, 2013, **25**, 422–426.

11 M. Irie, *Chem. Rev.*, 2000, **100**, 1685–1716.

12 R. Klajn, K. J. M. Bishop and B. A. Grzybowski, *Proc. Natl. Acad. Sci. U. S. A.*, 2007, **104**, 10305–10309.

13 M. Yamada, M. Kondo, J.-i. Mamiya, Y. Yu, M. Kinoshita, C. J. Barrett and T. Ikeda, *Angew. Chem., Int. Ed.*, 2008, **47**, 4986–4988.

14 O. Chovnik, R. Balgley, J. R. Goldman and R. Klajn, *J. Am. Chem. Soc.*, 2012, **134**, 19564–19567.

15 R. Klajn, K. J. M. Bishop, M. Fialkowski, M. Paszewski, C. J. Campbell, T. P. Gray and B. A. Grzybowski, *Science*, 2007, **316**, 261–264.

16 R. Klajn, K. P. Browne, S. Soh and B. A. Grzybowski, *Small*, 2010, **6**, 1385–1387.

17 H. M. D. Bandara and S. C. Burdette, *Chem. Soc. Rev.*, 2012, **41**, 1809–1825.

18 J. Henzl, M. Mehlhorn, H. Gawronski, K. H. Rieder and K. Morgenstern, *Angew. Chem., Int. Ed.*, 2006, **45**, 603–606.

19 W. Fuss, C. Kosmidis, W. E. Schmid and S. A. Trushin, *Angew. Chem., Int. Ed.*, 2004, **43**, 4178–4182.

20 J. Zhang, J. K. Whitesell and M. A. Fox, *Chem. Mater.*, 2001, **13**, 2323–2331.

21 V. I. Minkin, *Chem. Rev.*, 2004, **104**, 2751–2776.

22 G. Berkovic, V. Krongauz and V. Weiss, *Chem. Rev.*, 2000, **100**, 1741–1753.

23 R. Guglielmetti, in *Photochromism: Molecules and Systems*, ed. H. Durr and H. Bouas-Laurent, Elsevier, Amsterdam, 2003, pp. 314–466.

24 R. C. Bertelson, in *Organic Photochromic and Thermochromic Compounds*, vol. 1, Main Photochromic Families, ed. J. C. Crano and R. J. Guglielmetti, Kluwer Academic Publishers, 2002, pp. 11–83.

25 K. Matsuda and M. Irie, *J. Photochem. Photobiol. C*, 2004, **5**, 169–182.

26 T. Kudernac, S. J. van der Molen, B. J. van Wees and B. L. Feringa, *Chem. Commun.*, 2006, 3597–3599.

27 Y. Chen, C. M. Wang, M. G. Fan, B. L. Yao and N. Menke, *Opt. Mater.*, 2004, **26**, 75–77.

28 B. Heinz, S. Malkmus, S. Laimgruber, S. Dietrich, C. Schulz, K. Rueck-Braun, M. Braun, W. Zinth and P. Gilch, *J. Am. Chem. Soc.*, 2007, **129**, 8577–8584.

29 N. Koumura, R. W. J. Zijlstra, R. A. van Delden, N. Harada and B. L. Feringa, *Nature*, 1999, **401**, 152–155.

30 P. Zhao, C. F. Fang, C. J. Xia, Y. M. Wang, D. S. Liu and S. J. Xie, *Appl. Phys. Lett.*, 2008, **93**, 013113.

31 M. R. di Nunzio, P. L. Gentili, A. Romani and G. Favaro, *ChemPhysChem*, 2008, **9**, 768–775.

32 Y.-C. Jeong, D. G. Park, I. S. Lee, S. I. Yang and K.-H. Ahn, *J. Mater. Chem.*, 2009, **19**, 97–103.

33 R. Klajn, *Pure Appl. Chem.*, 2010, **82**, 2247–2279.

34 A. Setaro, P. Bluemmel, C. Maity, S. Hecht and S. Reich, *Adv. Funct. Mater.*, 2012, **22**, 2425–2431.

35 A. R. Jang, E. K. Jeon, D. Kang, G. Kim, B. S. Kim, D. J. Kang and H. S. Shin, *ACS Nano*, 2012, **6**, 9207–9213.

36 P. Joo, B. J. Kim, E. K. Jeon, J. H. Cho and B.-S. Kim, *Chem. Commun.*, 2012, **48**, 10978–10980.

37 A. Fontcuberta i Morral and F. Stellacci, *Nat. Mater.*, 2012, **11**, 272–273.

38 N. W. Tyer and R. S. Becker, *J. Am. Chem. Soc.*, 1970, **92**, 1289–1294.

39 M. Moniruzzaman, C. J. Sabey and G. F. Fernando, *Polymer*, 2007, **48**, 255–263.

40 H. Gorner, *Phys. Chem. Chem. Phys.*, 2001, **3**, 416–423.

41 S. A. Krysanov and M. V. Alfimov, *Chem. Phys. Lett.*, 1982, **91**, 77–80.

42 Z. Y. Tian, W. W. Wu, W. Wan and A. D. Q. Li, *J. Am. Chem. Soc.*, 2011, **133**, 16092–16100.

43 J. T. C. Wojtyk, A. Wasey, P. M. Kazmaier, S. Hoz and E. Buncel, *J. Phys. Chem. A*, 2000, **104**, 9046–9055.

44 M. Irie, A. Menju and K. Hayashi, *Macromolecules*, 1979, **12**, 1176–1180.

45 C. Lenoble and R. S. Becker, *J. Phys. Chem.*, 1986, **90**, 62–65.

46 D. A. Parthenopoulos and P. M. Rentzepis, *Science*, 1989, **245**, 843–845.

47 S. O. Konorov and A. M. Zheltikov, *Opt. Express*, 2003, **11**, 2440–2445.

48 O. Ivashenko, J. T. van Herpt, B. L. Feringa, P. Rudolf and W. R. Browne, *Langmuir*, 2013, **29**, 4290–4297.

49 M. C. George, A. Mohraz, M. Piech, N. S. Bell, J. A. Lewis and P. V. Braun, *Adv. Mater.*, 2009, **21**, 66–70.

50 A. S. Dvornikov, J. Malkin and P. M. Rentzepis, *J. Phys. Chem.*, 1994, **98**, 6746–6752.

51 J. Whelan, D. Abdallah, J. Wojtyk and E. Buncel, *J. Mater. Chem.*, 2010, **20**, 5727–5735.

52 S. Swansburg, E. Buncel and R. P. Lemieux, *J. Am. Chem. Soc.*, 2000, **122**, 6594–6600.

53 X. Q. Song, J. W. Zhou, Y. T. Li and Y. W. Tang, *J. Photochem. Photobiol. A*, 1995, **92**, 99–103.

54 R. Rosario, D. Gust, M. Hayes, J. Springer and A. A. Garcia, *Langmuir*, 2003, **19**, 8801–8806.

55 S. R. Keum, S. J. Roh, S. M. Ahn, S. S. Lim, S. H. Kim and K. Koh, *Dyes Pigm.*, 2007, **74**, 343–347.

56 K. Patel, A. Castillo-Muzquiz and M. C. Biewer, *Tetrahedron Lett.*, 2002, **43**, 5933–5935.

57 S. R. Keum, M. S. Hur, P. M. Kazmaier and E. Buncel, *Can. J. Chem.*, 1991, **69**, 1940–1947.

58 J. W. Zhou, Y. T. Li, Y. W. Tang, F. Q. Zhao, X. Q. Song and E. C. Li, *J. Photochem. Photobiol. A*, 1995, **90**, 117–123.

59 L. Florea, A. Hennart, D. Diamond and F. Benito-Lopez, *Sens. Actuators, B*, 2012, **175**, 92–99.

60 L. Florea, A. McKeon, D. Diamond and F. Benito-Lopez, *Langmuir*, 2013, **29**, 2790–2797.



61 Q. Shen, Y. Cao, S. Liu, M. L. Steigerwald and X. Guo, *J. Phys. Chem. C*, 2009, **113**, 10807–10812.

62 M. Levitus, G. Glasser, D. Neher and P. F. Aramendia, *Chem. Phys. Lett.*, 1997, **277**, 118–124.

63 M. Bletz, U. Pfeifer-Fukumura, U. Kolb and W. Baumann, *J. Phys. Chem. A*, 2002, **106**, 2232–2236.

64 H. Gruler, R. Vilanove and F. Rondelez, *Phys. Rev. Lett.*, 1980, **44**, 590–592.

65 R. Vilanove, H. Hervet, H. Gruler and F. Rondelez, *Macromolecules*, 1983, **16**, 825–831.

66 I. Panaiotov, S. Taneva, A. Bois and F. Rondelez, *Macromolecules*, 1991, **24**, 4250–4254.

67 J. Chen, F. Zeng and S. Z. Wu, *ChemPhysChem*, 2010, **11**, 1036–1043.

68 M. Q. Zhu, L. Y. Zhu, J. J. Han, W. W. Wu, J. K. Hurst and A. D. Q. Li, *J. Am. Chem. Soc.*, 2006, **128**, 4303–4309.

69 Y. Wu, X. Z. Qu, L. Y. Huang, D. Qiu, C. L. Zhang, Z. P. Liu, Z. Z. Yang and L. Feng, *J. Colloid Interface Sci.*, 2010, **343**, 155–161.

70 A. A. Garcia, S. Cherian, J. Park, D. Gust, F. Jahnke and R. Rosario, *J. Phys. Chem. A*, 2000, **104**, 6103–6107.

71 D. D. Perrin, B. Dempsey and E. P. Serjeant, *Prediction for Organic Acids and Bases*, Chapman and Hall, London, 1981.

72 R. A. Hall, P. J. Thistlethwaite and F. Grieser, *Langmuir*, 1994, **10**, 3743–3748.

73 K. Sumaru, M. Kameda, T. Kanamori and T. Shinbo, *Macromolecules*, 2004, **37**, 4949–4955.

74 C. D. Bain and G. M. Whitesides, *Langmuir*, 1989, **5**, 1370–1378.

75 F. M. Raymo and S. Giordani, *J. Am. Chem. Soc.*, 2001, **123**, 4651–4652.

76 J. T. C. Wojtyk, A. Wasey, N. N. Xiao, P. M. Kazmaier, S. Hoz, C. Yu, R. P. Lemieux and E. Buncel, *J. Phys. Chem. A*, 2007, **111**, 2511–2516.

77 S. R. Keum, K. B. Lee, P. M. Kazmaier and E. Buncel, *Tetrahedron Lett.*, 1994, **35**, 1015–1018.

78 R. Rosario, D. Gust, M. Hayes, F. Jahnke, J. Springer and A. A. Garcia, *Langmuir*, 2002, **18**, 8062–8069.

79 K. Wagner, R. Byrne, M. Zanoni, S. Gambhir, L. Dennany, R. Breukers, M. Higgins, P. Wagner, D. Diamond, G. G. Wallace and D. L. Officer, *J. Am. Chem. Soc.*, 2011, **133**, 5453–5462.

80 D. S. Tipikin, *Russ. J. Phys. Chem.*, 2001, **75**, 1720–1722.

81 Y. Shiraishi, M. Itoh and T. Hirai, *Phys. Chem. Chem. Phys.*, 2010, **12**, 13737–13745.

82 J. Ratner, N. Kahana, A. Warshawsky and V. Krongauz, *Ind. Eng. Chem. Res.*, 1996, **35**, 1307–1315.

83 K. Kinashi, S. Nakamura, Y. Ono, K. Ishida and Y. Ueda, *J. Photochem. Photobiol. A*, 2010, **213**, 136–140.

84 K. Kinashi, S. Nakamura, M. Imamura, K. Ishida and Y. Ueda, *J. Phys. Org. Chem.*, 2012, **25**, 462–466.

85 P. Calero, E. Aznar, J. M. Lloris, M. D. Marcos, R. Martinez-Manez, J. V. Ros-Lis, J. Soto and F. Sancenon, *Chem. Commun.*, 2008, 1668–1670.

86 J. Allouche, A. Le Beulze, J.-C. Dupin, J.-B. Ledeuil, S. Blanc and D. Gonbeau, *J. Mater. Chem.*, 2010, **20**, 9370–9378.

87 J. Sunamoto, K. Iwamoto, M. Akutagawa, M. Nagase and H. Kondo, *J. Am. Chem. Soc.*, 1982, **104**, 4904–4907.

88 I. Shimizu, H. Kokado and E. Inoue, *Bull. Chem. Soc. Jpn.*, 1969, **42**, 1730–1734.

89 C. P. McCoy, L. Donnelly, D. S. Jones and S. P. Gorman, *Tetrahedron Lett.*, 2007, **48**, 657–661.

90 S. Samanta and J. Locklin, *Langmuir*, 2008, **24**, 9558–9565.

91 V. A. Krongauz and E. S. Goldburt, *Nature*, 1978, **271**, 43–45.

92 T. Seki, K. Ichimura and E. Ando, *Langmuir*, 1988, **4**, 1068–1069.

93 H. Tachibana, Y. Yamanaka, H. Sakai, M. Abe and M. Matsumoto, *J. Lumin.*, 2000, **87–89**, 800–802.

94 P. Uznanski, *Synth. Met.*, 2000, **109**, 281–285.

95 Y. Unuma and A. Miyata, *Thin Solid Films*, 1989, **179**, 497–502.

96 E. Ando, J. Miyazaki, K. Morimoto, H. Nakahara and K. Fukuda, *Thin Solid Films*, 1985, **133**, 21–28.

97 I. Cabrera, F. Shvartsman, O. Veinberg and V. Krongauz, *Science*, 1984, **226**, 341–343.

98 I. Cabrera and V. Krongauz, *Macromolecules*, 1987, **20**, 2713–2717.

99 E. Goldburt and V. Krongauz, *Macromolecules*, 1986, **19**, 246–247.

100 E. Goldburt, F. Shvartsman, S. Fishman and V. Krongauz, *Macromolecules*, 1984, **17**, 1225–1230.

101 H. Tomioka and T. Itoh, *J. Chem. Soc., Chem. Commun.*, 1991, 532–533.

102 Y. Wu, C. L. Zhang, X. Z. Qu, Z. P. Liu and Z. Z. Yang, *Langmuir*, 2010, **26**, 9442–9448.

103 M. Piech, M. C. George, N. S. Bell and P. V. Braun, *Langmuir*, 2006, **22**, 1379–1382.

104 T. Seki and K. Ichimura, *J. Phys. Chem.*, 1990, **94**, 3769–3775.

105 H. Eckhardt, A. Bose and V. A. Krongauz, *Polymer*, 1987, **28**, 1959–1964.

106 H. R. Allcock and C. Kim, *Macromolecules*, 1991, **24**, 2846–2851.

107 E. Goldburt, F. Shvartsman and V. Krongauz, *Macromolecules*, 1984, **17**, 1876–1878.

108 M. Ueda, K. Kudo and K. Ichimura, *J. Mater. Chem.*, 1995, **5**, 1007–1011.

109 S. Gorelik, S. Hongyan, M. J. Lear and J. Hobley, *Photochem. Photobiol. Sci.*, 2010, **9**, 141–151.

110 M. Plaschke, R. Czolk and H. J. Ache, *Anal. Chim. Acta*, 1995, **304**, 107–113.

111 I. Oehme, S. Prattes, O. S. Wolfbeis and G. J. Mohr, *Talanta*, 1998, **47**, 595–604.

112 M. H. Lee, X. D. Li and E. Kim, *Mol. Cryst. Liq. Cryst.*, 2000, **349**, 51–54.

113 X. D. Li, E. Kim and M. H. Lee, *Polymer*, 2005, **29**, 25–31.

114 K. Arai, Y. Shitara and T. Ohyama, *J. Mater. Chem.*, 1996, **6**, 11–14.

115 M. Q. Zhu, G. F. Zhang, C. Li, M. P. Aldred, E. Chang, R. A. Drezek and A. D. Q. Li, *J. Am. Chem. Soc.*, 2011, **133**, 365–372.



116 Y.-H. Chan, M. E. Gallina, X. Zhang, I. C. Wu, Y. Jin, W. Sun and D. T. Chiu, *Anal. Chem.*, 2012, **84**, 9431–9438.

117 M. Irie, T. Iwayanagi and Y. Taniguchi, *Macromolecules*, 1985, **18**, 2418–2422.

118 G. Baillet, G. Giusti and R. Guglielmetti, *J. Photochem. Photobiol. A*, 1993, **70**, 157–161.

119 G. Baillet, M. Campredon, R. Guglielmetti, G. Giusti and C. Aubert, *J. Photochem. Photobiol. A*, 1994, **83**, 147–151.

120 X. L. Li, J. L. Li, Y. M. Wang, T. Matsuura and J. B. Meng, *J. Photochem. Photobiol. A*, 2004, **161**, 201–213.

121 R. Matsushima, M. Nishiyama and M. Doi, *J. Photochem. Photobiol. A*, 2001, **139**, 63–69.

122 M. Sakuragi, K. Aoki, T. Tamaki and K. Ichimura, *Bull. Chem. Soc. Jpn.*, 1990, **63**, 74–79.

123 J. Whelan, J. T. C. Wojtyk and E. Buncel, *Chem. Mater.*, 2008, **20**, 3797–3799.

124 A. Radu, R. Byrne, N. Alhashimy, M. Fusaro, S. Scarmagnani and D. Diamond, *J. Photochem. Photobiol. A*, 2009, **206**, 109–115.

125 N. S. Bell and M. Piech, *Langmuir*, 2006, **22**, 1420–1427.

126 S. Scarmagnani, Z. Walsh, C. Slater, N. Alhashimy, B. Paull, M. Macka and D. Diamond, *J. Mater. Chem.*, 2008, **18**, 5063–5071.

127 A. Radu, S. Scarmagnani, R. Byrne, C. Slater, K. T. Lau and D. Diamond, *J. Phys. D: Appl. Phys.*, 2007, **40**, 7238–7244.

128 C. Q. Huang, Y. Wang, C. Y. Hong and C. Y. Pan, *Macromol. Rapid Commun.*, 2011, **32**, 1174–1179.

129 D. S. Achilleos and M. Vamvakaki, *Macromolecules*, 2010, **43**, 7073–7081.

130 R. Adelmann, P. Mela, M. O. Gallyamov, H. Keul and M. Moller, *J. Polym. Sci., Part A: Polym. Chem.*, 2009, **47**, 1274–1283.

131 M. Bertoldo, S. Nazzi, G. Zampano and F. Ciardelli, *Carbohydr. Polym.*, 2011, **85**, 401–407.

132 J. Labsky, I. Koropecky, S. Nespurek and J. Kalal, *Eur. Polym. J.*, 1981, **17**, 309–313.

133 J. Labsky, J. Kalal and F. Mikes, *Polym. Photochem.*, 1982, **2**, 289–295.

134 J. Labsky, F. Mikes and J. Kalal, *Polym. Bull.*, 1980, **2**, 785–789.

135 R. J. Byrne, S. E. Stitzel and D. Diamond, *J. Mater. Chem.*, 2006, **16**, 1332–1337.

136 C. Bronner, G. Schulze, K. J. Franke, J. I. Pascual and P. Tegeder, *J. Phys.: Condens. Matter*, 2011, **23**, 484005.

137 Y. Imai, K. Adachi, K. Naka and Y. Chujo, *Polym. Bull.*, 2000, **44**, 9–15.

138 M. Tomasulo, I. Yildiz and F. M. Raymo, *Inorg. Chim. Acta*, 2007, **360**, 938–944.

139 Y. Kalisky and D. J. Williams, *Macromolecules*, 1984, **17**, 292–296.

140 D. J. Chung, Y. Ito and Y. Imanishi, *J. Appl. Polym. Sci.*, 1994, **51**, 2027–2033.

141 Y. Bardavid, I. Goykhman, D. Nozaki, G. Cuniberti and S. Yitzchaik, *J. Phys. Chem. C*, 2011, **115**, 3123–3128.

142 L. A. Connal, G. V. Franks and G. G. Qiao, *Langmuir*, 2010, **26**, 10397–10400.

143 S. Z. Wu, J. R. Lu, F. Zeng, Y. N. Chen and Z. Tong, *Macromolecules*, 2007, **40**, 5060–5066.

144 A. Warshawsky, N. Kahana, F. Buchholtz, A. Zelichonok, J. Ratner and V. Krongauz, *Ind. Eng. Chem. Res.*, 1995, **34**, 2825–2832.

145 Y. J. Oh, J. A. Nam, A. Al-Nahain, S. Lee, I. In and S. Y. Park, *Macromol. Rapid Commun.*, 2012, **33**, 1958–1963.

146 L. Hauser, A. C. Knall, M. Roth, G. Trimmel, M. Edler, T. Griesser and W. Kern, *Monatsh. Chem.*, 2012, **143**, 1551–1558.

147 S. R. Keum, S. M. Ahn, S. J. Roh and S. Y. Ma, *Dyes Pigm.*, 2010, **86**, 74–80.

148 B. B. Mistry, R. G. Patel and V. S. Patel, *J. Appl. Polym. Sci.*, 1997, **64**, 841–848.

149 J. Verborgt and G. Smets, *J. Polym. Sci., Polym. Chem. Ed.*, 1974, **12**, 2511–2523.

150 J. H. Su, J. Chen, F. Zeng, Q. M. Chen, S. Z. Wu and Z. Tong, *Polym. Bull.*, 2008, **61**, 425–434.

151 M. Moniruzzaman, G. F. Fernando and A. J. Bellamy, *Eur. Polym. J.*, 2006, **42**, 1455–1466.

152 Y. K. Choi, E. Y. Kim and S. R. Keum, *Tetrahedron Lett.*, 1998, **39**, 8861–8864.

153 H. Schenderlein, A. Voss, R. W. Stark and M. Biesalski, *Langmuir*, 2013, **29**, 4525–4534.

154 N. Negishi, K. Tsunemitsu, K. Ishihara, I. Shinohara, T. Okano, K. Kataoka, T. Akaike and Y. Sakurai, *Kobunshi Ronbunshu*, 1980, **37**, 287–291.

155 R. Nakao, N. Ueda, Y. Abe, T. Horii and E. Inoue, *Polym. Adv. Technol.*, 1994, **5**, 240–241.

156 R. Nakao, N. Ueda, Y. Abe, T. Horii and E. Inoue, *Polym. Adv. Technol.*, 1995, **6**, 243–247.

157 R. Nakao, N. Ueda, Y. Abe, T. Horii and H. Inoue, *Polym. Adv. Technol.*, 1996, **7**, 863–866.

158 J. H. Kim, S. Y. Ban, Q. Zhang, G. W. Kim, M. J. Cho and D. H. Choi, *Mol. Cryst. Liq. Cryst.*, 2006, **445**, 307–314.

159 J. Chen, F. Zeng, S. Z. Wu, J. Q. Zhao, Q. M. Chen and Z. Tong, *Chem. Commun.*, 2008, 5580–5582.

160 H. I. Lee, W. Wu, J. K. Oh, L. Mueller, G. Sherwood, L. Peteanu, T. Kowalewski and K. Matyjaszewski, *Angew. Chem., Int. Ed.*, 2007, **46**, 2453–2457.

161 C. H. Li, Y. X. Zhang, J. M. Hu, J. J. Cheng and S. Y. Liu, *Angew. Chem., Int. Ed.*, 2010, **49**, 5120–5124.

162 S. Guragain, B. P. Bastakoti, M. Ito, S.-i. Yusa and K. Nakashima, *Soft Matter*, 2012, **8**, 9628–9634.

163 Y. S. Park, Y. Ito and Y. Imanishi, *Macromolecules*, 1998, **31**, 2606–2610.

164 T. Wu, G. Zou, J. M. Hu and S. Y. Liu, *Chem. Mater.*, 2009, **21**, 3788–3798.

165 G. Smets and F. De Blauwe, *Pure Appl. Chem.*, 1974, **39**, 225–238.

166 G. O'Bryan, B. M. Wong and J. R. McElhanon, *ACS Appl. Mater. Interfaces*, 2010, **2**, 1594–1600.

167 C. K. Lee, D. A. Davis, S. R. White, J. S. Moore, N. R. Sottos and P. V. Braun, *J. Am. Chem. Soc.*, 2010, **132**, 16107–16111.

168 J. Kadokawa, Y. Tanaka, Y. Yamashita and K. Yamamoto, *Eur. Polym. J.*, 2012, **48**, 549–559.



169 S. L. Potisek, D. A. Davis, N. R. Sottos, S. R. White and J. S. Moore, *J. Am. Chem. Soc.*, 2007, **129**, 13808–13809.

170 B. A. Beiermann, D. A. Davis, S. L. B. Kramer, J. S. Moore, N. R. Sottos and S. R. White, *J. Mater. Chem.*, 2011, **21**, 8443–8447.

171 T. H. Mourey, I. Noh and H. Yu, *J. Chromatogr.*, 1984, **303**, 361–369.

172 K. Fukushima, A. J. Vandenbos and T. Fujiwara, *Chem. Mater.*, 2007, **19**, 644–646.

173 Y. Nakahara, J. Nakamura, N. Shirotani and K. Kimura, *Chem. Lett.*, 2012, 1142–1144.

174 W. L. Zhao and E. M. Carreira, *Org. Lett.*, 2005, **7**, 1609–1612.

175 L. Y. Zhu, M. Q. Zhu, J. K. Hurst and A. D. Q. Li, *J. Am. Chem. Soc.*, 2005, **127**, 8968–8970.

176 S. Manley, J. M. Gillette and J. Lippincott-Schwartz, in *Methods in Enzymology*, ed. N. G. Walter, Elsevier, San Diego, 2010, vol. 475, pp. 109–120.

177 E. Betzig, G. H. Patterson, R. Sougrat, O. W. Lindwasser, S. Olenych, J. S. Bonifacino, M. W. Davidson, J. Lippincott-Schwartz and H. F. Hess, *Science*, 2006, **313**, 1642–1645.

178 M. J. Rust, M. Bates and X. W. Zhuang, *Nat. Methods*, 2006, **3**, 793–795.

179 Z. Y. Tian and A. D. Q. Li, *Acc. Chem. Res.*, 2013, **46**, 269–279.

180 D. H. Hu, Z. Y. Tian, W. W. Wu, W. Wan and A. D. Q. Li, *J. Am. Chem. Soc.*, 2008, **130**, 15279–15281.

181 D. H. Hu, Z. Y. Tian, W. W. Wu, W. Wan and A. D. Q. Li, *Microsc. Microanal.*, 2009, **15**, 840–841.

182 Z. Y. Tian, A. D. Q. Li and D. H. Hu, *Chem. Commun.*, 2011, **47**, 1258–1260.

183 Z. Y. Tian, W. W. Wu, W. Wan and A. D. Q. Li, *J. Am. Chem. Soc.*, 2009, **131**, 4245–4252.

184 Y. Lv, H. Liu, B. Zhao, Z. Tian and A. D. Q. Li, *Isr. J. Chem.*, 2013, **53**, 294–302.

185 J. Chen, P. S. Zhang, G. Fang, C. Weng, J. Hu, P. G. Yi, X. Y. Yu and X. F. Li, *Polym. Chem.*, 2012, **3**, 685–693.

186 L. Y. Zhu, W. W. Wu, M. Q. Zhu, J. J. Han, J. K. Hurst and A. D. Q. Li, *J. Am. Chem. Soc.*, 2007, **129**, 3524–3526.

187 J. Chen, F. Zeng, S. Z. Wu, J. Su and Z. Tong, *Small*, 2009, **5**, 970–978.

188 J. Chen, F. Zeng, S. Z. Wu, Q. M. Chen and Z. Tong, *Chem.-Eur. J.*, 2008, **14**, 4851–4860.

189 I. S. Park, Y. S. Jung, K. J. Lee and J. M. Kim, *Chem. Commun.*, 2010, **46**, 2859–2861.

190 J. Chen, D. Wang, A. Turshatov, R. Munoz-Espi, U. Ziener, K. Koynov and K. Landfester, *Polym. Chem.*, 2013, **4**, 773–781.

191 M. Tomasulo, E. Deniz, R. J. Alvarado and F. M. Raymo, *J. Phys. Chem. C*, 2008, **112**, 8038–8045.

192 J. Chen, P. S. Zhang, X. Y. Yu, X. F. Li, H. W. Tao and P. G. Yi, *J. Macromol. Sci., Part A: Pure Appl. Chem.*, 2011, **48**, 637–643.

193 J. A. Chen, P. S. Zhang, G. Fang, P. G. Yi, X. Y. Yu, X. F. Li, F. Zeng and S. Z. Wu, *J. Phys. Chem. B*, 2011, **115**, 3354–3362.

194 J. Chen, P. S. Zhang, G. Fang, P. G. Yi, F. Zeng and S. Z. Wu, *J. Phys. Chem. B*, 2012, **116**, 4354–4362.

195 S. Mao, R. K. P. Benninger, Y. Yan, C. Petchprayoon, D. Jackson, C. J. Easley, D. W. Piston and G. Marriott, *Biophys. J.*, 2008, **94**, 4515–4524.

196 Y. Hirokawa and T. Tanaka, *J. Chem. Phys.*, 1984, **81**, 6379–6380.

197 R. Yoshida, K. Uchida, Y. Kaneko, K. Sakai, A. Kikuchi, Y. Sakurai and T. Okano, *Nature*, 1995, **374**, 240–242.

198 I. Dimitrov, B. Trzebicka, A. H. E. Muller, A. Dworak and C. B. Tsvetanov, *Prog. Polym. Sci.*, 2007, **32**, 1275–1343.

199 M. Irie, A. Menju, K. Hayashi and G. Smets, *J. Polym. Sci., Polym. Chem. Ed.*, 1979, **17**, 29–31.

200 A. Menju, K. Hayashi and M. Irie, *Macromolecules*, 1981, **14**, 755–758.

201 M. Irie, K. Hayashi and A. Menju, *Polym. Photochem.*, 1981, **1**, 233–242.

202 J. Edahiro, K. Sumaru, T. Takagi, T. Shinbo and T. Kanamori, *Langmuir*, 2006, **22**, 5224–5226.

203 V. A. Krongauz and A. Golinelli, *Polym. Bull.*, 1982, **6**, 259–262.

204 J. H. Kim, S. Y. Ban, S. Kaihua and D. H. Choi, *Dyes Pigm.*, 2003, **58**, 105–112.

205 D. H. Choi, S. Y. Ban and J. H. Kim, *Bull. Korean Chem. Soc.*, 2003, **24**, 441–445.

206 C. Konak, R. C. Rathi, P. Kopeckova and J. Kopecek, *Macromolecules*, 1997, **30**, 5553–5556.

207 C. Konak, R. C. Rathi, P. Kopeckova and J. Kopecek, *Polym. Adv. Technol.*, 1998, **9**, 641–648.

208 L. Ma, J. Li, D. Han, H. Geng, G. Chen and Q. Li, *Macromol. Chem. Phys.*, 2013, **214**, 716–725.

209 V. A. Krongauz and E. S. Goldburt, *Macromolecules*, 1981, **14**, 1382–1386.

210 T. Wismontski-Knittel and V. Krongauz, *Macromolecules*, 1985, **18**, 2124–2126.

211 B. Yan, J. He, P. Ayotte and Y. Zhao, *Macromol. Rapid Commun.*, 2011, **32**, 972–976.

212 D. S. Achilleos, T. A. Hatton and M. Vamvakaki, *J. Am. Chem. Soc.*, 2012, **134**, 5726–5729.

213 Y. Nakahara, Y. Okazaki and K. Kimura, *Soft Matter*, 2012, **8**, 3192–3199.

214 S. Kado, K. Uehara, Y. Nakahara and K. Kimura, *Bull. Chem. Soc. Jpn.*, 2011, **84**, 422–426.

215 V. K. Kotharangannagari, A. Sanchez-Ferrer, J. Ruokolainen and R. Mezzenga, *Macromolecules*, 2011, **44**, 4569–4573.

216 S. Menon, R. M. Ongungal and S. Das, *Polym. Chem.*, 2013, **4**, 623–628.

217 Q. A. Jin, G. Y. Liu and J. A. Ji, *J. Polym. Sci., Part A: Polym. Chem.*, 2010, **48**, 2855–2861.

218 Y. Arisaka, A. Tamura, K. Uchida and H. Yajima, *Chem. Lett.*, 2010, 58–59.

219 H. Feil, Y. H. Bae, J. Feijen and S. W. Kim, *Macromolecules*, 1993, **26**, 2496–2500.

220 A. E. Ivanov, N. L. Eremeev, P. O. Wahlund, I. Y. Galaev and B. Mattiasson, *Polymer*, 2002, **43**, 3819–3823.



221 K. Sumaru, M. Kameda, T. Kanamori and T. Shinbo, *Macromolecules*, 2004, **37**, 7854–7856.

222 J. I. Edahiro, K. Sumaru, T. Takagi, T. Shinbo, T. Kanamori and M. Sudoh, *Eur. Polym. J.*, 2008, **44**, 300–307.

223 M. Kameda, K. Sumaru, T. Kanamori and T. Shinbo, *Langmuir*, 2004, **20**, 9315–9319.

224 Y. Shiraishi, R. Miyamoto and T. Hirai, *Org. Lett.*, 2009, **11**, 1571–1574.

225 R. Byrne, C. Ventura, F. B. Lopez, A. Walther, A. Heise and D. Diamond, *Biosens. Bioelectron.*, 2010, **26**, 1392–1398.

226 A. Garcia, M. Marquez, T. Cai, R. Rosario, Z. B. Hu, D. Gust, M. Hayes, S. A. Vail and C. D. Park, *Langmuir*, 2007, **23**, 224–229.

227 A. Szilagyi, K. Sumaru, S. Sugiura, T. Takagi, T. Shinbo, M. Zrinyi and T. Kanamori, *Chem. Mater.*, 2007, **19**, 2730–2732.

228 Y. Zhao and L. Tremblay, *J. Polym. Sci., Part A: Polym. Chem.*, 2010, **48**, 4055–4066.

229 X. M. He, M. Aizenberg, O. Kuksenok, L. D. Zarzar, A. Shastri, A. C. Balazs and J. Aizenberg, *Nature*, 2012, **487**, 214–218.

230 T. Satoh, K. Sumaru, T. Takagi and T. Kanamori, *Soft Matter*, 2011, **7**, 8030–8034.

231 S. Sugiura, K. Sumaru, K. Ohi, K. Hiroki, T. Takagi and T. Kanamori, *Sens. Actuators, A*, 2007, **140**, 176–184.

232 S. Sugiura, A. Szilagyi, K. Sumaru, K. Hattori, T. Takagi, G. Filipcsei, M. Zrinyi and T. Kanamori, *Lab Chip*, 2009, **9**, 196–198.

233 K. Sumaru, K. Ohi, T. Takagi, T. Kanamori and T. Shinbo, *Langmuir*, 2006, **22**, 4353–4356.

234 F. Benito-Lopez, R. Byrne, A. M. Raduta, N. E. Vrana, G. McGuinness and D. Diamond, *Lab Chip*, 2010, **10**, 195–201.

235 T. Satoh, K. Sumaru, T. Takagi, K. Takai and T. Kanamori, *Phys. Chem. Chem. Phys.*, 2011, **13**, 7322–7329.

236 K. Kimura, H. Sakamoto and T. Nakamura, *J. Nanosci. Nanotechnol.*, 2006, **6**, 1741–1749.

237 S. Kurihara, M. Higuchi, T. Ogata and T. Nonaka, *J. Membr. Sci.*, 1994, **93**, 69–78.

238 S. Marx-Tibbon and I. Willner, *Chem. Commun.*, 1994, 1261–1262.

239 Z. Walsh, P. A. Levkin, S. Abele, S. Scarmagnani, D. Heger, P. Klan, D. Diamond, B. Paull, F. Svec and M. Macka, *J. Chromatogr., A*, 2011, **1218**, 2954–2962.

240 Z. Walsh, S. Scarmagnani, F. Benito-Lopez, S. Abele, F. Q. Nie, C. Slater, R. Byrne, D. Diamond, B. Paull and M. Macka, *Sens. Actuators, B*, 2010, **148**, 569–576.

241 I. Willner, S. Rubin, R. Shatzmiller and T. Zor, *J. Am. Chem. Soc.*, 1993, **115**, 8690–8694.

242 A. Nayak, H. Liu and G. Belfort, *Angew. Chem., Int. Ed.*, 2006, **45**, 4094–4098.

243 Y. Ito and Y. S. Park, *Polym. Adv. Technol.*, 2000, **11**, 136–144.

244 G. Smets, *Pure Appl. Chem.*, 1975, **42**, 509–526.

245 G. Smets, J. Braeken and M. Irie, *Pure Appl. Chem.*, 1978, **50**, 845–856.

246 D. A. Davis, A. Hamilton, J. L. Yang, L. D. Cremar, D. Van Gough, S. L. Potisek, M. T. Ong, P. V. Braun, T. J. Martinez, S. R. White, J. S. Moore and N. R. Sottos, *Nature*, 2009, **459**, 68–72.

247 B. A. Beiermann, S. L. B. Kramer, J. S. Moore, S. R. White and N. R. Sottos, *ACS Macro Lett.*, 2012, **1**, 163–166.

248 C. M. Kingsbury, P. A. May, D. A. Davis, S. R. White, J. S. Moore and N. R. Sottos, *J. Mater. Chem.*, 2011, **21**, 8381–8388.

249 C. K. Lee, B. A. Beiermann, M. N. Silberstein, J. Wang, J. S. Moore, N. R. Sottos and P. V. Braun, *Macromolecules*, 2013, **46**, 3746–3752.

250 J. D. Winkler, K. Deshayes and B. Shao, *J. Am. Chem. Soc.*, 1989, **111**, 769–770.

251 J. W. Zhou, Y. T. Li and X. Q. Song, *J. Photochem. Photobiol., A*, 1995, **87**, 37–42.

252 T. Suzuki, T. Kato and H. Shinozaki, *Chem. Commun.*, 2004, 2036–2037.

253 J. T. C. Wojtyk, P. M. Kazmaier and E. Buncel, *Chem. Commun.*, 1998, 1703–1704.

254 J. T. C. Wojtyk, P. M. Kazmaier and E. Buncel, *Chem. Mater.*, 2001, **13**, 2547–2551.

255 T. Suzuki, Y. Kawata, S. Kahata and T. Kato, *Chem. Commun.*, 2003, 2004–2005.

256 T. Suzuki, Y. Hirahara, K. Bunya and H. Shinozaki, *J. Mater. Chem.*, 2010, **20**, 2773–2779.

257 C. Ventura, R. Byrne, F. Audouin and A. Heise, *J. Polym. Sci., Part A: Polym. Chem.*, 2011, **49**, 3455–3463.

258 K. H. Fries, J. D. Driskell, S. Samanta and J. Locklin, *Anal. Chem.*, 2010, **82**, 3306–3314.

259 K. H. Fries, J. D. Driskell, G. R. Sheppard and J. Locklin, *Langmuir*, 2011, **27**, 12253–12260.

260 P.-J. Wu, J.-L. Chen, C.-P. Chen and Y.-H. Chan, *Chem. Commun.*, 2013, **49**, 898–900.

261 N. Kobayashi, S. Sato, K. Takazawa, K. Ikeda and R. Hirohashi, *Electrochim. Acta*, 1995, **40**, 2309–2311.

262 K. Kimura, M. Sumida and M. Yokoyama, *Chem. Commun.*, 1997, 1417–1418.

263 K. Kimura, M. Nakamura, H. Sakamoto, R. M. Uda, M. Sumida and M. Yokoyama, *Bull. Chem. Soc. Jpn.*, 2003, **76**, 209–215.

264 K. Kimura, H. Sakamoto and R. M. Uda, *Macromolecules*, 2004, **37**, 1871–1876.

265 M. Kojima, T. Nakanishi, Y. Hirai, H. Yabu and M. Shimomura, *Chem. Commun.*, 2010, **41**, 3970–3972.

266 T. Nakanishi, Y. Hirai, M. Kojima, H. Yabu and M. Shimomura, *J. Mater. Chem.*, 2010, **20**, 6741–6745.

267 N. Negishi, T. Iida, K. Ishihara and I. Shinohara, *Makromol. Chem., Rapid Commun.*, 1981, **2**, 617–620.

268 Y. Shiraishi, S. Sumiya, K. Manabe and T. Hirai, *ACS Appl. Mater. Interfaces*, 2011, **3**, 4649–4656.

269 L. Angiolini, T. Benelli, L. Giorgini and F. M. Raymo, *Polymer*, 2009, **50**, 5638–5646.

270 L. Angiolini, T. Benelli, L. Giorgini and F. M. Raymo, *Macromol. Chem. Phys.*, 2008, **209**, 2049–2060.



271 L. Angiolini, T. Benelli, E. Bicciocchi, L. Giorgini and F. M. Raymo, *React. Funct. Polym.*, 2012, **72**, 469–477.

272 I. Cabrera, V. Krongauz and H. Ringsdorf, *Mol. Cryst. Liq. Cryst.*, 1988, **155**, 221–230.

273 S. Yitzchaik, G. Berkovic and V. Krongauz, *Macromolecules*, 1990, **23**, 3539–3541.

274 S. Yitzchaik, I. Cabrera, F. Buchholtz and V. Krongauz, *Macromolecules*, 1990, **23**, 707–713.

275 E. J. C. Kellar, G. Williams, V. Krongauz and S. Yitzchaik, *J. Mater. Chem.*, 1991, **1**, 331–337.

276 I. Cabrera, V. Krongauz and H. Ringsdorf, *Angew. Chem., Int. Ed. Engl.*, 1987, **26**, 1178–1180.

277 L. V. Natarajan, T. J. Bunning and S. Y. Kim, *Macromolecules*, 1994, **27**, 7248–7253.

278 L. V. Natarajan, V. Tondiglia, T. J. Bunning, R. L. Crane and W. W. Adams, *Adv. Mater. Opt. Electron.*, 1992, **1**, 293–297.

279 A. Y. Bobrovsky, N. I. Boiko and V. P. Shibaev, *Adv. Mater.*, 1999, **11**, 1025–1028.

280 A. Y. Bobrovsky, N. I. Boiko and V. P. Shibaev, *Liq. Cryst.*, 2000, **27**, 57–62.

281 A. K. Bobrovsky, N. I. Boiko and V. P. Shibaev, *Liq. Cryst.*, 2000, **27**, 219–223.

282 I. Cabrera and V. Krongauz, *Nature*, 1987, **326**, 582–585.

283 S. Yitzchaik, G. Berkovic and V. Krongauz, *Adv. Mater.*, 1990, **2**, 33–36.

284 S. Yitzchaik, G. Berkovic and V. Krongauz, *Chem. Mater.*, 1990, **2**, 162–168.

285 S. Yitzchaik, G. Berkovic and V. Krongauz, *Opt. Lett.*, 1990, **15**, 1120–1122.

286 M. Kamenjicki Maurer, I. K. Lednev and S. A. Asher, *Adv. Funct. Mater.*, 2005, **15**, 1401–1406.

287 Q. S. Liu, K. J. Jiang, Y. Q. Wen, J. X. Wang, J. Luo and Y. L. Song, *Appl. Phys. Lett.*, 2010, **97**, 253304.

288 M. Sommer and H. Komber, *Macromol. Rapid Commun.*, 2013, **34**, 57–62.

289 J. H. Yang and M. K. Ng, *Synthesis*, 2006, 3075–3079.

290 K. Wagner, M. Zanoni, A. B. S. Elliott, P. Wagner, R. Byrne, L. Florea, D. Diamond, K. C. Gordon, G. G. Wallace and D. L. Officer, *J. Phys. Chem. C*, 2013, **1**, 3913–3916.

291 J. Pennakalathil and J. D. Hong, *ACS Nano*, 2011, **5**, 9232–9237.

292 G. Montagnoli, O. Pieroni and S. Suzuki, *Polym. Photochem.*, 1983, **3**, 279–294.

293 P. H. Vandewyer and G. Smets, *J. Polym. Sci., Part A-1: Polym. Chem.*, 1970, **8**, 2361–2374.

294 G. Smets, *Pure Appl. Chem.*, 1972, **30**, 1–24.

295 F. Ciardelli, D. Fabbri, O. Pieroni and A. Fissi, *J. Am. Chem. Soc.*, 1989, **111**, 3470–3472.

296 T. M. Cooper, L. V. Natarajan and C. G. Miller, *Photochem. Photobiol.*, 1999, **69**, 173–176.

297 T. M. Cooper, K. A. Obermeier, L. V. Natarajan and R. L. Crane, *Photochem. Photobiol.*, 1992, **55**, 1–7.

298 A. Fissi, O. Pieroni, F. Ciardelli, D. Fabbri, G. Ruggeri and K. Umezawa, *Biopolymers*, 1993, **33**, 1505–1517.

299 N. Higashi, K. Shimizu and M. Niwa, *J. Colloid Interface Sci.*, 1997, **185**, 44–48.

300 B. Mecheri, P. Baglioni, O. Pieroni and G. Caminati, *Mater. Sci. Eng., C*, 2003, **23**, 893–896.

301 N. Angelini, B. Corrias, A. Fissi, O. Pieroni and F. Lenci, *Biophys. J.*, 1998, **74**, 2601–2610.

302 O. Pieroni, A. Fissi, F. Ciardelli and D. Fabbri, *Mol. Cryst. Liq. Cryst.*, 1994, **246**, 191–194.

303 R. Pachter, T. M. Cooper, L. V. Natarajan, K. A. Obermeier, R. L. Crane and W. W. Adams, *Biopolymers*, 1992, **32**, 1129–1140.

304 O. Pieroni, A. Fissi, A. Viegi, D. Fabbri and F. Ciardelli, *J. Am. Chem. Soc.*, 1992, **114**, 2734–2736.

305 T. M. Cooper, M. O. Stone, L. V. Natarajan and R. L. Crane, *Photochem. Photobiol.*, 1995, **62**, 258–262.

306 A. Fissi, O. Pieroni, N. Angelini and F. Lenci, *Macromolecules*, 1999, **32**, 7116–7121.

307 O. Pieroni, A. Fissi and F. Ciardelli, *React. Funct. Polym.*, 1995, **26**, 185–199.

308 K. Fujimoto, M. Amano, Y. Horibe and M. Inouye, *Org. Lett.*, 2006, **8**, 285–287.

309 T. Sakata, Y. L. Yan and G. Marriott, *Proc. Natl. Acad. Sci. U. S. A.*, 2005, **102**, 4759–4764.

310 K. Namba and S. Suzuki, *Chem. Lett.*, 1975, 947–950.

311 M. Aizawa, K. Namba and S. Suzuki, *Arch. Biochem. Biophys.*, 1977, **180**, 41–48.

312 M. Aizawa, K. Namba and S. Suzuki, *Arch. Biochem. Biophys.*, 1977, **182**, 305–310.

313 E. Zahavy, S. Rubin and I. Willner, *J. Chem. Soc., Chem. Commun.*, 1993, 1753–1755.

314 E. Zahavy, S. Rubin and I. Willner, *Mol. Cryst. Liq. Cryst.*, 1994, **246**, 195–199.

315 I. Willner, S. Rubin and Y. Cohen, *J. Am. Chem. Soc.*, 1993, **115**, 4937–4938.

316 M. Lion-Dagan and I. Willner, *J. Photochem. Photobiol., A*, 1997, **108**, 247–252.

317 I. Karube, Y. Nakamoto, K. Namba and S. Suzuki, *Biochim. Biophys. Acta*, 1976, **429**, 975–981.

318 I. Willner, M. Lion-Dagan and E. Katz, *Chem. Commun.*, 1996, 623–624.

319 M. Lion-Dagan, E. Katz and I. Willner, *J. Am. Chem. Soc.*, 1994, **116**, 7913–7914.

320 D. G. Weston, J. Kirkham and D. C. Cullen, *Biochim. Biophys. Acta*, 1999, **1428**, 463–467.

321 Y. Ito, N. Sugimura, O. H. Kwon and Y. Imanishi, *Nat. Biotechnol.*, 1999, **17**, 73–75.

322 I. Karube, S. Suzuki, Y. Nakamoto and M. Nishida, *Biotechnol. Bioeng.*, 1977, **19**, 1549–1552.

323 I. Karube, S. Suzuki, Y. Nakamoto and M. Nishida, *J. Mol. Catal.*, 1979, **6**, 51–56.

324 Y. Nakamoto, I. Karube, S. Terawaki and S. Suzuki, *J. Ferment. Technol.*, 1977, **55**, 409–413.

325 Y. Nakamoto, I. Karube, S. Terawaki and S. Suzuki, *J. Solid-Phase Biochem.*, 1976, **1**, 143–149.

326 I. Karube, Y. Nakamoto and S. Suzuki, *Biochim. Biophys. Acta*, 1976, **445**, 774–779.

327 Y. Nakamoto, M. Nishida, I. Karube and S. Suzuki, *Biotechnol. Bioeng.*, 1977, **19**, 1115–1123.



328 Y. Nakamoto, I. Karube and S. Suzuki, *J. Ferment. Technol.*, 1975, **53**, 595–598.

329 I. Karube, Y. Yugeta, H. Matsuoka and S. Suzuki, *J. Mol. Catal.*, 1983, **18**, 135–140.

330 Y. Nakamoto, I. Karube, I. Kobayashi, M. Nishida and S. Suzuki, *Arch. Biochem. Biophys.*, 1979, **193**, 117–121.

331 I. Karube, Y. Ishimori and S. Suzuki, *J. Solid-Phase Biochem.*, 1977, **2**, 9–17.

332 I. Karube, Y. Ishimori, S. Suzuki and T. Sato, *Biotechnol. Bioeng.*, 1978, **20**, 1775–1783.

333 I. Karube, Y. Ishimori and S. Suzuki, *Anal. Biochem.*, 1978, **86**, 100–106.

334 H. Asanuma, K. Shirasuka, T. Yoshida, T. Takarada, X. G. Liang and M. Komiya, *Chem. Lett.*, 2001, 108–109.

335 P. Zhang, J. B. Meng, T. Matsuura and Y. M. Wang, *Chin. Chem. Lett.*, 2002, **13**, 299–302.

336 C. Beyer and H. A. Wagenknecht, *Synlett*, 2010, 1371–1376.

337 D. W. Urry, *Angew. Chem., Int. Ed. Engl.*, 1993, **32**, 819–841.

338 M. Alonso, V. Reboto, L. Guiscardo, A. San Martin and J. C. Rodríguez-Cabello, *Macromolecules*, 2000, **33**, 9480–9482.

339 T. Hirakura, Y. Nomura, Y. Aoyama and K. Akiyoshi, *Biomacromolecules*, 2004, **5**, 1804–1809.

340 A. Kocer, M. Walko, W. Meijberg and B. L. Feringa, *Science*, 2005, **309**, 755–758.

341 W. Szymanski, D. Yilmaz, A. Kocer and B. L. Feringa, *Acc. Chem. Res.*, 2013, DOI: 10.1021/ar4000357.

342 K. Yoshimura, A. Batiza, M. Schroeder, P. Blount and C. Kung, *Biophys. J.*, 1999, **77**, 1960–1972.

343 E. Kato, T. Ueda, S. Kimura and Y. Imanishi, *Biophys. Chem.*, 1994, **49**, 215–222.

344 T. Ueda, K. Nagamine, S. Kimura and Y. Imanishi, *J. Chem. Soc., Perkin Trans. 2*, 1995, 365–368.

345 K. Y. Tomizaki and H. Mihara, *J. Mater. Chem.*, 2005, **15**, 2732–2740.

346 K. Y. Tomizaki, X. He and H. Mihara, *Bioorg. Med. Chem. Lett.*, 2005, **15**, 1731–1735.

347 K. Y. Tomizaki and H. Mihara, *J. Am. Chem. Soc.*, 2007, **129**, 8345–8352.

348 K. Y. Tomizaki and H. Mihara, *Mol. Biosyst.*, 2006, **2**, 580–589.

349 B. Liao, J. A. Chen, H. W. Huang, X. F. Li and B. Q. He, *J. Mater. Chem.*, 2011, **21**, 5867–5869.

350 D. B. Liu, W. W. Chen, K. Sun, K. Deng, W. Zhang, Z. Wang and X. Y. Jiang, *Angew. Chem., Int. Ed.*, 2011, **50**, 4103–4107.

351 W. H. Binder, R. Sachsenhofer, C. J. Straif and R. Zirbs, *J. Mater. Chem.*, 2007, **17**, 2125–2132.

352 M. James, S. Ciampi, T. A. Darwish, T. L. Hanley, S. O. Sylvester and J. J. Gooding, *Langmuir*, 2011, **27**, 10753–10762.

353 F. May, M. Peter, A. Hutten, L. Prodi and J. Mattay, *Chem.-Eur. J.*, 2012, **18**, 814–821.

354 I. L. Medintz, S. A. Trammell, H. Mattoussi and J. M. Mauro, *J. Am. Chem. Soc.*, 2004, **126**, 30–31.

355 M. Tomasulo, I. Yildiz and F. M. Raymo, *Aust. J. Chem.*, 2006, **59**, 175–178.

356 B. Liao, P. Long, B. Q. He, S. J. Yi, B. L. Ou, S. H. Shen and J. Chen, *J. Mater. Chem. C*, 2013, **1**, 3716–3721.

357 C. Zhang, C. H. Xu, L. D. Sun and C. H. Yan, *Chem.-Asian J.*, 2012, **7**, 2225–2229.

358 M. Ueda, H. B. Kim and K. Ichimura, *J. Mater. Chem.*, 1994, **4**, 883–889.

359 M. Ueda, H. B. Kim and K. Ichimura, *Mater. Lett.*, 1994, **20**, 245–249.

360 M. Piech and N. S. Bell, *Macromolecules*, 2006, **39**, 915–922.

361 E. A. Osborne, B. R. Jarrett, C. Q. Tu and A. Y. Louie, *J. Am. Chem. Soc.*, 2010, **132**, 5934–5935.

362 B. I. Ipe, S. Mahima and K. G. Thomas, *J. Am. Chem. Soc.*, 2003, **125**, 7174–7175.

363 M. H. Yang and M. C. Biewer, *Tetrahedron Lett.*, 2005, **46**, 349–351.

364 L. de Leon and M. C. Biewer, *Tetrahedron Lett.*, 2000, **41**, 3527–3530.

365 B. C. Bunker, B. I. Kim, J. E. Houston, R. Rosario, A. A. Garcia, M. Hayes, D. Gust and S. T. Picraux, *Nano Lett.*, 2003, **3**, 1723–1727.

366 S. Kado, K. Yamada, T. Murakami and K. Kimura, *J. Am. Chem. Soc.*, 2005, **127**, 3026–3030.

367 D. Kessler, F. D. Jochum, J. Choi, K. Char and P. Theato, *ACS Appl. Mater. Interfaces*, 2011, **3**, 124–128.

368 Y. Aburaya, H. Nomura, M. Kageshima, Y. Naitoh, Y. J. Li and Y. Sugawara, *J. Appl. Phys.*, 2011, **109**, 064308.

369 T. A. Darwish, Y. Tong, M. James, T. L. Hanley, Q. Peng and S. Ye, *Langmuir*, 2012, **28**, 13852–13860.

370 R. Rosario, D. Gust, A. A. Garcia, M. Hayes, J. L. Taraci, T. Clement, J. W. Dailey and S. T. Picraux, *J. Phys. Chem. B*, 2004, **108**, 12640–12642.

371 D. Dattilo, L. Armelao, G. Fois, G. Mistura and M. Maggini, *Langmuir*, 2007, **23**, 12945–12950.

372 D. Wang, P. Jiao, J. Wang, Q. Zhang, L. Feng and Z. Yang, *J. Appl. Polym. Sci.*, 2012, **125**, 870–875.

373 G. Joseph, J. Pichardo and G. F. Chen, *Analyst*, 2010, **135**, 2303–2308.

374 W. Barthlott and C. Neinhuis, *Planta*, 1997, **202**, 1–8.

375 H. S. Lim, W. H. Lee, S. G. Lee, D. Lee, S. Jeon and K. Cho, *Chem. Commun.*, 2010, **46**, 4336–4338.

376 Y. Nakahara, Y. Yamaguchi, H. Iwamoto, H. Sakamoto and K. Kimura, *Anal. Methods*, 2012, **4**, 4025–4029.

377 A. K. Bohaty, M. R. Newton and I. Zharov, *J. Porous Mater.*, 2010, **17**, 465–473.

378 G. Wang, A. K. Bohaty, I. Zharov and H. S. White, *J. Am. Chem. Soc.*, 2006, **128**, 13553–13558.

379 M. Zhang, X. Hou, J. Wang, Y. Tian, X. Fan, J. Zhai and L. Jiang, *Adv. Mater.*, 2012, **24**, 2424–2428.

380 I. Vlassiouk, C. D. Park, S. A. Vail, D. Gust and S. Smirnov, *Nano Lett.*, 2006, **6**, 1013–1017.

381 I. Vlassiouk, F. Rios, S. A. Vail, D. Gust and S. Smirnov, *Langmuir*, 2007, **23**, 7784–7792.

382 R. Q. Albuquerque, J. Kuehni, P. Belser and L. De Cola, *ChemPhysChem*, 2010, **11**, 575–578.

383 C. T. Burns, S. Y. Choi, M. L. Dietz and M. A. Firestone, *Sep. Sci. Technol.*, 2008, **43**, 2503–2519.



384 L. Malfatti, S. Costacurta, T. Kidchob, P. Innocenzi, M. Casula, H. Amenitsch, D. Dattilo and M. Maggini, *Microporous Mesoporous Mater.*, 2009, **120**, 375–380.

385 Z. Zhang, D. Balogh, F. Wang, R. Tel-Vered, N. Levy, S. Y. Sung, R. Nechushtai and I. Willner, *J. Mater. Chem. B*, 2013, **1**, 3159–3166.

386 M. Natali and S. Giordani, *Chem. Soc. Rev.*, 2012, **41**, 4010–4029.

387 E. Del Canto, M. Natali, D. Movia and S. Giordani, *Phys. Chem. Chem. Phys.*, 2012, **14**, 6034–6043.

388 R. Byrne and D. Diamond, *Nat. Mater.*, 2006, **5**, 421–424.

389 S. Heng, M.-C. Nguyen, R. Kostecki, T. M. Monro and A. D. Abell, *RSC Adv.*, 2013, **3**, 8308–8317.

390 G. Wen, J. Yan, Y. Zhou, D. Zhang, L. Mao and D. Zhu, *Chem. Commun.*, 2006, 3016–3018.

391 M. Riskin, E. Katz, V. Gutkin and I. Willner, *Langmuir*, 2006, **22**, 10483–10489.

392 M. Riskin and I. Willner, *Langmuir*, 2009, **25**, 13900–13905.

393 M. Riskin, V. Gutkin, I. Felner and I. Willner, *Angew. Chem., Int. Ed.*, 2008, **47**, 4416–4420.

394 E. Aznar, R. Casasus, B. Garcia-Acosta, M. D. Marcos and R. Martinez-Manez, *Adv. Mater.*, 2007, **19**, 2228–2231.

395 D. Balogh, R. Tel-Vered, R. Freeman and I. Willner, *J. Am. Chem. Soc.*, 2011, **133**, 6533–6536.

396 I. Willner and R. Blonder, *Thin Solid Films*, 1995, **266**, 254–257.

397 R. Blonder, S. Levi, G. L. Tao, I. BenDov and I. Willner, *J. Am. Chem. Soc.*, 1997, **119**, 10467–10478.

398 E. Kaganer, R. Pogreb, D. Davidov and I. Willner, *Langmuir*, 1999, **15**, 3920–3923.

399 F. Patolsky, B. Filanovsky, E. Katz and I. Willner, *J. Phys. Chem. B*, 1998, **102**, 10359–10367.

400 A. Higuchi, A. Hamamura, Y. Shindo, H. Kitamura, B. O. Yoon, T. Mori, T. Uyama and A. Umezawa, *Biomacromolecules*, 2004, **5**, 1770–1774.

401 A. Gelmi, M. Zanoni, M. J. Higgins, S. Gambhir, D. L. Officer, D. Diamond and G. G. Wallace, *J. Mater. Chem. B*, 2013, **1**, 2162–2168.

402 T. Okano, N. Yamada, H. Sakai and Y. Sakurai, *J. Biomed. Mater. Res.*, 1993, **27**, 1243–1251.

403 J. Edahiro, K. Sumaru, Y. Tada, K. Ohi, T. Takagi, M. Kameda, T. Shinbo, T. Kanamori and Y. Yoshimi, *Biomacromolecules*, 2005, **6**, 970–974.

404 Y. Tada, K. Sumaru, M. Kameda, K. Ohi, T. Takagi, T. Kanamori and Y. Yoshimi, *J. Appl. Polym. Sci.*, 2006, **100**, 495–499.

405 K. Kikuchi, K. Sumaru, J.-I. Edahiro, Y. Ooshima, S. Sugiura, T. Takagi and T. Kanamori, *Biotechnol. Bioeng.*, 2009, **103**, 552–561.

406 I. Willner, R. Blonder and A. Dagan, *J. Am. Chem. Soc.*, 1994, **116**, 9365–9366.

407 A. Doron, E. Katz, G. L. Tao and I. Willner, *Langmuir*, 1997, **13**, 1783–1790.

408 R. Blonder, I. BenDov, A. Dagan, I. Willner and E. Zisman, *Biosens. Bioelectron.*, 1997, **12**, 627–644.

409 D. J. Gavadhan and S. W. Feldberg, *J. Electroanal. Chem.*, 2000, **491**, 103–110.

410 E. Katz, M. Lion-Dagan and I. Willner, *J. Electroanal. Chem.*, 1995, **382**, 25–31.

411 E. Katz and I. Willner, *Electroanalysis*, 1995, **7**, 417–419.

412 R. Blonder, I. Willner and A. F. Buckmann, *J. Am. Chem. Soc.*, 1998, **120**, 9335–9341.

413 M. Lion-Dagan, E. Katz and I. Willner, *J. Chem. Soc., Chem. Commun.*, 1994, 2741–2742.

414 I. Willner, M. Lion-Dagan, S. Marxtibon and E. Katz, *J. Am. Chem. Soc.*, 1995, **117**, 6581–6592.

415 I. Willner, A. Doron, E. Katz, S. Levi and A. J. Frank, *Langmuir*, 1996, **12**, 946–954.

416 T. Niazov, B. Shlyahovsky and I. Willner, *J. Am. Chem. Soc.*, 2007, **129**, 6374–6375.

417 S. Friedle and S. W. Thomas, III, *Angew. Chem., Int. Ed.*, 2010, **49**, 7968–7971.

418 K. Aoki, K. Ichimura, T. Tamaki, T. Seki and Y. Kawanishi, *Kobunshi Ronbunshu*, 1990, **47**, 771–777.

419 K. Ichimura, Y. Hayashi and N. Ishizuki, *Chem. Lett.*, 1992, 1063–1066.

420 K. Ichimura, Y. Hayashi, K. Goto and N. Ishizuki, *Thin Solid Films*, 1993, **235**, 101–107.

421 J. M. Galvin and G. B. Schuster, *Supramol. Sci.*, 1998, **5**, 89–100.

422 E. Fischer and Y. Hirschberg, *J. Chem. Soc.*, 1952, 4522–4524.

423 T. M. Cooper, V. Tondiglia, L. V. Natarajan, M. Shapiro, K. Obermeier and R. L. Crane, *Appl. Opt.*, 1993, **32**, 674–677.

424 Z. Tokarski, L. V. Natarajan, B. L. Epling, T. M. Cooper, K. L. Hussong, T. M. Grinstead and W. W. Adams, *Chem. Mater.*, 1994, **6**, 2063–2069.

425 R. Klajn, P. J. Wesson, K. J. M. Bishop and B. A. Grzybowski, *Angew. Chem., Int. Ed.*, 2009, **48**, 7035–7039.

426 R. F. Khairutdinov, M. E. Itkis and R. C. Haddon, *Nano Lett.*, 2004, **4**, 1529–1533.

427 E. Del Canto, K. Flavin, M. Natali, T. Perova and S. Giordani, *Carbon*, 2010, **48**, 2815–2824.

428 Y. J. Song, C. Xu, W. L. Wei, J. S. Ren and X. G. Qu, *Chem. Commun.*, 2011, **47**, 9083–9085.

429 T. Stafforst and D. Hilvert, *Chem. Commun.*, 2009, 287–288.

430 S. Biswas, K. Kinbara, N. Oya, N. Ishii, H. Taguchi and T. Aida, *J. Am. Chem. Soc.*, 2009, **131**, 7556–7557.

431 R. H. Kramer, D. L. Fortin and D. Trauner, *Curr. Opin. Neurobiol.*, 2009, **19**, 544–552.

432 N. Caporale, K. D. Kolstad, T. Lee, I. Tochitsky, D. Dalkara, D. Trauner, R. Kramer, Y. Dan, E. Y. Isacoff and J. G. Flannery, *Mol. Ther.*, 2011, **19**, 1212–1219.

433 A. S. Reddy, A. Izmitli and J. J. de Pablo, *J. Chem. Phys.*, 2009, **131**, 085101.

434 A. Fissi, O. Pieroni, G. Ruggeri and F. Ciardelli, *Macromolecules*, 1995, **28**, 302–309.

435 K. Fries, S. Samanta, S. Orski and J. Locklin, *Chem. Commun.*, 2008, 6288–6290.

